Universidad de Sonora

Postgrado en Nanotecnología

Departamento de Física

Stochastic properties of cooperative and non-cooperative enzymatic reactions at nanoscale

by

Juan Miguel Castellanos-Jaramillo

Dissertation submitted in fulfillment of the requirements

of the degree of Doctor in Nanotechnology.

Thesis advisor: Arnulfo Castellanos Moreno   Co-advisor: Adalberto Corella Madueño

Hermosillo, Sonora, México.   Noviembre, 2021

Universidad de Sonora

Repositorio Institucional UNISON
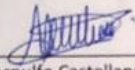
VOTOS APROBATORIOS

DR. MARIO ENRIQUE ÁLVAREZ RAMOS
Coordinador de Posgrado en Nanotecnología.

Por medio de la presente, nos permitimos informarle que los miembros del Jurado designado para revisar la Tesis de Doctorado intitulada:
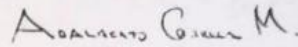
"Stochastic properties of cooperative and non-cooperative enzymatic reactions at nanoscale",

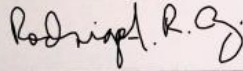presentada por:

Juan Miguel Castellanos Jaramillo

Hemos revisado y dado su VOTO APROBATORIO ya que cumple con los requisitos para la obtención del Título de Grado de Doctor en Nanotecnología:
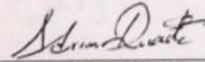
Dr. Arnulfo Castellanos Moreno

Dr. Adalberto Corella Madueño

Dr. Rodrigo Arturo Rosas Burgos

Dr. Roberto Pedro Duarte Zamorano

Dr. Francisco Adrían Duarte Alcaraz
(EXTERNO)

I Content

I Content

II Figure index

as the reaction progresses. (c) shows the correlation between the fluctuations of the substrate and enzyme-substrate complex, it increases.

III Acknowledgement

I would like to express thanks to my committee for their aid in improving and completing this thesis in a timely manner. I am also grateful to Doctor Josué Elías Juarez Onofre, whose comments, and opinions proved invaluable in bringing up questions, discussions and answers that nourished and assisted the development of this research.

I'd like to extend my gratitude to Doctor Mario Enrique Álvarez Ramos, academic coordinator of the PhD program, for his guidance and support.

And finally, to my family and friends. Thank you, and good bye.

1 Introduction

Many of the different processes of synthesis of nanostructured material frequently use catalysts whose rates and properties are studied under stationary regimes. As far as our understanding goes, the most common approach is the Michaelis-Menten model, or a modified version of it, where the rate of change of the enzyme-substrate complex concentration is slow enough that it can be approximated as if it was zero [1].

Although it is common to see the Michaelis-Menten model being used in diverse circumstances, the validity of the algebraic expression known as the Michaelis-Menten equation ($V = \frac{V_{max}[S]}{K_M+[S]}$ where V is the rate of product formation, V_{max} the maximum rate of product formation, $[S]$ is the substrate concentration and K_M is known as the Michaelis-Menten constant), has been widely studied [2], [3], and a variety of methods have been used to study the dynamics of the reaction [4]–[6]. From the point of view of stochastic processes, it is worth to mention A. F. Bartholomay [7], who formulated the problem of chemical reactions as a probability density that was a function of time and of the concentrations of substrate and enzyme-substrate complex. He obtained the corresponding master equation and demonstrated that the time evolution of the means of the concentrations match with the non-linear differential equations known in the textbooks of chemical kinetics. Sandra Hasstedt [8] studied the same problem with bivalued variables {0,1}, to indicate the presence or absence of a single enzyme molecule. Arányi & Thöt [9] developed a similar approach for states with zero or one enzyme molecule but an unlimited amount of substrate molecules. After 1990, the advancements in technology and measurement techniques using Raman spectroscopy and methods of photo-physics and photochemistry [10]–[12], have made the study of random fluctuations a necessity. In the XXI century the study of stochastic systems has proliferated [13]–[15] brought to attention to the fact that, in the smaller dimensions inside of the cell, enzymes are subject to random fluctuations due to the Brownian motion, causing random displacements of these, therefore changing the reaction rates. After noting that the number of proteins is also very small, the authors of the last references above questioned the description of reactions based in the continuous flow of matter and proposed a formulation in terms of discrete stochastic equations. Puchaka and Kierzek [16] suggested a method named "maximal time step method" aimed at stochastic simulation of systems composed of metabolic reactions and regulatory processes involving small quantities of molecules. Turner *et al.* [17] reviewed the efforts intended to include the effects of fluctuations in the structural organization of the cytoplasm and the limited diffusion of molecules due to molecular aggregation, and discussed the advantages of these for the modelling of intracellular reactions. In 2008 Valdus Saks *et al.* [18] showed that cells have a highly compartmentalized inner structure, thus they are not to be considered as simple bags of protein where enzymes diffuse as a gas. Also, this type of works has inspired specialists to design drugs, who have initiated studies about the required sizes for better substrate processing. Among these, one analyzed pairs of compartments in cyanobacterias, which contain two compartments named α-carboxysome and β-carboxysome, with dimensions of the order of nanometers [19]. These

elements lead us to maintain our position that the analysis of random fluctuations of substance concentrations are relevant in biochemical systems.

While there are many enzyme reactions that can be described by the Michaelis-Menten model, it is better suited for cases that follow two conditions:

1. The number of substrate species that can bind to an enzyme is one.

2. The system does not exhibit cooperativity, therefore the curve of the reaction velocity, as a function of substrate concentration, has a hyperbolic shape.

Advancements in fluorescence spectroscopy have allowed tracking single catalytic molecules, providing fundamental knowledge about the reactions being catalyzed. Noticing that the proportions of enzyme molecules fluctuate drastically compared to its mean values, Kumar *et al.* [20] suggest that a stochastic approach demonstrates the appearance of a cooperative dynamic in the chemical reaction kinetics such that, when the number of enzymes participating in the catalysis are few, there is a combined effect of the enzyme fluctuation that renders the Michaelis-Menten model ineffective. The classical model, they affirm, is useful only in cases where substrate concentration is much greater than enzyme concentration, consequently giving rise to modifications being made to the model to introduce parallel pathway mechanisms, which translate to the addition of reaction rates to the Michaelis-Menten model.

Many of such pathways involve allosteric regulation of enzymes by different mechanisms. Allosteric regulation occurs when particles (ions or molecules) usually bind reversibly to active or allosteric sites on the enzyme, activating or inhibiting its catalytic activity; therefore, modulating the kinetic behavior of the ensemble of enzymes. Such particles are often given the name of regulators or modulators, and these can be products formed by the enzymatic activity, or products from other reactions from other processes occurring in a larger scale.

Unlike single active site enzymes, such as beta-lactamase or the oxygen carrier myoglobin, which have a hyperbolic binding curve; enzymes with multiple binding sites, such as the oxygen carrier hemoglobin, present a sigmoid curve. This shape results from what is called a cooperative binding behavior and can be understood as follows: An enzyme that cooperatively binds its substrates, at low substrate concentration, will behave as if it had poor affinity to it. But as substrate concentration levels increase and more substrate binds to it, the affinity of the enzyme to its substrate also increases.

Said another way: From the perspective of a single, multisite enzyme, the first substrate particle that binds to one of the sites will have a hard time binding to it, but as more sites are occupied, the easier it will be for other substrate particles to bind to other sites of the same enzyme, eventually saturating it.

In the case of hemoglobin, it is considered that this behavior occurs because its structure undergoes a conformational change from a lower affinity state (T state) to a higher affinity state (R state). It is

the substrate the one responsible with regulating the oxygenation process. This kind of regulation is called homoalloesteric.

Another mechanism of enzymatic regulation is known as heteroallosteric that activate or inhibit enzyme function, by binding and shifting the conformational state of the structure from T to R (in the case of an activator) or R to T (in the case of an inhibitor). In the hemoglobin, these particles are the CO_2, biphosphoglycerate (BPG), and H+ ions that regulate the liberation of the oxygen in tissues that require the payload carried by the protein.

In our aim to develop a model capable of simulating cooperative binding, we opted to focus on studying the oxygenation process of hemoglobin since its dissociation curve (ODC) presents the sigmoid shape that is characteristic to this type of binding behavior, as well as being a system that has been well studied in the medical sciences.

In medical practice, the oxygen dissociation curve of the hemoglobin (ODC) is used to determine the oxygenation capacity of a living being. This is a curve on a plane where the O_2 saturation of an Hb is measured in respect to the partial pressure of oxygen, PO_2 [21], [22]. There exist a variety of algebraic expression that attempt to parametrize the ODC [23]–[26] and one of the simpler ones is the Hill equation [27], where two parameters are enough to determine its geometry.

Although there have been attempts in past research, spanning over a century, to understand the phenomenon of oxygenation of Hb, there still exist aspects of it that remain obscure. As can be seen in physical statistics textbooks, this law rests on the hypothesis of equilibrium [28], but as we will see here, this is not a sufficient description because it does not consider how it reaches equilibrium if the oxygenation process, which consists in the penetration of O_2 into the erythrocyte, is a non-equilibrium phenomenon.

The relaxation process towards equilibrium has been studied for decades. Using modified diffusion equations, W. Moll [29] studied in 1968 the rate of O_2 transportation from the instant it binds to the Hb to when it is released to the tissues. With a similar approach, Baxley *et al.* [30] in 1983 studied O_2 transport through capillary vessels. Clark *et al.* [31] also analyzed the release of O_2 considering that the diffusion coefficient is different inside the carrier cell from the diffusion near the cell-membrane. A general review, updated in 1989, was written by Popel [32], who discusses at length the kinetics of Hb and O_2 in the transport process of blood flowing through different geometries.

Fischer *et al.* [33] developed a dissolution model of a bubble of O_2 immersed in blood, trying to understand the dynamics of the diffusion process of this gas in blood.

The rise in computational techniques in the last four decades has allowed scientists to study the transport phenomenon using numerical methods. An example is the work by Hyakutake and Kishimoto [34], who studied oxygen carriers based in Hb, approaching diffusion equations with various parameters, among them the P_{50} value, diffusion constant D, length of a blood vessel and CO_2 concentration.

A great deal of interest has been given to understanding how O_2 molecules diffuse through liquid membranes to reach Hb molecules, or membranes similar to biological tissues. This is with the express goal of designing external and internal respirators or oxygen concentrators aimed to help patients with respiratory deficiencies [35]–[38].

In a line of research close to our work, recently Scrima *et al.* [39] studied the out of equilibrium oxygen-hemoglobin dissociation curve (ODC). It is an experimental approach where, among other results, they obtain the sigmoidal shape of the curve, as well as values of equilibrium constants for the four oxygenation states, and also identify a source of sequential cooperativity and of conformational cooperativity.

Moreover, Agliari *et al.* [40], [41] have developed a very interesting connection between three apparently dissimilar fields of knowledge: enzyme kinetics, ferromagnetism and neural networks. Particularly, they have used Hopfield neural networks at the thermodynamic limit, which theoretically consist in an infinite number of neurons, and have established various connections between these three phenomena. Their approach consists in using a McCulloch-Pitts neuron as a model for a binding site, so the output of this neuron is $+1$ if the binding site is occupied and -1 if it is vacant. If the network consists of N neurons, this can also be understood as an Ising spin model system of N spins [42].

This work is divided into two chapters:

The first chapter is an application that expands our previous work [43] in the extension of the Michaelis-Menten model. We use our extended version to study the hydrolization of rifampicin (a member of the penicillin family of antibiotics) by beta-lactamase enzymes. There are two new contributions:

1. After studying the formalism of stochastic velocities, this approach was used to analyze the quasi-stationary state of the reaction process, as well as its entropy.

2. One of the results previously found was the decrease in entropy in purely theoretical simulated reactions. We replicate this result using experimental data for the simulations, as well as propose an explanation of this phenomenon based on the formalism stated in the previous point. We suggest that a decrease in entropy is possible due to work being done on the system, also propose that the source of this energy comes from the normal vibration modes of the enzyme, which have well defined vibration frequencies. This is a relevant result, because the specificity of enzyme catalysis could be related to a process of resonance between the active site of the enzyme and the molecular structure of the substrate. The approach developed here is useful for any number of participating enzymes and substrate molecules, provided that the initial number of enzymes is smaller than the initial number of molecules; therefore, it is applicable to nano-scaled systems.

The second chapter is a new approach to the simulation of enzymatic reactions in reduced spaces that present cooperative behavior. This model is based in the use of finite Hopfield neural networks, taking as type case the oxygenation of a cluster of hemoglobin molecules. Our results are valid for

a finite number of participating oxygen molecules, therefore it is useful for micro and nano devices that could be placed inside living organisms that are suffering from diminished oxygenation capacity.

2 Chapter I: Entropy and stochastic properties in catalysis at nanoscale

2.1 Objective:

As a first part of this work, we calculate the entropy of fluctuations and present kinematics that describe the behavior of these fluctuations from the point of view of their state space, given the name of *fluctuation space*. We introduce various stochastic velocities and take advantage of two of these to describe the regions of higher and lower probability. It will be shown that, during the course of the chemical reaction, an entropy of fluctuation arises that presents two characteristics:

1. The initial increment is positive, which guarantees the spontaneous nature of the reaction.

2. There is a subsequent decrease in entropy, which in turn reveals two aspects:

   a. There exists a source of energy in the process.

   b. This decrease in the change of entropy translates into the heat capacity at constant pressure, C_p, is negative in the catalysis. This is a result that has been confirmed in previous literature.

The stochastic velocities surged as part of the efforts to understand quantum phenomena as a probabilistic problem [44]–[47]. However, the mathematical expansion is valid for any stochastic phenomenon that can be described by diffusion equations. These velocities have been previously used to study the active Brownian motion [48]; in this work they are applied to the field mentioned in this section.

For the sake of completeness and for a uniform notation throughout this work and the ones referenced, the initial sections are dedicated to a short examination of the master equation and the van Kampen method for the separation of the problem into a deterministic and stochastic parts. A Fokker-Planck equation (FPE) is obtained in the latter part, which is then used as grounds to discuss the formalism of stochastic velocities and the entropy of the system. The results are discussed based on the references cited in this work.

This chapter is organized as follows:

We begin by defining the physical system and present the results of a simulated reaction using the Gillespie algorithm. In the following section, based on the graphs obtained from it, we review the theory developed by Bartholomay, which is used to split the state space in two: one for the average concentrations and another for their fluctuations (the latter one receiving the name of *fluctuation space*). In this same section we clarify what is understood by a *state of equilibrium* in this work, and its difference with the *stationary state* under study.

In the next section we analyze the behavior of the state points in the fluctuation space obtained previously and do a short review of the stochastic velocities formalism, as well as obtain the expression for the entropy in this system. We pay special attention to the form of these velocities in time dependent Ornstein-Uhlenbeck processes. We examine what it means to reach a state of

equilibrium in the simulated reaction, and the conduct of the probability density of the state points in the fluctuation space during the quasi-stationary state.

We then retake the discussion of the entropy, performing an estimation of its value at different points in time of the reaction. We find that, during the evolution of the reaction, the Michaelis-Menten model is capable of describing an expected decrease of the entropy of the system.

We close this chapter by discussing the results obtained and our conclusions.

2.2 Physical system

The physical system under consideration are the chemical reactions described by the following reaction equation:

$$E + S \underset{k_r}{\overset{k_f}{\rightleftharpoons}} ES \xrightarrow{k_{cat}} E + P$$
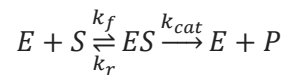
where E stands for enzyme molecules, S for substrate molecules, ES for enzyme-substrate complex and P for product. During the time interval $t < 0$, enzyme and substrate molecules exist without interaction within a fluid that serves as a medium that is in thermodynamic equilibrium. At time $t = 0$ the system suffers a change that gives way to the start of the reaction, an event that could be, for example, the stirring of the fluid with the enzymes and substrate molecules. During the interval $t > 0$ the system undergoes the process of a catalytic reaction until all substrate molecules have been depleted.

We started by simulating a reaction using the Gillespie algorithm [49]. One hundred realizations are carried out with the following initial conditions: $E = 100, S = 4900, ES = 0, P = 0$. The reaction rates were taken from the work by Weilandt *et al.* [50] and selecting the special case where the reaction is irreversible, thus $k_2^b = 0$. In this work the notation used for the reaction rates are presented in Table 1.

k_1'	1.52×10^5	$\left(\dfrac{1}{seg \cdot M}\right)$
k_2	10	$\left(\dfrac{1}{s}\right)$
k_3	22	$\left(\dfrac{1}{s}\right)$
r	6.5579×10^{-5}	dimensionless
k_M	2.105×10^{-4}	(M)

Table 1. Reaction rate used in the simulation.

The simulation results were data structures for (t, E, S, ES, P), where t is the time between reactions. An example of a time evolution of E and ES as it progresses towards a stationary state is given in Figure 1
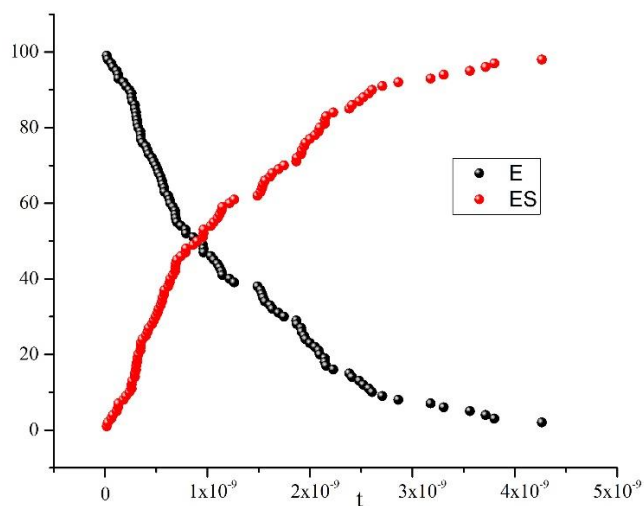
Figure 1. Time evolution of the number of enzyme molecules (black) and ES complex (red) reaching stationary states. One realization with the Gillespie algorithm. Initial conditions: E=100, S=4900, ES=0, P=0 (product and substrate not pictured).

We found that as the reaction progresses, the number of enzymes decreases to almost zero due to them having transitioned to the enzyme-substrate complex state. Once in this state, the quantity of ES is kept almost constant in time. The amount of S decreases as it is consumed to form P, and when the process is nearing depletion of S the same occurs to ES, returning the amount of free enzyme E to its initial value. The evolution of E and ES is shown in Figure 2.
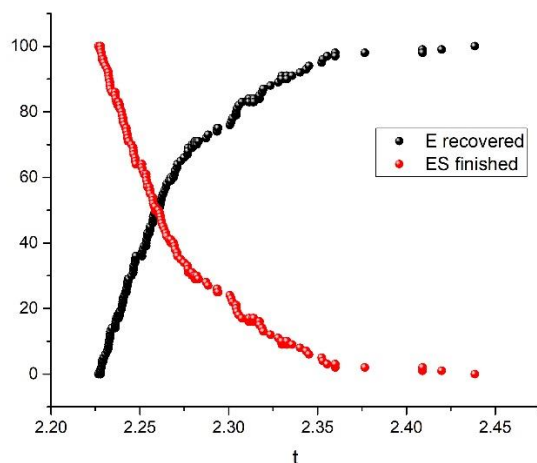
Figure 2. Time evolution of the number of enzyme molecules (black) and ES complexes (red). The number of ES go to zero. One realization with the Gillespie algorithm. Initial conditions: E=100, S=4900, ES=0, P=0 (product and substrate not pictured).

Between the initial and final stages exists a stage called the quasi-stationary state of the chemical reaction. This is presented in Figure 3 and is the regime that will be addressed in greater detail in this chapter.
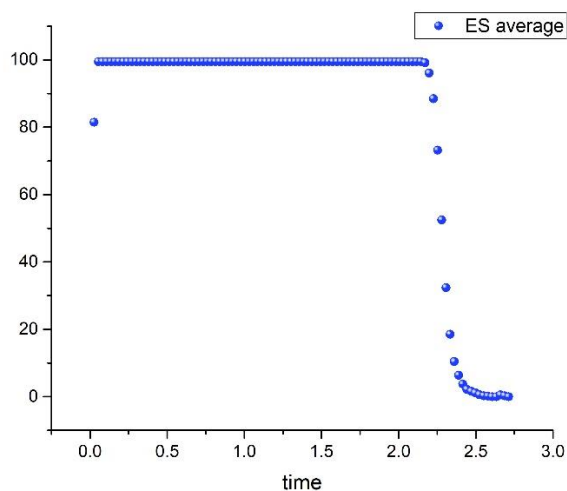
Figure 3. The number of ES complexes is almost constant. This is the state considered as stationary in this work. Average over 100 realizations with the Gillespie algorithm. Initial conditions: E=100, S=4900, ES=0, P=0.

Figures 1 and 2 show the stochastic nature of this process, and these random fluctuations are the focal point of our work. An adequate treatment for this kind of problems was developed in the past; this is presented in the section below.

One of the results obtained predicts that the profile of the mean of the ES complex is a decreasing curve. This occurs when the product is reaching its constant value and the amount of substrate is nearly depleted. We will also demonstrate that this is what is called the state of equilibrium.

2.3 Master equation and the van Kampen omega expansion

The usual mathematical treatment sets off from the consideration of a process where a number of N_{10} enzyme molecules and N_{20} substrate molecules react, first to form an enzyme-substrate complex in a reversible reaction, followed by an irreversible reaction that can form a product plus a free enzyme. We model this system through 4 amounts that at a given time t have: N_1 enzyme particles, N_2 substrate particles, N_3 enzyme-substrate complexes, and N_4 product particles.

Two laws of conservation are followed:

1. The number of enzyme molecules at any given time are conserved and can be described by:

$$N_{10} = N_1 + N_3 \tag{1}$$

2. The number of substrate molecules at any given time are conserved and can be described by:

$$N_{20} = N_2 + N_3 + N_4 \tag{2}$$

From above follows that there are only two independent variables, therefore $\{N_2, N_3\}$ are taken as the state variables that evolve with time, and to introduce $P(N_2, N_3, t)$ as the probability that there are N_2 substrate particles and N_3 enzyme-substrate complexes at time t. From now on these will be called $\{N, M\}$, to ease reading and to connect with the notation used in reference [51]. The time evolution equation of $P(N, M, t)$ is obtained on the basis of three transitions that can occur in the state space representable in a two-dimensional plane, as shown in Figure 4.
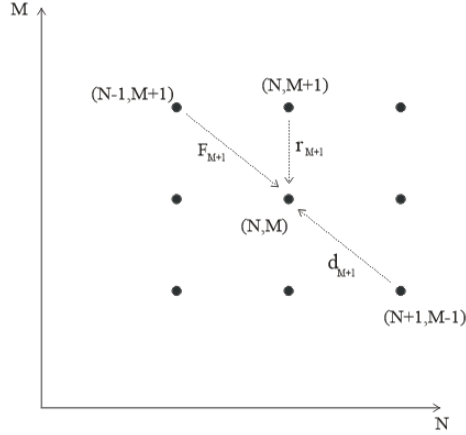
Figure 4. State space. The number of complexes M versus the number of substrates N. The arrows show the transitions needed to build the master equation.

The probability $P(N, M, t + \Delta t)$ can be calculated considering the conservation of probability. Each term consists of two factors, such that each factor is the probability of an independent event. For instance, in the event where the state transitions from $(N - 1, M + 1)$ to (N, M) in the interval $(t, t + \Delta t)$, considers the product of the probability of the state to be at $(N - 1, M + 1)$ at time t, and the probability of the transition to be towards (N, M). A similar argument is applicable for each of the three transitions drawn in Figure 4. There also exist the passive transition, that consists of the system already being at state (N, M) at time t, and stays in that state during the time interval $(t, t + \Delta t)$. The general formulation of this can be consulted in [51]. The resulting master equation is:

$$\frac{\partial P(N, M, t)}{\partial t} = \hat{L} P(N, M, t) \tag{3}$$

where

$$\hat{L} = (\mathcal{E}_N \mathcal{E}_M^{-1} - 1) d_M + (\mathcal{E}_M - 1) r_M + (\mathcal{E}_N^{-1} \mathcal{E}_M - 1) F_M \tag{4}$$

with step operators:

$$\mathcal{E}_N^{\pm 1} f(N, M, t) = f(N \pm 1, M, t)$$
$$\mathcal{E}_M^{\pm 1} f(N, M, t) = f(N, M \pm 1, t)$$

The van Kampen omega expansion allows one to separate the state space represented in Figure 4 in two distinct spaces, one for the deterministic side of the problem, and another for the random fluctuations. For this purpose, the next intensive variables are defined:

$$n = \frac{N}{\Omega} = \psi + \frac{1}{\sqrt{\Omega}} q_1 \ , \qquad m = \frac{M}{\Omega} = \phi + \frac{1}{\sqrt{\Omega}} q_2 \tag{5}$$

with $\Omega = N_{10} + N_{20}$. It is important to note that, while it is common practice to define concentration as the quotient between the number of molecules within a volume, in this work it is defined in respect to the total number of reactants in the system. The relation between both ratios is a constant.

The pair (ψ, ϕ) represent the deterministic conduct (also called the macroscopic description) of the particle densities (concentrations), and the pair (q_1, q_2) are their respective random fluctuations.

The step operator acts as shown in equation (6) below:

$$\mathcal{E}_N^{\pm 1} N = \mathcal{E}_N^{\pm 1} \left(\Omega\psi + \sqrt{\Omega} q_1 \right) = \Omega\psi + \sqrt{\Omega} \left(q_1 \pm \frac{1}{\sqrt{\Omega}} \right) \tag{6}$$

Such that the action of this step operator causes the change $q_1 \to q_1 \pm \frac{1}{\sqrt{\Omega}}$. There is an analogous expression for $\mathcal{E}_M^{\pm 1}$. Working with an arbitrary function, of which the second derivatives exists, from their Taylor expansion follows that an approximation for the operators can be expressed as:

$$\mathcal{E}_N^{\pm 1} \cong 1 + \frac{1}{\sqrt{\Omega}} \frac{\partial}{\partial q_1} + \frac{1}{2\Omega} \frac{\partial^2}{\partial q_1^2}$$

$$\mathcal{E}_M^{\pm 1} \cong 1 + \frac{1}{\sqrt{\Omega}} \frac{\partial}{\partial q_2} + \frac{1}{2\Omega} \frac{\partial^2}{\partial q_2^2} \tag{7}$$

These will be used in expression (4), along with transition rates $\{d_M, r_M, F_M\}$.

If one is looking for a probabilistic treatment where a well-defined probability density is obtained, in the sense that it is non-negative for every value of time t in all the fluctuation space (q_1, q_2), the only option is to cut (7) at its second order. Higher order expansions allow working with statistical moments or cumulants, but the pseudoprobability being used is not well defined; non-negativity is only recovered if all the terms in the series are used, in other words, if $\mathcal{E}_N$ is of the form shown in the expression below:

$$\mathcal{E}_N = exp \left\{ \sum_{j=0}^{\infty} \frac{1}{j! \, (\Omega)^{j/2}} \frac{\partial^j}{\partial q_1^j} \right\}$$

The other three operators involved would also have to have analogous expressions. In other words, according to the Pawula theorem, the expansion should stop after the first term or after the second term. On the contrary, it must contain an infinite number of terms for the solution to the equation to be interpretable as a probability density function [52].

The transition rates are usually introduced by means of the law of mass action, resulting in

$$d_M = k_1 N_1 N_2 \ , \quad r_M = k_3 N_3 \ , \quad F_M = k_2 N_3 \tag{8}$$

with $\{k_1, k_2, k_3\}$ as the reaction rates given by the Arrhenius law. The description in the state space $\{N, M\}$ is recovered by considering $N_1 = N_{10} - M$ in d_M.

Substituting (5) in (8) and rescaling $\Omega k_1 = k_1'$ results in

$$d_M = \Omega k_1'(n_{10} - \phi)\psi + \sqrt{\Omega}[(n_{10} - \phi)q_1 + \psi q_2] \tag{9}$$

$$F_M = k_2\left(\Omega\phi + \sqrt{\Omega}q_2\right) \tag{10}$$

$$r_M = k_3\left(\Omega\phi + \sqrt{\Omega}\right) \tag{11}$$

Also, now the probability $P(N, M, t)$ has the following functional dependence for every pair of (N, M)

$$P(N, M, t) = P\left(\Omega\psi + \sqrt{\Omega}q_1, \Omega\phi + \sqrt{\Omega}q_1, t\right) = \Pi(q_1, q_2, t) \tag{12}$$

Substituting (7) and (9) to (11) in (4), the right-hand side of the master equation (3) takes the following form:

$$\hat{\mathcal{L}} = \sqrt{\Omega}G_1 + \Omega^0 G_2 \tag{13}$$

The left-hand side is also rewritten as:

$$\frac{\partial P(N, M, t)}{\partial t} = \frac{\partial \Pi(q_1, q_2, t)}{\partial t} - \Omega^{1/2}\frac{d\psi}{dt}\frac{\partial \Pi(q_1, q_2, t)}{\partial q_1} - \Omega^{1/2}\frac{d\phi}{dt}\frac{\partial \Pi(q_1, q_2, t)}{\partial q_2} \tag{14}$$

Substituting (13) and (14) in the master equation, and comparing terms with like coefficients it is possible to obtain:

For $\Omega^{1/2}$

$$-\frac{d\psi}{dt}\frac{\partial \Pi(q_1, q_2, t)}{\partial q_1} - \frac{d\phi}{dt}\frac{\partial \Pi(q_1, q_2, t)}{\partial q_2} = G_1 \tag{15}$$

For Ω^0

$$\frac{\partial \Pi(q_1, q_2, t)}{\partial t} = G_2 \tag{16}$$

The equations for the deterministic part of the problem, also called the macroscopic part, can be obtained through G_1, and the partial differential equation that allows the study of the random fluctuations can be obtained through G_2. The procedures for these are widely covered in the literature [47]. From here onwards we will be using them in the context of the notation initially proposed in this work as was done in [51].

2.3.1   Deterministic equations

The equations for the mean substrate concentration, ψ, and the mean concentration of enzyme-substrate complex, ϕ, that describe the macroscopic part are:

$$\frac{d\psi}{dt} = -k_1'(n_{10} - \phi)\psi + k_2\phi$$
$$\frac{d\phi}{dt} = k_1'(n_{10} - \phi)\psi - (k_2 + k_3)\phi$$

(17)

This approach is versatile enough to be of use at any enzyme-substrate ratio, since these differential equations can be solved numerically for different initial conditions; but it will be used with the usual proportions of reactants found in in-vitro experiments, where the initial substrate concentration is much greater than the initial enzyme concentration. The logic behind this is that smaller quantities of enzyme can catalyze much larger quantities of substrate, thus it is a topic of efficiency; however, this is not the only situation that can be studied in the laboratories. Albe *et al.* [53] report the progress of a chemical reaction with different enzyme-substrate ratios, including cases where these ratios are inverted, so that the amount of enzyme exceeds that of the substrate.

Equations (17) can take a very practical form when multiplied by $\frac{1}{k_1'}$, and one can define the evolution parameter $s = k_1't$, with units of $\frac{1}{M}$. The resulting expressions are:

$$\frac{d\psi}{ds} = -(n_{10} - \phi)\psi$$
$$+ r\phi$$
$$\frac{d\phi}{dt}$$
$$= (n_{10} - \phi)\psi - k_M\phi$$

(18)

Where $r = k_2/k_1'$ is an efficiency parameter that measures the rate of dissociation of the ES complex that is not transformed into product.

2.3.2 Quasi-stationary state

The quasi-stationary state that is of interest in the in-vitro experiments is obtained through the condition that the density of enzyme-substrate complex changes very little across time, which is mathematically expressed as $\frac{d\phi_s}{dt} \cong 0$. This is the topic of discussion in this subsection.

In terms of the densities, the conservation laws take the form of

$$n_{10} = e(t) + \phi(t), \quad n_{20} = \psi(t) + \phi(t) + P(t)$$

(19)

Where $e(t)$ and $P(t)$ are the densities of the enzyme and the product, respectively. It is possible to demonstrate that the time evolution equations can be obtained through the following expressions:

$$\frac{de}{dt} = -\frac{d\phi}{dt} , \quad \frac{dP}{dt} = -k_3\phi(t)$$

(20)

Introducing the quasi-stationary condition in the time evolution equation of $\phi(t)$ in (17) results in

$$k_1'(n_{10} - \phi_s)\psi_s - (k_2 + k_3)\phi_s \cong 0$$

The conservation laws yield the relation $(n_{10} - \phi_s) = e_s$, such that

$$\phi_s \cong \frac{k_1' e_s \psi_s}{k_2 + k_3} = \frac{e_s \psi_s}{k_M} \tag{21}$$

where $k_M = \frac{k_2 + k_3}{k_1'}$ and receives the well-known name of the Michaelis-Menten constant.

Denoting as V the rate of growth of the product density $P(t)$, one obtains:

$$V = \frac{dP(t)}{dt}$$

The in-vitro experiments are performed with amounts on the order micromoles. In such cases the behavior observed is of a slow decrease of the functions $\psi(t)$ and $\phi(t)$. It is then where the condition of $\frac{d\phi_s}{dt}$ is applicable.

From the deterministic equation for $\frac{d\phi}{dt}$ in (18) results

$$(n_{10} - \phi)\psi - k_M \phi \cong 0 \tag{22}$$

One can obtain the following expression for the mean concentration of enzyme-substrate complex:

$$\phi_s \cong \frac{n_{10}\psi_s}{k_M + \psi_s}$$

Using de definition $V = \frac{dP(t)}{dt}$ and the time evolution of $P(t)$ in (20), the demonstration of the following expression is straightforward.

$$V \cong \frac{V_{max}\psi_s}{k_M + \psi_s}$$

Where $V_{max} = k_3 n_{10}$. The usual notation is recovered by simply rewriting ψ_s as $[S]$.

2.3.3   Equilibrium state

It is common practice to indistinctively use the terms "stationary" and "equilibrium" as synonyms, but it is imperative to establish a clear distinction between them. This section is dedicated to this purpose, showing the difference between a stationary state achieved in in-vitro experiments and the equilibrium state. This latter one corresponds to the mathematical condition:

$$\frac{d\psi}{dt} = 0, \qquad \frac{d\phi}{dt} = 0 \tag{23}$$

such that the following equations are followed:

$$-k_1'(n_{10} - \phi_e)\psi_e + k_2 \phi_e = 0 \tag{24}$$
$$k_1'(n_{10} - \phi_e)\psi_e - (k_2 + k_3)\phi_e = 0$$

The algebraic solution is $\psi_e = 0, \phi_e = 0$, it corresponds to the complete consumption of the substrate and enzyme-substrate complex. It is for this reason that the state of equilibrium is only

15

attainable when all the substrate has been consumed, such that only the initial amounts of free enzymes and the product remain in the system.

It is possible to study the stability of the equilibrium state. Linearizing the differential equations around $(\psi_e, \phi_e) = (0,0)$ results in:

$$\frac{d}{dt}\begin{pmatrix}\psi(t)\\\phi(t)\end{pmatrix} = \begin{pmatrix}-k_1'n_{10} & k_2\\ k_1'n_{10} & -(k_2+k_3)\end{pmatrix}\begin{pmatrix}\psi\\\phi\end{pmatrix}$$

To ease reading, we introduce a shorter notation:

$$A = k_1'n_{10}, \quad C = k_2, D = k_3, \quad R = \sqrt{-4AD + (A + C + D)^2}$$

Thus, the eigenvalues of the matrix above are given as:

$$\lambda_{1,2} = -\frac{1}{2}(A + C + D \pm R)$$

The transition rates and initial conditions are defined positive, this results in the eigenvalues satisfying the inequality: $\lambda_{1,2} < 0$. The fundamental solutions $\{e^{\lambda_1 t}, e^{\lambda_2 t}\}$ generate the most general solution:

$$\begin{pmatrix}\psi(t)\\\phi(t)\end{pmatrix} = \begin{pmatrix}Ae^{\lambda_1 t} + Be^{\lambda_2 t}\\ Ee^{\lambda_1 t} + Fe^{\lambda_2 t}\end{pmatrix}$$

Which will always converge towards the equilibrium state. This mathematic expression explains the profile of the curve for the ES complex seen in Figure 1 and the decreasing stage shown in Figure 14.

2.4 Analysis of the random fluctuations

2.4.1 General solution

The following equation is called the Fokker-Planck equation (FPE):

$$\frac{\partial P(\vec{q}, t)}{\partial t} = \frac{\partial [A_\mu(\vec{q}, \psi, \phi)P(\vec{q}, t)]}{\partial q_\mu} + \frac{1}{2}\sum_{\mu=1}^{2}\sum_{\nu=1}^{2}D_{\mu\nu}(\psi, \phi)\frac{\partial^2 P(\vec{q}, t)}{\partial q_\mu q_\nu} \tag{25}$$

The expression above describes the probability that the fluctuation of substrate concentration takes the value q_1, and the fluctuation of enzyme-substrate complex concentration takes the value q_2, at time t. The systematic term can be written as:

$$A_\mu(\vec{q}, \psi, \phi) = \sum_{\nu=1}^{2}L_{\mu\nu}(\psi, \phi)\, q_\nu \tag{26}$$

Where A_μ is the flux of random concentration fluctuations of S and ES.

And its general solution [54] is a gaussian function of the form:

$$P(\vec{q},t) = \frac{1}{2\pi\sqrt{Det(\Xi(t))}} e^{-\frac{1}{2}(q_\mu - \langle q_\mu(t)\rangle)\Xi^{-1}(t)(q_\nu - \langle q_\nu(t)\rangle)} \tag{27}$$

with $\Xi(t) = \langle q_\mu q_\nu\rangle - \langle q_\mu\rangle\langle q_\nu\rangle$ as the self-correlation matrix, and $\Xi^{-1}(t)$ as its inverse. This is the matrix that contains the variance of the random fluctuations of E and ES concentrations, as well as their correlations.

In the case under study, the elements of $\{L_{\mu\nu}\}$ and $\{D_{\mu\nu}\}$ are given by:

$$L_{11} = -k_1'(n_{10} - \phi), \quad L_{12} = k_1'\psi + k_2$$
$$L_{21} = k_1'(n_{10} - \phi), \quad L_{22} = -k_1'\psi - k_2 - k_3 \tag{28}$$

$$D_{11} = k_1'(n_{10} - \phi)\psi + (1 + k_2)\phi$$
$$D_{22} = k_1'(n_{10} - \phi)\psi + (k_2 + k_3)\phi \tag{29}$$
$$D_{12} = -k_1'(n_{10} - \phi)\psi - k_2\phi$$

Given a physical magnitude $g(\vec{q},t)$ that is relevant to the system, its mean can be calculated by:

$$\langle g(\vec{q},t)\rangle(t) = \int_{-\infty}^{\infty}\int_{-\infty}^{\infty} g(\vec{q},t)P(\vec{q},t)dq_1 dq_2 \tag{30}$$

The time evolution equations of the mean of the fluctuations of the concentrations of E and ES take the form of:

$$\frac{d}{dt}\begin{pmatrix}\langle q_1\rangle(t)\\\langle q_2\rangle(t)\end{pmatrix} = \begin{pmatrix}L_{11} & L_{12}\\L_{21} & L_{22}\end{pmatrix}\begin{pmatrix}\langle q_1\rangle(t)\\\langle q_2\rangle(t)\end{pmatrix} \tag{31}$$

and the time evolution equations for the self-correlation functions are:

$$\frac{d}{dt}\begin{pmatrix}\Xi_{11}(t)\\\Xi_{12}(t)\\\Xi_{22}(t)\end{pmatrix} = \begin{pmatrix}2L_{11} & 2L_{12} & 0\\L_{21} & L_{11}+L_{22} & L_{12}\\0 & 2L_{21} & 2L_{22}\end{pmatrix}\begin{pmatrix}\Xi_{11}(t)\\\Xi_{12}(t)\\\Xi_{22}(t)\end{pmatrix} + \begin{pmatrix}D_{11}(t)\\D_{12}(t)\\D_{22}(t)\end{pmatrix} \tag{32}$$

Defining $\vec{\Xi}(t) = [\Xi_{11}(t), \Xi_{12}(t), \Xi_{22}(t)]$ and $\vec{D}(t) = [D_{11}(t), D_{12}(t), D_{22}(t)]$, the equation above can be rewritten as follows:

$$\frac{d\vec{\Xi}(t)}{dt} = M(t)\vec{\Xi}(t) + \vec{D}(t) \tag{33}$$

where

$$M(t) = \begin{pmatrix}2L_{11}(t) & 2L_{12}(t) & 0\\L_{12}(t) & L_{11}(t)+L_{22}(t) & L_{12}(t)\\0 & 2L_{21}(t) & 2L_{22}(t)\end{pmatrix} \tag{34}$$

Defining the entropy of fluctuation of the concentrations of E and ES as

$$S(t) = -\langle \ln P(\vec{q}, t) \rangle = - \int_{-\infty}^{\infty} \int_{-\infty}^{\infty} P(\vec{q}, t) \, \ln[P(\vec{q}, t)] \, dq_1 dq_2 \tag{35}$$

Substituting the general solution in the expression for the entropy (35), results in expression (36) seen below:

$$S(t) = \frac{1}{2} \ln\big[Det\big(\varXi(t)\big)\big] + \ln(2\pi e) \tag{36}$$

Given two temporal points such that $t_1 < t_2$, the change in entropy is:

$$\varDelta S = S(t_2) - S(t_1) = \frac{1}{2} \ln \left[\frac{Det\big(\varXi(t_2)\big)}{Det\big(\varXi(t_1)\big)} \right] \tag{37}$$

so, the condition of $\varDelta S \geq 0$ translates into the following condition:

$$\frac{Det\big(\varXi(t_2)\big)}{Det\big(\varXi(t_1)\big)} > 1 \tag{38}$$

Expression (38) will later be utilized to confirm that the entropy of fluctuation decreases when the reaction is taking place. Expression (27) provides the mathematical form of the time dependent probability density for the fluctuation variables which, as will be shown in the numerical example in a later section, performs a clockwise turning motion as the reaction progresses. This result showcases the importance of fluctuations in the dynamics of catalysis; therefore, in-depth study of this topic is relevant.

If the phenomenon is analyzed using the dynamics of stochastic velocities, the behavior observed can be better understood. Thus, the section below is dedicated to the introduction of this formalism that may prove useful to the uninitiated reader.

2.4.2   Stochastic velocities

The time evolution of the fluctuations can be described by the motion of a state point $\vec{q}$. It is common to assume that its study is completed once its behavior has been formulated, as we did in the previous section. We will see that it is possible to extract new knowledge to better understand the behavior of the state point $\vec{q}$.

In this section we present an intuitive approach to stochastic velocities. We begin with an analysis of the difficulty found when attempting to define velocities in stochastic processes. The typical example given of a stochastic process is the Brownian motion; this describes the conduct of a micrometric mass floating inside a liquid at temperature T. Seen through a modern video camera, its movement takes place in two dimensions, but for ease of writing mathematical expressions, we consider only one dimension. The model treats the Brownian particle as if it is a point mass, and due to the movement possessing random behavior, each point z has a time dependent probability associated to it. This probability is a probability density function, denoted as $\rho(z, t)$, such that a

given interval, $(z, z + dz)$, on the line of accessible positions, the expression $\rho(z, t)dz$ yields the probability of the particle being found within that interval at time t.

It can be demonstrated that $\rho(z, t)$ follows an equation of the form shown below:

$$\frac{\partial \rho(z, t)}{\partial t} = D \frac{\partial^2 \rho(z, t)}{\partial z^2} \tag{39}$$

where D is named the diffusion coefficient. With the initial condition $\rho(z, t = 0) = \delta(z - z_0)$ the solution obtained for (39) is

$$\rho(z, t) = \frac{1}{\sqrt{4\pi Dt}} e^{-\frac{(z - z_0)^2}{4\pi Dt}} \tag{40}$$

In this case, the probability densities evolve with time. From (40), the statistical properties $\langle z \rangle = 0$ and $\langle z^2 \rangle = 2Dt$ can be demonstrated. It is important to note that the mean movement is zero and that the standard deviation changes with time as $t^{1/2}$. In the approach presented by Paul Langevin in 1908, the Second Law of Newton is applied to a Brownian particle of mass m with a force $F(x)$ acting upon it plus a friction force proportional to the velocity, $-\beta v$, plus a stochastic force, $\eta(t)$, with the following properties:

$$\langle \eta(t) \rangle = 0, \langle \eta(t)\eta(s) \rangle = C\delta(t - s) \tag{41}$$

where C is a constant. There are technical reasons for calling white noise a random magnitude that displays these properties. The fundamental dynamic law resulting from this is called the Langevin equation, and is written as shown below:

$$m \frac{dv}{dt} = F(x) - \beta v + \eta(t) \tag{42}$$

Using the method of moments, one obtains similar results for the Brownian motion. If the trajectories as functions of time t are to be plotted, the resulting graphs would present functions with very sharp peaks and valleys, therefore one can perceive intuitively that there would be problems when attempting to define the displacement velocity as $v = \frac{dx}{dt}$. Next, we will focus on this dilemma with close attention.

In mathematical terms, the Weiner process has been defined to formalize the events that follow the Brownian motion. Taking as a starting point the case where $D = 1$ and denoting the process as $W(t)$, the postulated properties are:

1. $W(t = 0) = 0$.

2. $W(t)$ is continuous.

3. $W(t)$ has independent increments, that is to say, if it follows that $0 \leq s_1 \leq t_1 \leq s_2 \leq t_2$, then the differences $W(t_1) - W(s_1)$ and $W(t_2) - W(s_2)$ are independent random variables.

4. $W(t-s)$ is a random variable with normal distribution of mean $\mu = 0$ and variance $\sigma^2 = t - s$.

In rigorous terms, equation (42) presents a difficulty that is analyzed next. Using the traditional concepts of defining the rate of change in a trajectory $z(t)$, we take the quotient of finite increments:

$$\frac{\Delta z}{\Delta t} = \frac{z(t+h) - z(t)}{h} \tag{43}$$

but from the fourth postulate one must have $z(t+h) - z(t) = \sqrt{h}$, where it follows that $\frac{\Delta z}{\Delta t} = \frac{\sqrt{h}}{h}$. Therefore, the quotient diverges in the limit $h \to 0$; consequently, it is impossible to define the rate of change through traditional methods.

For the issue encountered above, instead of using the Langevin equation, as it was originally formulated, it is better to consider an approach using finite differences to suggest an equation that avoids the use of derivatives and translates all calculations to integrals, giving place to two types of integral calculus: that of Kiyoshi Ito and of Ruslan Stratonovich [55]. A less known option is the one developed by Edward Nelson, based in a system of averages over the realizations of the stochastic processes, and gives place to the concept of stochastic velocities [45], [56]. These have been used to describe quantum phenomena from a stochastic perspective, giving rise to a line of work called stochastic mechanics. In this work we take advantage of the mathematical tools developed and use them in our topic of interest. The condition is that the stochastic process must be describable by means of Fokker-Planck equations (FPE) [48].

When an ensemble is associated to a stochastic process $\vec{x} = (x_1, \ldots, x_n)$, a state space of dimension n is available in which a point at a time t corresponds to each member of the ensemble. A large number of members of the ensemble produce a cloud of points that move at random as time progresses; this idea allows the introduction of an analogy with a gas, such that it is possible to include in the description some properties typical of fluids. One of these is that of vorticity, which lets us know if the cloud of state points tends to rotate, or if it behaves like a fluid whose velocity is irrotational. This gives us the opportunity of using this concept to analyze the manner with which the agitation of this cloud of state points occurs, and with it establish a difference between a stationary process and that of a process at equilibrium. The former abides to the condition that the statistical moment of order m must be time invariant:

$$\langle x_1(t)x_2(t) \ldots x_m(t) \rangle = \langle x_1(t+\tau)x_2(t+\tau) \ldots x_3(t+\tau) \rangle \tag{44}$$

while the latter also follows the condition that each of the possible transitions must be balanced out by a transition that occurs on the opposite side. This condition is given the name of detailed balance. If the detailed balance is not present, then the cloud of state points tends to rotate, therefore, the use of the concept of vorticity contributes to the understanding of the dynamics of the gas cloud. Vorticity is defined as the curl of the velocity thus it is necessary to revise this point.

The mean over the realizations, as originally developed by Nelson, can be understood with the concept of moving averages used in the study of time series. In this section we introduce these concepts.

Let $\vec{x}(t)$ be a stochastic process that occurs inside a state space $\mathcal{U}$, and let the points $\{\vec{x}', \vec{x}, \vec{x}''\} \in \mathcal{U}$, such that they are reached by some realizations of the stochastic process $\vec{x}$ at times t', t, t'', respectively, where $t' < t < t''$. Let the increments be $\Delta_+\vec{x} = \vec{x}'' - \vec{x}, \Delta_-\vec{x} = \vec{x} - \vec{x}'$, see Figure 5.
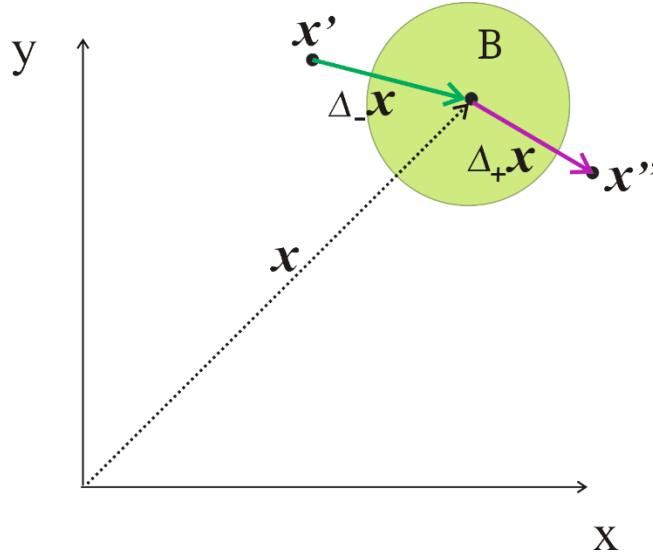
Figure 5. The state space $\mathcal{U}$. The neighborhood of the point $\vec{x}(t)$, $\mathcal{B}$, is the region of interest where we determine the state points going inside or outside. One can arrive to the definition of the access and exit velocities if the times are considered. The stochastic process $\vec{x}(t)$ can jump to points: $\{\vec{x}' \; or \; \vec{x}''\}$. The velocities are defined depending on the jump. Each point is reached at times $t' < t < t''$. The increments considered in the definitions are: $\Delta_+\vec{x} = \vec{x}'' - \vec{x}, and \; \Delta_-\vec{x} = \vec{x} - \vec{x}'$.

Next, we will explain the relations that must be followed between the time intervals involved in the description; for that purpose, we continue using the Brownian movement as a case study. Suppose there is a camera capable of registering the random movements of a state point; due to the difference in mass, the collision of a single molecule against the Brownian particle does not produce an effect that is registerable by the lab instrument. What moves the Brownian particle is the difference in the number of collisions that it receives because of the random fluctuations of the density of particles comprising the surrounding medium. By this manner, the path traced by the Brownian particle, as observed by a camera recording through an optical microscope, are polygonal shaped. However, because of the easiness in the mathematical language, we say that a collision occurs each time there is a change in the path taken by the particle of interest.

There are three instants of time that are relevant in this approach:

1. t_c, the time required to accumulate enough collisions capable of causing a registerable random change in the path of the particle.

2. T_0, the time that passes between two successive frames captured by the camera. If T_0 is too short, the displacements registered may follow the relation $\Delta x \sim t$, as is the case in classical mechanics; but it is more common to find $\langle \Delta x \rangle \sim t^{1/2}$ in the Brownian case. For the latter conduct it is necessary that $T_0 \gg t_c$.

3. Δt, the time necessary to smoothen trajectories by the moving averages method. To study the movement of the state points, the stochastic trajectories are smoothed by introducing moving averages; these are calculated in time intervals Δt that must be long enough to include various spikes of the trajectory, as can be seen in Figure 7, but also short enough that the camera registering the data cannot tell that the trajectory has been smoothed.

Therefore, $\Delta t \gg T_0 \gg t_c$ must be followed. This regime is called the coarse grain time scale, as shown in Figure 6 below.
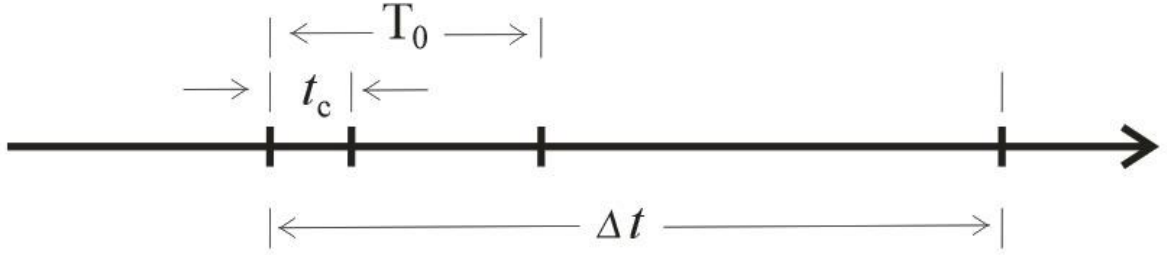
Figure 6. t_c is the time required to accumulate enough collisions to achieve a random motion. T_0 is the time between two successive images, or measurements, taken by a camera, or measuring device. ΔT is the time required to calculate a moving average.

The moving average of p points is defined as $x_k = \frac{1}{p}\sum_{i=k-\frac{p}{2}}^{k+\frac{p}{2}} x_i$, where i takes values such that the sum is not out of the bounds of the interval. For continuous signals, the moving average is defined as: $\langle x \rangle_{\Delta t}(t) \equiv \frac{1}{\Delta t}\int_{t'}^{t'+\Delta t} x(s)\, ds$. We now set out to study the derivative of a function $g(\vec{x}, t)$. For this purpose, we establish a set of times expressed in (45) below:

$$t_1 < t_2 < \cdots < t_M \tag{45}$$

and considering finite increments of the function $g(\vec{x}, t)$: $\Delta g_k = g(\vec{x}, t_k + 1) - g(\vec{x}, t_k)$, with $k = 1, \ldots, M - 1$, one can write:

$$g(\vec{x}, t_M) = g(\vec{x}, t_1) + \Delta g_1 + \Delta g_2 + \cdots + \Delta g_{M-1} \tag{46}$$

Rearranging and multiplying by $\frac{1}{2\Delta t}$ gives:

$$\frac{g(\vec{x}, t_M) - g(\vec{x}, t_1)}{2\Delta t} = \frac{1}{2\Delta t} \int_{t'}^{t'+2\Delta t} \frac{\partial g(\vec{x}, s)}{\partial s} ds \qquad (47)$$

This expression receives the name of coarse grain time derivative. Notice the incorporation of the sum of finite differences inside a moving average within an interval of width $2\Delta t$. Once the smoothening process has been applied, the resulting trajectories can be studied using the usual tools of calculus. An illustrative example is given in Figure 7.
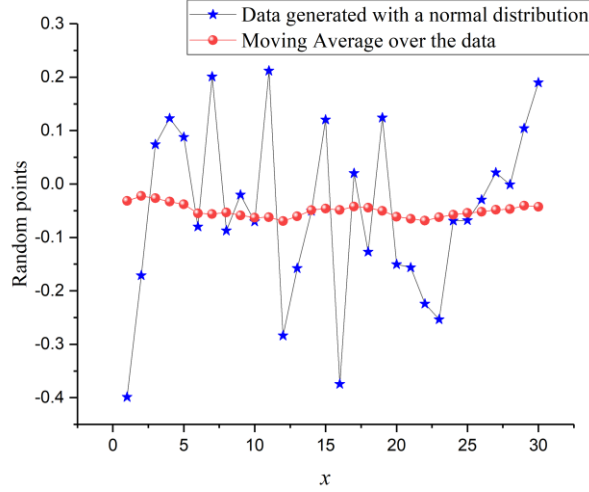
Figure 7. The result of the smoothening process is a curve without the spikes that are characteristic of the Brownian motion.

2.4.2.2 *The study of smoothened stochastic functions*

2.4.2.2.1 Points in the state space and a statistical description of their movement

Suppose a statistical ensemble of equally prepared experiments at a macro scale. Each of these carry out a realization of the stochastic process $\vec{x}$. At a given point in time, we have a cloud of points whose number is theoretically infinite. If one is to let the clock run out, a static image (like that of a photograph) would be substituted for a series of images of points moving at random, similar to a swarm of mosquitos swirling in summer. These will enter and exit of the previously marked region $\mathcal{B}$, as seen in Figure 5. The question that follows is: How many points enter or exit $\mathcal{B}$ in a second? This problem is similar as counting the number of smoke particles in a given region of space.

The concept of systematic velocity, which has already been presented, measure the net number of state points that cross $\mathcal{B}$ per second.

2.4.2.2.2 Systematic derivative and systematic velocity

We define the systematic derivative as the mean over the ensemble of all the realizations:

$$D_c g(\vec{x}, t) \equiv \frac{\langle g(\vec{x}, t'') - g(\vec{x}, t') \rangle}{2\Delta t} \qquad (48)$$

23

To have an analytical representation of the previous definition, we introduce various hypotheses that lead to the Taylor series expansion. These hypotheses are:

- The stochasticity of the physical phenomenon is introduced by a source that is: stationary, isotropic and homogenous.

- The second statistical moments of the increments $\Delta_+\vec{x}$ and $\Delta_-\vec{x}$ are such that they follow:

$$
\begin{aligned}
&\langle \Delta_+ x_i \Delta_+ x_j \rangle \\
&= \langle \Delta_- x_i \Delta_- x_j \rangle \\
&\langle \Delta_+ x_i \Delta_- x_j \rangle = 0
\end{aligned}
\tag{49}
$$

The diffusion matrix can be defined as

$$
D_{ij} \equiv \frac{1}{2\Delta t} \langle \Delta_+ x \Delta_+ x_j \rangle
\tag{50}
$$

or also as

$$
D_{ij} \equiv \frac{1}{2\Delta t} \langle \Delta_- x_i \Delta_- x_j \rangle
\tag{51}
$$

Notice that the increments grow as $(\Delta t)^{1/2}$ so that the average that appears in the definition above grows as (Δt). It also must be noted that the products of increments appear as coefficients in the second order derivatives of any function $d(x,t)$ expanded using Taylor series.

To work at higher orders of (Δt) would involve considering Taylor expansions with derivatives of orders of 3,4, …; although it is mathematically possible, there exist a restriction when the problem is translated to determining the probability $P(\vec{x},t)$ by means of a partial differential equation. The function $P(\vec{x},t)$ that satisfies an equation of order higher than 2 ceases to be defined as nonnegative for all $\vec{x}$ and t, therefore it cannot be interpreted as a probability density function.

In vector calculus, a function $f(\vec{x},t)$ has a total time derivative that is of the form:

$$
\begin{aligned}
\frac{df(\vec{x},t)}{dt} &= \frac{\partial f(\vec{x},t)}{\partial t} + \sum_{i=1}^{n} \frac{\partial f}{\partial x_i} \frac{dx_i}{dt} \\
\frac{df(\vec{x},t)}{dt} &= \frac{\partial f(\vec{x},t)}{\partial t} + \vec{v}_c \cdot \nabla f(\vec{x},t)
\end{aligned}
\tag{52}
$$

where $\vec{v}_c = \frac{d\vec{x}}{dt}$ is the velocity. The expression above is called the convective derivative.

This concept can be adapted to the case where the function $g(\vec{x},t)$ depends on a stochastic process $\vec{x}$. This is the systematic derivative:

$$
D_c g(\vec{x},t) = \frac{\partial g(\vec{x},t)}{\partial t} + \vec{v}_c \cdot \nabla g(\vec{x},t)
\tag{53}
$$

such that the systematic velocity is as given in (54) below:

$$\vec{v}_c = D_c\vec{x}(t) \equiv \frac{\langle \vec{x}(t'') - \vec{x}(t') \rangle}{2\Delta t} \tag{54}$$

2.4.2.2.3   Access velocities, of exit and of diffusion

In fluid dynamics appears the phenomenon of swirls, or eddies, that cannot be understood with the systematic velocity alone; an illustrative example would be the that of cigar smoke traveling upwards through the air. To approach this topic let us consider a point $\vec{x}$ in the state space and both displacements, $\Delta_+\vec{x}$ and $\Delta_-\vec{x}$, as shown in Figure 5. We have the next relations:

$$\vec{x}'' = \vec{x} + \Delta_+\vec{x} \; , \; \vec{x}' = \vec{x} + \Delta_-\vec{x} \tag{55}$$

If $\vec{x}$ is a state point contained in vicinity $\mathcal{B}$, it is understood that the displacement towards $\vec{x}''$, in a time interval Δt, is related to the exit of state points. Likewise, the displacement from $\vec{x}'$ towards $\vec{x}$, also in a time interval Δt, is related with the entry of state points into vicinity $\mathcal{B}$.

Let us suppose we track a state point whose route is as follows:

- At instant $t - \Delta t$ the state point is located at $\vec{x}'$.

- At instant t the state point is located at $\vec{x}''$.

Separating by components and working them individually, one can obtain

$$\Delta_+ x_i = x_i'' - x_i \tag{56}$$
$$\Delta_- x_i = x_i' - x_i$$

We now consider the physical magnitude of the system denoted as $g(\vec{x}'')$. To treat the displacement from $\vec{x}$ to $\vec{x}''$, the function is expanded in Taylor series as shown below:

$$\begin{aligned}
g(\vec{x}'', t + \Delta t) &= g(\vec{x} + \Delta_+\vec{x}, t + \Delta t) \\
&= g(\vec{x}, t) + \frac{\partial g(\vec{x}, t)}{\partial t}\Delta t + \frac{\partial g(\vec{x}, t)}{\partial x_i}(x_i'' - x_i) \\
&\quad + \frac{1}{2}\frac{\partial^2 g(\vec{x}, t)}{\partial x_i \partial x_j}(x_i'' - x_i)(x_j'' - x_j) + \cdots
\end{aligned} \tag{57}$$

such that repeated indexes indicate a sum.

In the same fashion, one can study the displacement from $\vec{x}'$ to $\vec{x}$, resulting in:

$$\begin{aligned}
g(\vec{x}', t - \Delta t) &= g(\vec{x} + \Delta_-\vec{x}, t - \Delta t) \\
&= g(\vec{x}, t) - \frac{\partial g(\vec{x}, t)}{\partial t}\Delta t - \frac{\partial g(\vec{x}, t)}{\partial x_i}(x_i - x_i') \\
&\quad + \frac{1}{2}\frac{\partial^2 g(\vec{x}, t)}{\partial x_i \partial x_j}(x_i - x_i')(x_j - x_j') + \cdots
\end{aligned} \tag{58}$$

The difference between $g(\vec{x}'')$ and $g(\vec{x}')$ is:

$$g(\vec{x}'') - g(\vec{x}') = \frac{\partial g(\vec{x},t)}{\partial t} 2\Delta t + \frac{\partial g}{\partial x_i}[x_i'' - x_i + x_i - x_i']$$
$$+ \frac{1}{2}\frac{\partial^2 g}{\partial x_i \partial x_j}\left[(x_i'' - x_i)(x_j'' - x_j)\right. \tag{59}$$
$$\left. - (x_i - x_i')(x_j - x_j')\right] + \cdots$$

It is possible to find that the next relations are followed:

$$x_i'' - x_i + x_i - x_i' = \Delta_+ x_i + \Delta_- x_i \tag{60}$$
$$(x_i'' - x_i)(x_j'' - x_j) - (x_i - x_i')(x_j - x_j') = \Delta_+ x_i \Delta_+ x_j - \Delta_- x_i \Delta_- x_j$$

Such that (59) can be written as:

$$g(\vec{x}'') - g(\vec{x}') = \frac{\partial g(\vec{x},t)}{\partial t} 2\Delta t + \frac{\partial g}{\partial x_i}[\Delta_+ x_i + \Delta_- x_i] + \frac{1}{2}\frac{\partial^2}{\partial x_i \partial x_j}\left[\Delta_+ x_i \Delta_+ x_j - \Delta_- x_i \Delta_- x_j\right] + \cdots \tag{61}$$

Multiplying by $\frac{1}{2\Delta t}$ and calculating the mean results in

$$\frac{\langle g(\vec{x}'') - g(\vec{x}')\rangle}{2\Delta t} = \frac{\partial g(\vec{x},t)}{\partial t} + \frac{\partial g}{\partial x_i}\frac{\langle x_i'' - x_i'\rangle}{2\Delta t} + \frac{1}{2}\frac{\partial^2}{\partial x_i \partial x_j}\frac{\langle \Delta_+ x_i \Delta_+ x_j - \Delta_- x_i \Delta_- x_j\rangle}{2\Delta t} + \cdots \tag{62}$$

From (54) we have that the coefficient of the first derivative with respect to the position, is the i-th component of the systematic velocity, v_i, which has been previously found. We also find the following:

$$\langle \Delta_+ x_i \Delta_+ x_j - \Delta_- x_i \Delta_- x_j\rangle = 2\Delta t\left(D_{ij} - D_{ij}\right) = 0 \tag{63}$$

Also, the expression $\frac{\langle g(\vec{x}'') - g(\vec{x}')\rangle}{2\Delta t}$ is the systematic derivative of $g(\vec{x},t)$, thus, we have:

$$D_c g(\vec{x},t) = \frac{\partial g(\vec{x},t)}{\partial t} + v_i^c \frac{\partial g(\vec{x},t)}{\partial x_i} \tag{64}$$

From (64) it is easy to identify the systematic derivative operator as:

$$D_c \equiv \frac{\partial}{\partial t} + v_i^c \frac{\partial}{\partial x_i} \tag{65}$$

If one takes as a special case the identity function: $g(\vec{x},t) = \vec{x}(t)$, the expression is reduced to the systematic velocity in vicinity $\mathcal{B}$.

Adding (57) and (58), it results:

$$g(\vec{x}'', t + \Delta t) + g(\vec{x}', t - \Delta t)$$
$$= 2g(\vec{x},t) + \frac{\partial g(\vec{x},t)}{\partial x_i}(x_i'' - x_i - x_i + x_i')$$
$$+ \frac{\partial^2 g(\vec{x},t)}{\partial x_i \partial x_j}\left[(x_i'' - x_i)(x_j'' - x_j) + (x_i - x_i')(x_j - x_j')\right]$$

Rearranging, multiplying by $\frac{1}{2\Delta t}$ and calculating the mean value, one obtains:

$$\frac{\langle g(\vec{x}'', t + \Delta t) + g(\vec{x}', t - \Delta t) - 2g(\vec{x}, t)\rangle}{2\Delta t}$$
$$= \frac{\partial g(\vec{x}, t)}{\partial x_i} \frac{\langle \Delta_+ x_i + \Delta_- x_i \rangle}{2\Delta t}$$
$$+ \frac{\partial^2 g(\vec{x}, t)}{\partial x_i \partial x_j} \frac{\langle (x_i'' - x_i)(x_j'' - x_j) + (x_i - x_i')(x_j - x_j') \rangle}{2\Delta t}$$
(66)

The term that accompanies the first derivative with respect to the positions is used to define the diffusion velocity in vicinity $\mathcal{B}$:

$$u_i \equiv \frac{\langle \Delta_+ x_i + \Delta_- x_i \rangle}{2\Delta t}$$
(67)

Which is useful to measure the stirring that the state point undergoes in each subset $\mathcal{B}$ in the fluctuations space. We can back up this definition if we add the systematic velocity and the diffusion presented above, resulting in:

$$\frac{\langle \vec{x}'' - \vec{x}' \rangle}{2\Delta t} + \frac{\langle \vec{x}'' - 2\vec{x} + \vec{x}' \rangle}{2\Delta t} = \frac{\langle \vec{x}'' - \vec{x} \rangle}{\Delta t}$$
(68)

Which can be interpreted as a total velocity measuring the mean path of state points from $\vec{x}$ to $\vec{x}''$ in the time interval Δt. In that case it follows that:

$$\vec{v} = \vec{v}_c + \vec{u}$$
(69)

such that the cigarette smoke phenomenon can be described in terms of two velocities, one of translation and other of swirling for each of the $\mathcal{B}$ vicinities in the fluctuation space.

With these conceptual tools, one can identify the operators that allow the calculation of the velocities mentioned in this work. Combining results, we find the next expression:

$$\frac{\langle g(\vec{x}'', t + \Delta t) + g(\vec{x}', t - \Delta t) - 2g(\vec{x}, t)\rangle}{2\Delta t} = u_i \frac{\partial g(\vec{x}, t)}{\partial x_i} + D_{ij} \frac{\partial^2 g(\vec{x}, t)}{\partial x_i \partial x_j}$$
(70)

where

$$D_{ij} = \frac{\langle \Delta_- x_i \Delta_- x_j + \Delta_- x_i \Delta_- x_j \rangle}{2\Delta t}$$
(71)

With the elements considered up until now, we identify the left-hand side as the stochastic derivative, or of diffusion, of the function $g(\vec{x}, t)$ and identify the operator of the stochastic derivative as

$$D_s = u_i \frac{\partial}{\partial x_i} + D_{ij} \frac{\partial^2}{\partial x_i \partial x_j}$$
(72)

such that, when $g(\vec{x}, t) = \vec{x}$, it results in:

$$D_s g(\vec{x}, t) = u_i \tag{73}$$

To study the exit velocity, $\vec{v}^e$, we study the displacement from $\vec{x}$ to $\vec{x}''$ in a Δt time interval. For this purpose, we reuse the Taylor expansion given in (57) and rearrange it as:

$$g(\vec{x}'', t + \Delta t) - g(\vec{x}, t)$$
$$= \frac{\partial g(\vec{x}, t)}{\partial t} \Delta t + \frac{\partial g(\vec{x}, t)}{\partial x_i} (x_i'' - x_i) + \frac{1}{2} \frac{\partial^2 g(\vec{x}, t)}{\partial x_i \partial x_j} (x_i'' - x_i)(x_j'' - x_j)$$
$$+ \cdots$$

Multiplying by $\frac{1}{\Delta t}$ and calculating the mean

$$\frac{\langle g(\vec{x}'', t + \Delta t) - g(\vec{x}, t) \rangle}{\Delta t} = \frac{\partial g(\vec{x}, t)}{\partial t} + \frac{\partial g(\vec{x}, t)}{\partial x_i} \frac{\langle x_i'' - x_i \rangle}{\Delta t} + \frac{1}{2} \frac{\partial^2 g(\vec{x}, t)}{\partial x_i \partial x_j} \frac{\langle (x_i'' - x_i)(x_j'' - x_j) \rangle}{\Delta t} + \cdots \tag{74}$$

Defining the i-th component of the exit velocity as follows

$$v_i^e \equiv \frac{\langle x_i'' - x_i \rangle}{\Delta t} \tag{75}$$

and identifying that

$$\frac{1}{2} \frac{\langle (x_i'' - x_i)(x_j'' - x_j) \rangle}{\Delta t} = \frac{1}{2\Delta t} \langle \Delta_+ x_i \Delta_+ x_j \rangle = D_{ij} \tag{76}$$

thus, we have

$$\frac{\langle g(\vec{x}'', t + \Delta t) - g(\vec{x}, t) \rangle}{\Delta t} = \frac{\partial g(\vec{x}, t)}{\partial t} + v_i^e \frac{\partial g(\vec{x}, t)}{\partial x_i} + D_{ij} \frac{\partial^2 g(\vec{x}, t)}{\partial x_i \partial x_j} \tag{77}$$

Defining the left-hand side as a forward derivative of function $g(\vec{x}, t)$ and introducing the forward operator as:

$$D^e \equiv \frac{\partial}{\partial t} + v_i^e \frac{\partial}{\partial x_i} + D_{ij} \frac{\partial^2}{\partial x_i \partial x_j} \tag{78}$$

Such that we represent the forward derivative as $D^e g(\vec{x}, t)$. In the case when $g(\vec{x}, t) = x_i$ one obtains the i-th component of the exit velocity in vicinity $\mathcal{B}$.

$$D^e x_i = v_i^e \tag{79}$$

Finally, one can relate the entry velocity with the translation of the state point from $\vec{x}'$ to $\vec{x}$ in time interval Δt (see Figure 5). Now consider the Taylor series expansion:

$$g(\vec{x}', t - \Delta t) = g(\vec{x}, t) - \frac{\partial g(\vec{x}, t)}{\partial t} \Delta t - \frac{\partial g(\vec{x}, t)}{\partial x_i} (x_i - x_i') + \frac{1}{2} \frac{\partial^2 g(\vec{x}, t)}{\partial x_i \partial x_j} (x_i - x_i')(x_j - x_j') + \cdots \text{ (80)}$$

Rearranging, multiplying by $\frac{1}{\Delta t}$ and calculating the mean:

$$\frac{\langle g(\vec{x}', t - \Delta t) - g(\vec{x}, t) \rangle}{\Delta t} = -\frac{\partial g(\vec{x}, t)}{\partial t} - \frac{\partial g(\vec{x}, t)}{\partial x_i} \frac{\langle x_i - x_i' \rangle}{\Delta t} + \frac{1}{2} \frac{\partial^2 g(\vec{x}, t)}{\partial x_i \partial x_j} \frac{\langle (x_i - x_i')(x_j - x_j') \rangle}{\Delta t} \text{ (81)}$$

Defining the i-th component of the entry velocity in vicinity $\mathcal{B}$ as:

$$v_i^a \equiv \frac{\langle x_i - x_i' \rangle}{\Delta t} \tag{82}$$

and identifying

$$\frac{1}{2} \frac{\langle (x_i - x_i')(x_j - x_j') \rangle}{\Delta t} = D_{ij} \tag{83}$$

It is possible to rewrite (81) as:

$$\frac{\langle g(\vec{x}', t - \Delta t) - g(\vec{x}, t) \rangle}{\Delta t} = -\frac{\partial g(\vec{x}, t)}{\partial t} - v_i^a \frac{\partial g(\vec{x}, t)}{\partial x_i} + D_{ij} \frac{\partial^2 g(\vec{x}, t)}{\partial x_i \partial x_j} \tag{84}$$

Defining the backwards derivative operator as

$$D_a \equiv -\frac{\partial}{\partial t} - v_i^a \frac{\partial}{\partial x_i} + D_{ij} \frac{\partial^2}{\partial x_i \partial x_j} \tag{85}$$

And rewriting (84) as

$$D_a g(\vec{x}, t) = -\frac{\partial g(\vec{x}, t)}{\partial t} - v_i^a \frac{\partial g(\vec{x}, t)}{\partial x_i} + D_{ij} \frac{\partial^2 g(\vec{x}, t)}{\partial x_i \partial x_j} \tag{86}$$

Once again, if $g(\vec{x}, t) = x_i$ one can obtain

$$D_a x_i = v_i^a \tag{87}$$

which is the i-th component of the entry velocity in vicinity $\mathcal{B}$.

2.4.2.2.4   Combining operators

Passing the operators through an algebraic process, one can obtain the following expressions:

$$D^e \equiv \frac{\partial}{\partial t} + v_i^e \frac{\partial}{\partial x_i} + D_{ij} \frac{\partial^2}{\partial x_i \partial x_j} \tag{88}$$

$$D_a \equiv \frac{\partial}{\partial t} + v_i^a \frac{\partial}{\partial x_i} - D_{ij} \frac{\partial^2}{\partial x_i \partial x_j} \tag{89}$$

If we were to add (88) and (89), then multiply by $\frac{1}{2}$

$$\frac{1}{2}(D^e + D_a) = \frac{\partial}{\partial t} + \frac{v_i^e + v_i^a}{2}\frac{\partial}{\partial x_i} \qquad (90)$$

Defining

$$\frac{v_i^e + v_i^a}{2} \equiv v_i^c \qquad (91)$$

we have

$$\frac{1}{2}(D^e + D_a) = \frac{\partial}{\partial t} + \frac{v_i^e + v_i^a}{2}\frac{\partial}{\partial x_i} = \frac{\partial}{\partial t} + v_i^c\frac{\partial}{\partial x_i} = D^c \qquad (92)$$

Now, calculating the difference between (88) and (89) and multiplying by $\frac{1}{2}$

$$\frac{1}{2}(D^e - D_a) = \frac{v_i^e - v_i^a}{2}\frac{\partial}{\partial x_i} + D_{ij}\frac{\partial^2}{\partial x_i \partial x_j} \qquad (93)$$

such that it is convenient to define:

$$\frac{v_i^e - v_i^a}{2} \equiv u_i \qquad (94)$$

So (93) can be rewritten as:

$$\frac{1}{2}(D^e - D_a) = u_i\frac{\partial}{\partial x_i} + D_{ij}\frac{\partial^2}{\partial x_i \partial x_j} = D^s \qquad (95)$$

The stochastic velocities provide a description at the level of vicinities such that it is possible to calculate a variety of means previously mentioned. Table 2 summarizes the previous results:

Velocity	Notation	Operator
Access entry	$\vec{v}^a$	$D^e\vec{x}(t) = \left(\dfrac{\partial}{\partial t} + v_i^e\dfrac{\partial}{\partial x_i} + D_{ij}\dfrac{\partial^2}{\partial x_i \partial x_j}\right)\vec{x}(t)$
Exit	$\vec{v}^e$	$D^a\vec{x}(t) = \left(\dfrac{\partial}{\partial t} + v_i^a\dfrac{\partial}{\partial x_i} - D_{ij}\dfrac{\partial^2}{\partial x_i \partial x_j}\right)\vec{x}(t)$
Systematic	$\vec{v}^c$	$D^c\vec{x}(t) = \left(\dfrac{\partial}{\partial t} + v_i^c\dfrac{\partial}{\partial x_i}\right)\vec{x}(t)$
Diffusion	$\vec{u}$	$D^s\vec{x}(t) = \left(u_i\dfrac{\partial}{\partial x_i} + D_{ij}\dfrac{\partial^2}{\partial x_i \partial x_j}\right)\vec{x}(t)$

Table 2. Stochastic velocities. Notation and associated operator

In their current form, their usefulness is not very clear. In the following section we will see a version of these that allows us to study the quasi-local conduct of the state points in the fluctuation space.

30

Figures 5 and 7 lead to a description where the idea of instantaneous velocities, used regularly in the context of classical mechanics, has to be abandoned. In the topic under study there is a necessity to associate the concepts of velocities to vicinities that are small enough, but without reducing their size to an infinitesimal area, as is the standard in differential calculus.

2.4.3 Stochastic velocities in time dependent Ornstein-Uhlenbeck process

The stochastic velocities have a practical application in time dependent Ornstein-Uhlenbeck stochastic processes because they can be written in terms of the convection, diffusion and self-correlation matrices of these processes. To make the understanding of the conduct of the state point in the fluctuation space more accessible, in this section we obtain the form of these velocities for the system under consideration.

The time dependent Ornstein-Uhlenbeck processes are normally distributed, $P(\vec{q}, t)$, in which their means and self-correlation function change with time. The forward Fokker-Planck equation (FPE) that satisfies $P(\vec{q}, t)$ is written as follows:

$$\frac{\partial P(\vec{q}, t)}{dt} = \frac{\partial\left[F_\mu(\vec{q}, t)P(\vec{q}, t)\right]}{\partial q_\mu} + \frac{\partial^2\left[D_{\mu\nu}(t)P(\vec{q}, t)\right]}{\partial q_\mu \partial q_\nu} \tag{96}$$

The factor of $\frac{1}{2}$ frequently used when writing a FPE has been absorbed by $D_{\mu\nu}$, and the repeated indexes run from 1 to p, with p denoting the number of degrees of liberty of the system. The flux term, F_μ, is linear in the noise $\vec{q}$, as shown below:

$$F_\mu(\vec{q}, t) = -L_{\mu\nu}q_\nu \tag{97}$$

where $L_{\mu\nu}$ is called the convection matrix.

The probability distribution that satisfies the forward FPE is given in (98)

$$P(\vec{q}, t) = \frac{1}{(2\pi)^{p/2}\sqrt{Det\left(\Xi(t)\right)}} e^{-\frac{1}{2}(q_\mu - \langle q_\mu(t)\rangle))[\Xi^{-1}(t)]_{\mu\nu}(q_\nu - \langle q_\nu(t)\rangle))} \tag{98}$$

We can identify the exit velocity $\vec{v}_e$ with the flux term, thus we have:

$$v_\mu^e = -L_{\mu\nu}q_\nu \tag{99}$$

so, we can rewrite the forward FPE as

$$\frac{\partial P(\vec{q}, t)}{dt} = -v_\mu^e \frac{\partial P(\vec{q}, t)}{\partial q_\mu} + D_{\mu\nu}(t)\frac{\partial^2 P(\vec{q}, t)}{\partial q_\mu \partial q_\nu} \tag{100}$$

On the other hand, the backward FPE that corresponds to this process takes the following form:

$$\frac{\partial P(\vec{q}, t)}{dt} = -F_\mu(\vec{q}, t)\frac{\partial P(\vec{q}, t)}{\partial q_\mu} - D_{\mu\nu}(t)\frac{\partial^2 P(\vec{q}, t)}{\partial q_\mu \partial q_\nu} \tag{101}$$

In a similar fashion, the backward FPE is related to the operator D_a and with the entry velocity, resulting in

$$\frac{\partial P(\vec{q},t)}{dt} = -v_\mu^a \frac{\partial P(\vec{q},t)}{\partial q_\mu} - D_{\mu\nu}(t)\frac{\partial^2 P(\vec{q},t)}{\partial q_\mu \partial q_\nu} \tag{102}$$

There is an analytical solution when the diffusion velocity has zero divergence. Calculating the difference between (100) and (102) and multiplying by $\frac{1}{2}$

$$0 = \frac{\partial}{\partial q_\mu}\left[u_\mu P(\vec{q},t) - D_{\mu\nu}(t)\frac{\partial P(\vec{q},t)}{\partial q_\nu}\right] \tag{103}$$

The term between brackets is a magnitude with divergence of zero:

$$J_\mu = u_\mu P(\vec{q},t) - D_{\mu\nu}(t)\frac{\partial P(\vec{q},t)}{\partial q_\nu} \tag{104}$$

thus, it can be interpreted as a magnitude that is conserved:

$$J_\mu = u_\mu P(\vec{q},t) - D_{\mu\nu}(t)\frac{\partial P(\vec{q},t)}{\partial q_\nu} = C \tag{105}$$

where C is a constant that can be taken as equal to zero, then u_μ is given in terms of $P(\vec{q},t)$ and $D_{\mu\nu}$:

$$u_\mu = D_{\mu\nu}(t)\frac{1}{P(\vec{q},t)}\frac{\partial P(\vec{q},t)}{\partial q_\nu} = D_{\mu\nu}(t)\frac{\partial \ln|P(\vec{q},t)|}{\partial q_\nu} \tag{106}$$

From above it results that the diffusion velocity can be obtained if $P(\vec{q},t)$ is known. This is the case for time dependent Ornstein-Uhlenbeck processes.

Substituting (98) in (106) and using the short notation of: $G(t) = \frac{1}{2}y_\alpha(t)[\Xi^{-1}(t)]_{\alpha\beta}y_\beta(t)$, one obtains

$$u_\mu = D_{\mu\nu}(t)\frac{\partial}{\partial q_\nu}\ln\left\{\frac{1}{(2\pi)^{p/2}\sqrt{Det(\Xi(t))}}e^{-G(t)}\right\} \tag{107}$$

where we have written $y(t) = q_\mu(t) - \langle q_\mu(t)\rangle$ to simplify notation. Working (107) some more results in:

$$u_\mu = -D_{\mu\nu}(t)\frac{\partial G(t)}{\partial q_\nu} \tag{108}$$

Calculating the derivative and using that $(\Xi^{-1})_{\alpha\beta}$ is symmetric results that

$$u_\mu = -D_{\mu\nu}(t)[\Xi^{-1}(t)]_{\nu\beta}\left[q_\beta(t) - \langle q_\beta(t)\rangle\right] \tag{109}$$

From previous results we have the next relations for the velocities:

$$\vec{v}^c = \frac{1}{2}(\vec{v}^e + \vec{v}^a) \tag{110}$$

$$\vec{u} = \frac{1}{2}(\vec{v}^e - \vec{v}^a) \tag{111}$$

Relation (111) leads to

$$\vec{v}^a = -2\vec{u} + \vec{v}^e$$

Substituting this result in (110) gives:

$$\vec{v}^c = \vec{v}^e - \vec{u}$$

so, the components of the entry velocity have the form:

$$v_\mu^a = -2u_\mu + v_\mu^e = 2D_{\mu\nu}[\Xi^{-1}(t)]_{\nu\beta}\big[q_\beta(t) - \langle q_\beta(t)\rangle\big] - L_{\mu\nu}q_\nu \tag{112}$$

and the components of the systematic velocity are:

$$v_\mu^c = -L_{\mu\nu}q_\nu + D_{\mu\nu}(t)[\Xi^{-1}(t)]_{\nu\beta}\big[q_\beta(t) - \langle q_\beta(t)\rangle\big] \tag{113}$$

With this, the set of stochastic velocities in terms of the probability density is now complete. The results above can be written in matrix notation. Table 3 displays the four stochastic velocities for time dependent Ornstein-Uhlenbeck processes:

Velocity	Notation	Operator
entry	$\vec{v}^a$	$2D\Xi^{-1}(t)(\vec{q} - \langle\vec{q}\rangle) - L\vec{q}$
Exit	$\vec{v}^e$	$\vec{v}^e = -L\vec{q}$
Systematic	$\vec{v}^c$	$D\Xi^{-1}(t)(\vec{q} - \langle\vec{q}\rangle) - L\vec{q}$
Diffusion	$\vec{u}$	$-D\Xi^{-1}(t)(\vec{q} - \langle\vec{q}\rangle)$

Table 3. Stochastic velocity operators for Ornstein-Uhlenbeck processes.

The diffusion velocity and the systematic velocity will be used below to describe the behavior of a state point in each vicinity $\mathcal{B}$ in the fluctuation space.

2.4.4   Reaching the state of thermodynamic equilibrium

The analysis of the simulated catalysis reaction allows the determination of when thermodynamic equilibrium has been reached. From expression (37), it is evident that the determinant can be used for that purpose. The state of equilibrium is reached if $\det\big(\Xi(t_2)\big) = \det\big(\Xi(t_1)\big)$, where $t_1 < t_2$. In numerical calculation it is possible to define a tolerance

$$\text{tol} = \frac{\det(\Xi(t_2))}{\det(\Xi(t_1))} < 10^{-5}$$

This is the regime called equilibrium state, and it corresponds to the moment when substrate and enzyme-substrate complex have been depleted. It is achieved at $t \geq 0.013$.

The quasi-stationary process is studied through the numerical solution of equations (32). The expressions for the time evolution of the substrate and enzyme-substrate complex presented in

Table 6 in section *Entropy of Fluctuations* are utilized to calculate the autocorrelation functions shown in Figure 8 below:

(a) (b) (c)
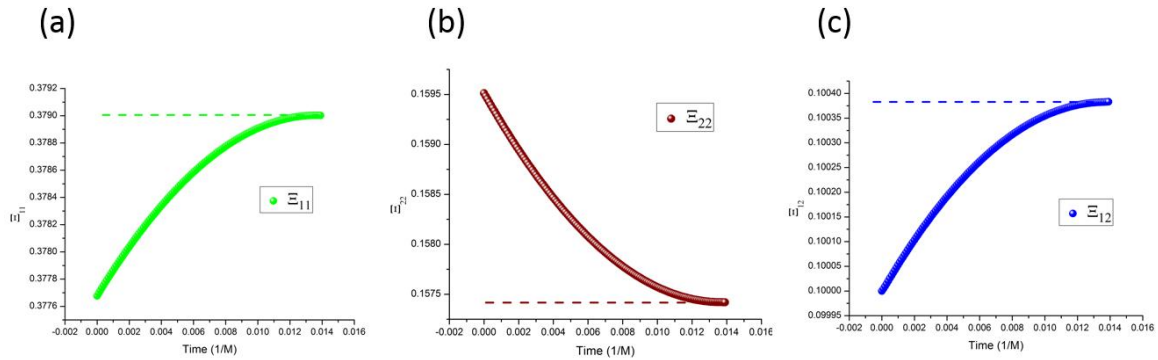
Figure 8. At the end of the quasi-stationary state, all correlations tend to a constant value. (a) is the variance of the fluctuations of the substrate concentration, it increases as the reaction progresses. (b) is the enzyme-substrate complex concentration, it diminishes as the reaction progresses. (c) shows the correlation between the fluctuations of the substrate and enzyme-substrate complex, it increases.

Figure 8a exhibits the autocorrelation of the fluctuation of the substrate, Figure 8b is the graph of the autocorrelation of the fluctuation of the enzyme-substrate complex, and Figure 8c the correlation of both. The numerical analysis could be performed up to $t = 0.015$, but the description would no longer correspond to the state under study, the quasi-stationary state; instead, it would be a state with only the remnants of the noise of the substrate and complex concentrations, which is of little practical interest in this work.

2.4.5   Probability density

The probability density can be calculated with expression (27). Figure 9 shows its initial form at $t = 0.0001$, and its final form at $t = 0.0158$ once it reaches the end of the quasi-stationary state. At first glance the differences between the gaussian distributions at its initial and final states are not apparent. But a more careful observation reveals that there has been a clockwise rotation of approximately $-4°$, as shown in Figure 10.
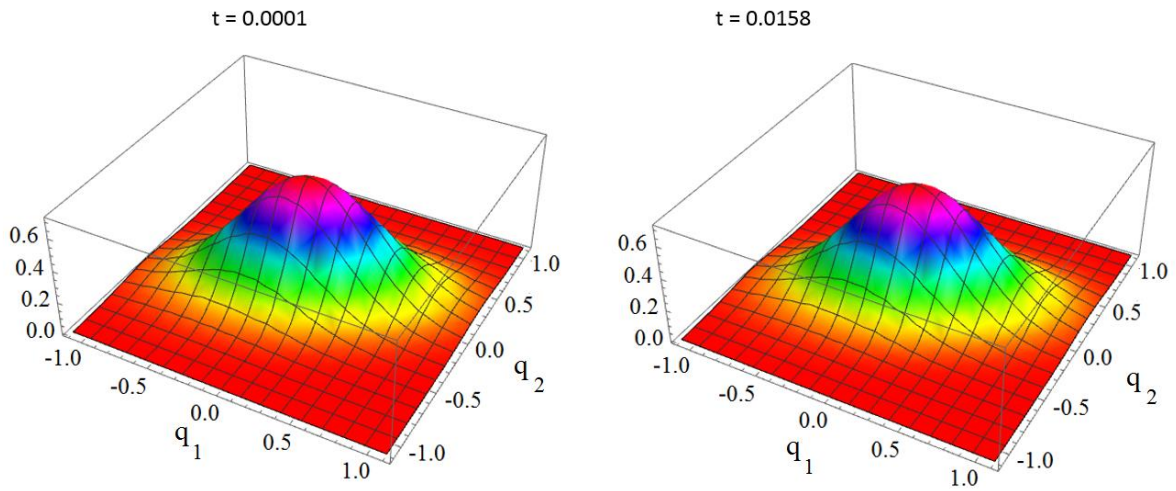
Figure 9. Comparison of the probability density at the start and at the end of the quasi-stationary state.
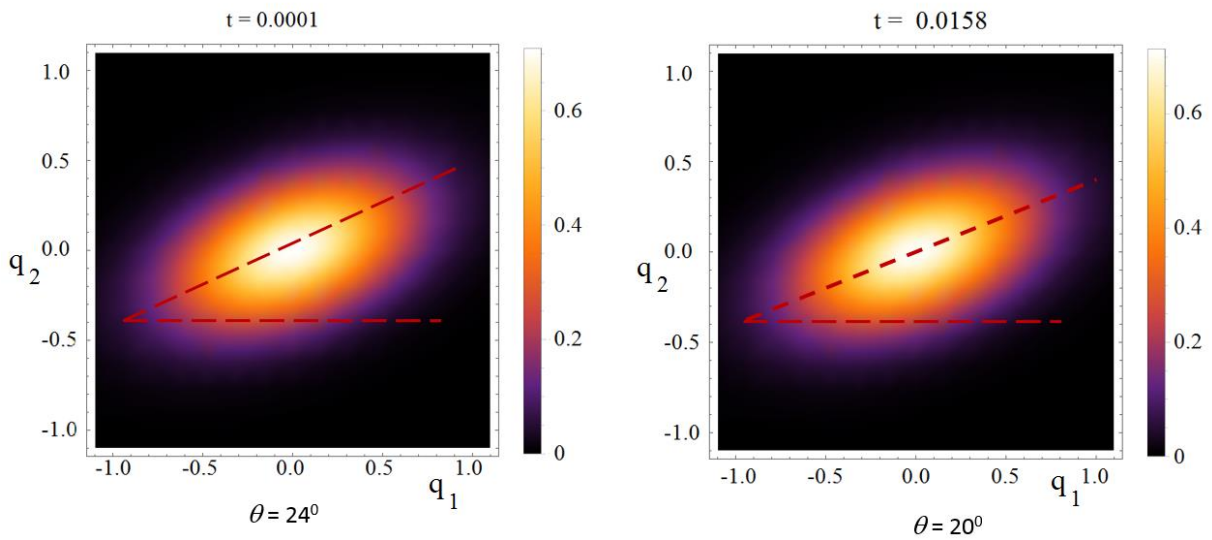
Figure 10. The longest axis of symmetry of the probability density rotates clockwise during the quasi-stationary state.

An analytical way of detecting a change is by calculating the difference between probability densities at $t_f = 0.0158$ and $t_i = 0.0001$, $P(\vec{q}, t_f) - P(\vec{q}, t_i)$. The result can be seen in Figure 11, where there is a region at the center with higher probability, while above and below there is a region with lower probability. What this means is that, during the quasi-stationary state of the catalytic process, the probability density shifts towards the center.
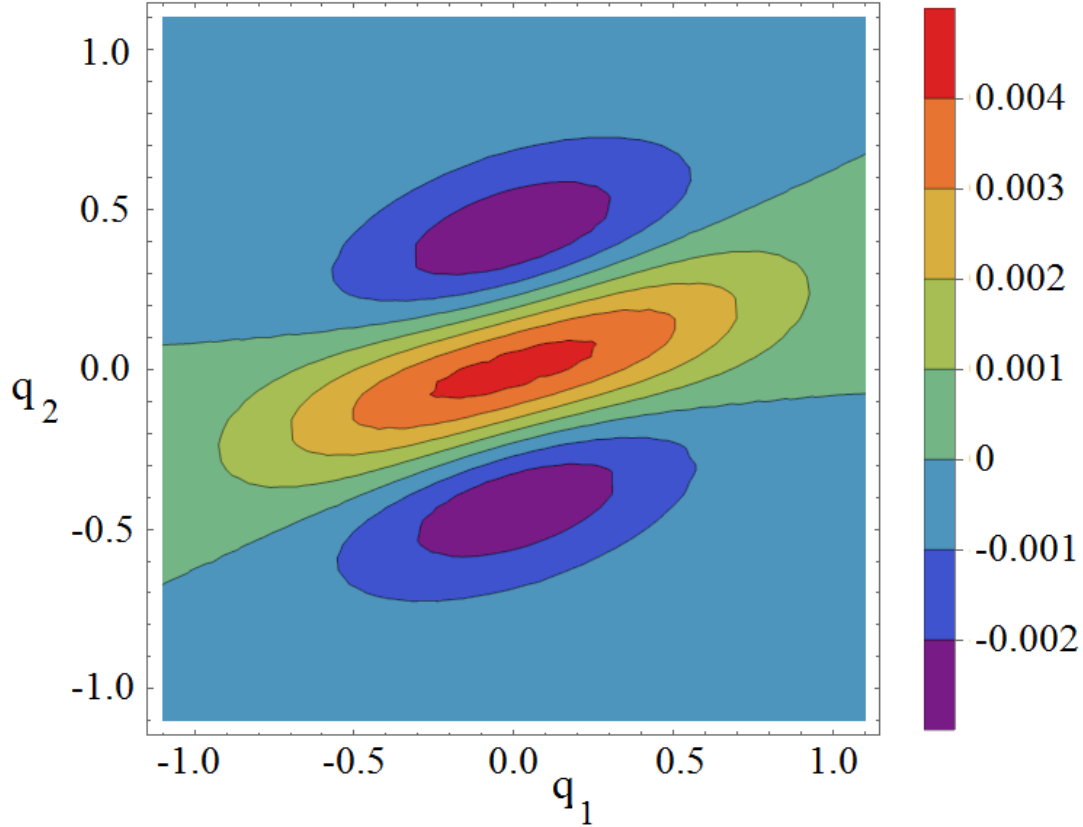
Figure 11. The difference between the last probability density and the initial probability density during the quasi-stationary state. It displays the transition of the probability from the upper and lower regions towards the center. It becomes narrower due to the decrease of magnitude of $\Xi_{22}(t)$.

This is an expected outcome once proper attention is paid to the graphs of $\Xi_{11}(t)$ and $\Xi_{22}(t)$ in figure 8, where the former increases as the latter decreases over time. Further details on information contained within the quasi-stationary state, that is relevant to the understanding of the biochemical process, will be addressed in a later section titled *Entropy of Fluctuations*.

Before going to the next section, where we address the topic of the entropy in this model, let us focus on the total stochastic velocity, which results from the sum of the systematic velocity and the diffusion velocity. Figure 12 shows a comparison between the initial state, at $t = 0.0001$, and a state close to equilibrium, at $t = 0.014$, of the total stochastic velocity.
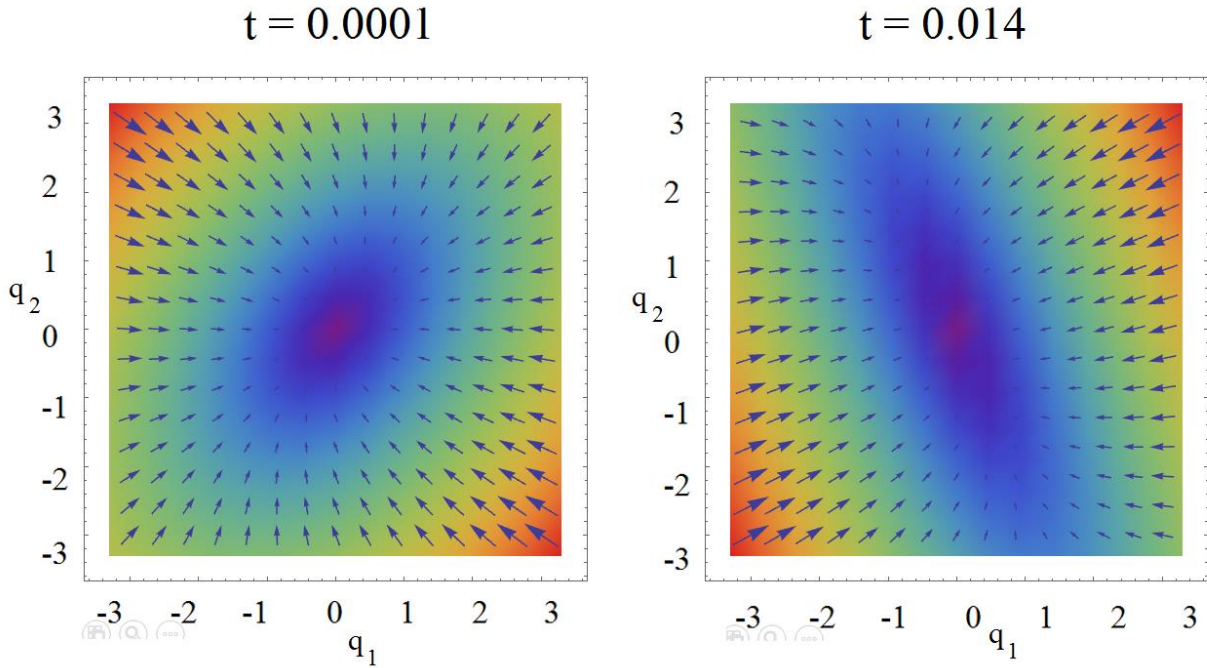
Figure 12. The total stochastic velocity at the start and the end of the quasi-stationary state. The state points $\vec{q}$ farthest from the center move at a greater velocity, while the points in the center are comparatively static. The velocities in the $\mathcal{B}$ regions indicate the increase in probability at the central region.

The total stochastic velocity, shown in Figure 12, is a two-dimensional field that plots the tendency of the state points $\vec{q}$ to move towards a region in the center, which intuitively coincides with the plot of the probability density. At the start of the reaction ($t = 0.0001$) it is mainly the points from the second and fourth quadrant that move at a greater velocity, contributing the most in keeping the saturation on the center. In contrast, when very close to the equilibrium ($t = 0.014$) the roles have reversed, and it is now the first and third quadrants responsible of keeping the saturation in the center.

We calculate the curl of the total stochastic velocity to further explore this behavior, as shown in Figure 13. From a geometrical viewpoint, the tendency of the field to rotate suggests that the averaged transitions performed by the state points, $\vec{q}$, within each region $\mathcal{B}$ occur due to the lack of balance between the displacements $\pm q_x$, which is something that is also reflected by the averaged $\pm q_y$. This conduct causes the semi-axes of symmetry of the probability distribution to not remain static. The magnitude of this phenomenon diminishes over time, corresponding to the end of the quasi-stationary stage.
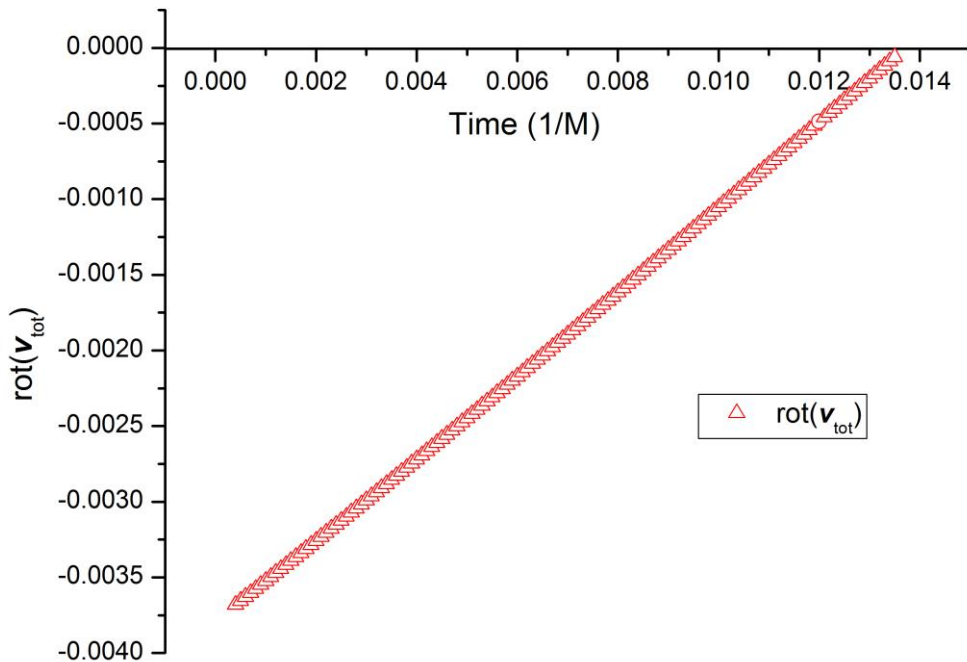
Figure 13. The curl of the total stochastic velocities is negative. We associate it with the tendency of the probability distribution to rotate clockwise during the quasi-stationary state.

2.5 About the different terms of the entropy of the Michaelis-Menten model

In this section we retake the discussion about the entropy of the system left pending in expressions (36), (37) and (38). The system under study is a laboratory experiment that progresses through time:

- At an initial stage, at a time interval we label as $t < 0$, the enzyme and substrate molecules exist separate from one another.
- At an instant $t = 0$ both substances get in contact with each other within a fluid that serves as a medium, at this point in time the reaction has not started. While the system is at $t = 0$, where the reaction is yet to begin, the system can be considered as being in a state of thermodynamic equilibrium: It is for this reason that its entropy can be calculated using standard methods found in physical statistics.
- Let us suppose that the physical system is stirred to aid the start of the reaction. Once it starts, the time interval is $t > 0$, which corresponds to the random process that has been discussed in previous sections. It is then than the entropy of fluctuations given in expression (36) makes itself apparent.

This section is dedicated to the study of entropy of the substrate and the enzyme-substrate complex. The working hypothesis is that the substrate and enzyme molecules are diluted in an aqueous medium, where they perform irregular motions. The physical system can be illustrated by the antibiotic penicillin playing the role of the substrate, and the beta-lactamase acting as the enzyme. The latter is used by bacteria to protect itself against the antibiotic.

At instant $t = 0$, when the reaction is about to start, we consider the substrate and enzyme molecules as if they are two ideal gasses with their respective entropy, which are originated by their degrees of freedom: translational, rotational and electronic. At instant $t \leq 0$, the entropy of equilibrium, denoted as S_{eq}, contains the terms shown in (114):

$$S_{eq} = S_{tr} + S_{mix} + S_v + S_r + S_e \tag{114}$$

Where S_{tr} is the translational entropy, S_{mix} is the entropy of mixing, S_v is the vibrational entropy, S_r is the rotational entropy, and S_e is the electronic entropy. Save for S_e, we will calculate estimates for the values of the entropy of each contribution mentioned with the purpose of knowing an estimated value of S_{eq}.

In this work we also add the fluctuation entropy, $S_f(t)$, for substrate and enzyme, which arises due to the dynamics of the Michaelis-Menten model. The resulting total entropy is given by (115):

$$S_T(t) = S_{eq} + S_f(t) \tag{115}$$

It is compulsory to note the non-uniqueness of the definition of entropy in non-equilibrium systems. The definition of $S(t)$ is based in the one used in the theory of stochastic processes, but it should be made clear that there is no expression available for it that is generally accepted. In 2019, de Decker [57] demonstrated that, in the case of non-equilibrium systems, there are at least two definitions of entropy that, being both physically sound, differ in the time evolution of the production of entropy, even if both reproduce the same equilibrium state. However, even though the uniqueness of the time evolution is under contention, we consider appropriate the study of the special case of entropy in the processes that can be described by the Michaelis-Menten model.

2.5.1   Requirements for the decrease of entropy

The second law of thermodynamics establishes that, in the absence of external work being done on a system, entropy follows the inequality shown in (116):

$$\Delta S \geq 0 \tag{116}$$

Such that the equal sign is present once the state of equilibrium is reached.

Instead, entropy can diminish if energy is applied to a system through appropriate processes. We see that this is the case in enzymatic catalysis that are studied with the Michaelis-Menten model.

From the definition of Markov processes [57], it is clear that, in mathematical terms, the decrease of entropy through time is not forbidden. For a physical system with microscopic states numbered with n, and its probability is denoted by $P_n(t)$, its entropy can be expressed as seen in (117):

$$S(t) = -\sum_n P_n(t) \ln P_n(t) \tag{117}$$

Its rate of change is given by (118):

$$\frac{dS(t)}{dt} = -\sum_n \frac{\partial P_n(t)}{\partial t} [\ln P_n(t) + 1] \tag{118}$$

From $0 \le P_n(t) \le 1$, results that $-\infty < \ln P_n(t) \le 0$. Therefore, the inequality $\frac{dS(t)}{dt} < 0$ can be fulfilled if either of the conditions (119) or (120) are followed.

$$\frac{\partial P_n(t)}{\partial t} < 0 \quad \text{and} \quad \ln P_n(t) < -1 \tag{119}$$

$$\frac{\partial P_n(t)}{\partial t} > 0 \quad \text{and} \quad \ln P_n(t) > -1 \tag{120}$$

2.5.2 Calculating an estimation of the entropy of equilibrium

In this section we study the entropy in the time interval $t \le 0$ up to equation (135). From that point on, the contribution of the entropy of fluctuations is added to the Michaelis-Menten model of the penicillin hydrolysis by the beta-lactamase. This is the case when the initial state of equilibrium is broken, then begins a process where the most important stage is the quasi-stationary state of the reaction, that reaches a state of equilibrium once the substrate has been exhausted.

The entropy of a system in statistical physics is calculated by $S = k_B \left(\frac{\partial T \ln Q}{\partial T} \right)_{N,V}$, where Q is the partition function. But as stated before, we will suppose that the system behaves like an ideal gas system. Therefore, for an ideal gas of N particles of mass m, the expression for the entropy is given by:

$$S_{ideal}^{(i)} = N_i k_B \ln \left[\left(\frac{2\pi m_i k_B T}{h^2} \right)^{3/2} \frac{q^{5/2}}{c_i} \right]$$

Where $c_i = c_1, c_2$, with $c_1 = \frac{N_S}{\Omega}, c_2 = \frac{N_E}{\Omega}$, and N_S the number of substrate particles, N_E the number of enzyme particles, and Ω is the initial number of substrate and enzymes in the system. In this expression m_i denotes the masses, m_1 is the mass of a substrate particle and m_2 is the mass of the enzyme particle.

2.5.2.1 Translation entropy

For the substrate, let us consider as an example the antibiotic rifampicin, which is part of the family of penicillin. The enzyme considered is the beta-lactamase. The data used to model these molecules is shown in table 4 next:

$$M_{enz} = 4.981616763 \times 10^{-23} \text{ kg} \qquad M_{sus} = 5.73314 \times 10^{-25} \text{ kg}$$

$$N_{enz} = 100 \qquad\qquad N_{sus} = 4999$$

Table 4. Values of the mass and number of molecules for enzyme and substrate.

With a temperature of $T = 36.5°C = 309.65$ K, the translation entropy of substrate and enzyme are given in (121) and (122), respectively.

$$S_{tr}^{(sus)} = 80.3875 N_{sus} k_B \tag{121}$$

$$S_{tr}^{(enz)} = 1.82029 \eta N_{sus} k_B \tag{122}$$

Where $\eta = \frac{N_{enz}}{N_{sus}} = \frac{100}{4999} = 0.02$. The total translation entropy is given by (123):

$$S_{tr} = S_{tr}^{(sus)} + S_{tr}^{(enz)} = N_{sus} k_B [80.3875 + \eta 1.82029] \tag{123}$$

2.5.2.2 Mixing entropy

This contribution to the total entropy exists due to the existence of two gasses mixing inside a volume. The mixing entropy can be expressed as:

$$S_{mix} = -\Omega k_B (c_{sus} \ln c_{sus} + c_{enz} \ln c_{enz})$$

Where $c_{sus} = \frac{N_{sus}}{\Omega} = \frac{4999}{4999+100} = \frac{4999}{5099} = 0.98039$ and $c_{enz} = \frac{N_{enz}}{\Omega} = 1.9612 \times 10^{-2}$. The estimate of the mixing entropy is given by (124):

$$S_{mix} = 0.0984549(1 + \eta) N_{sus} k_B \tag{124}$$

2.5.2.3 Vibrational entropy

Here we study the contribution to the entropy by the vibrations of enzyme and substrate molecules. We begin with the substrate.

2.5.2.3.1 Vibrational entropy of the substrate

The rifampicin molecule is relatively small when compared to that of the beta-lactamase. For this analysis we suppose that the molecules can be considered as oscillating nuclei that can be detected by IR spectroscopy, therefore we model the substrate as p independent harmonic oscillators, where ν_k denotes the frequencies, with $k = 1, 2, \ldots, p$. The contribution to the entropy due to the vibrational degrees of freedom of the substrate can be calculated with:

$$S_v^{(sus)} = k_B \left\{ \frac{\partial}{\partial T} \left[T \ln \left(\prod_{k=1}^{p} \left(\frac{1}{1 - e^{-\beta h \nu_k}} \right)^{N_{sus}} \right) \right] \right\}$$

This results in (125):

$$S_v^{(sus)} = N_{sus} k_B \left[-\sum_{k=1}^{p} \ln \left(1 - e^{-\frac{h\nu_k}{k_B T}} \right) + \sum_{k=1}^{p} \frac{\frac{h\nu_k}{k_B T}}{e^{\frac{h\nu_k}{k_B T}} - 1} \right] \tag{125}$$

Ivashchenko [58] provides a set of wave numbers that, when transformed to frequencies, provide the following values:

$$\nu = \{3.71, 4.12, 4.30, 4.36, 4.60, 4.68, 4.87, 4.95, 5.16, 8.77, 9.14, 10.04\} \times 10^{13} \text{Hz}$$

For a temperature of $T = 36.5°C = 309.65$ K the vibrational entropy contribution of the substrate is shown in (126):

$$S_v^{(sus)} = 12.0203 N_{sus} k_B \tag{126}$$

2.5.2.3.2 Vibrational entropy of the enzyme

The enzyme is a sizeable molecule, compared to the substrate, but its dimensions are still within the order of nanometers. For it we use the oscillatory theory of very small solids with the added correction necessary for such scales. The shape also plays an important role, but we will suppose it is a sphere of diameter between 3 to 7 nm, with a homogenously distributed mass.

Bu-Xuan Wang [59] argues that the theory of specific heats of Einstein can be applied to nanoparticles, thus, we use the partition function of solids [28] given as:

$$Q_v^{(enz)} = -\int_0^\infty \left[\ln\left(1 - e^{-\beta h v}\right) + \frac{1}{2}\beta h v \right] g(v) dv$$

Using the hypothesis by Einstein of $g(v) = 3N_{enz}\delta(v - v_E)$, with v_E being the Einstein frequency, and using the empirical adjustment parameter known as the Einstein temperature, $\Theta_E = \frac{h v_E}{k_B}$, the expression for the vibrational entropy of the enzyme can be obtained, as shown in (127):

$$S_v^{(enz)} = -3k_B N_{enz} \left\{ \frac{\partial}{\partial T} \left[T \ln\left(1 - e^{-\Theta_E/T}\right) + \frac{\Theta_E}{2} \right] \right\}$$

$$= 3k_B N_{enz} \left\{ \frac{\Theta_E f(T)}{g(T) \, ln[\Theta_E + 2T \, ln \, g(T)]} - ln\left(\frac{\Theta_E}{2T}\right) + ln \, g(T) \right\} \tag{127}$$

Where $f(T) = e^{\Theta_E/T} + 1$ and $g(T) = e^{\Theta_E/T} - 1$.

According to E Gamsjäger [60], $\Theta_E \cong \sqrt{\frac{3}{5}}\Theta_D \cong 1200$ K, for a temperature of $T = 309.65$ K, the value of the vibrational entropy contribution of the enzyme is given in (128):

$$S_v^{(enz)} = 0.0127706 \eta k_B N_{sus} \tag{128}$$

2.5.2.4 Entropy of rotation

A more precise treatment of the entropy of a large molecule, such as a protein or an enzyme, requires knowing its energy levels to be able to calculate its partition function. This has been considered a very complicated problem [61], [62], therefore we suggest the approach mentioned above, to treat it as a sphere of homogenously distributed mass.

The substrate, on the other hand, is by comparison a much smaller molecule. This can be modelled as if it was a nanometric ellipsoid with a homogeneously distributed mass M, with its axes denoted by a, b and c. Taking its principal axes as the coordinated system, the tensor of inertia is diagonalized, and only three quantities are needed to describe it [63]:

$$I_1 = \frac{1}{5}M(b^2 + c^2) \quad , \quad I_2 = \frac{1}{5}M(a^2 + c^2) \quad , \quad I_3 = \frac{1}{5}M(a^2 + b^2)$$

The partition function resulting from the rotational degrees of freedom is denoted as such:

$$Q_r = q_r^N = \left[\frac{\sqrt{\pi}}{\sigma} \left(\frac{8\pi^2 k_B T}{h^2} \right)^{3/2} \sqrt{I_1 I_2 I_3} \right]^N$$

Which, defining $\alpha = \frac{\sqrt{\pi}}{\sigma} \left(\frac{8\pi^2 k_B}{h^2} \right)^{3/2} \sqrt{I_1 I_2 I_3}$, can be compacted as seen in (129):

$$q_r = \alpha T^{3/2} \tag{129}$$

The resulting entropy of rotation is of the form (130):

$$S_r = N k_B \ln\left(\alpha e^{3/2} T^{3/2} \right) \tag{130}$$

The underlying difference between the contribution from the substrate and from the enzyme is contained in the values of N and α.

2.5.2.4.1   Entropy of rotation of the substrate

We suggest that, when the substrate molecule rotates, the shape is similar to a spheroidal prolate. With this in consideration, it is possible to estimate its size based on the length of its $N - N$ bonds (1.346 Å); therefore, its semiaxes would be:

$$a = 1.346 \times 12 \text{ Å} = 16.152 \times 10^{-10} \text{ m}$$
$$b = c = 1.346 \times 8 \text{ Å} = 10.768 \times 10^{-10} \text{ m}$$

With its mass given as:

$$M_{sus} = 5.73314 \times 10^{-25} \text{ kg}$$

The moments of inertia are of the form:

$$I_1 = I_a = \frac{2}{5}Mb^2 = 5.9858 \times 10^{-43} \text{ kg m}^2$$
$$I_2 = I_3 = I_b = \frac{1}{5}M(a^2 + b^2) = 4.3209 \times 10^{-43} \text{ kg m}^2$$

Since we have no information about its symmetry, we assume $\sigma = 1$, which gives the result:

$$S_r^{(sus)} = N_{sus} k_B \ln\left(\alpha e^{3/2} T^{3/2} \right) \tag{131}$$

At a temperature of $T = 309.65 \text{ K}$, the value of the estimation of the entropy of rotation contribution by the substrate is given by (132):

$$S_r^{(sus)} = 20.8999 N_{sus} k_B \tag{132}$$

2.5.2.4.2 Entropy of rotation of the enzyme

For the estimation of the contribution to the entropy of rotation by the enzyme we consider the beta-lactamase, which will be modelled by a sphere of homogeneously distributed mass M_{enz}. Its measurements are presented below:

$$M_{enz} = 4.981616763 \times 10^{-23} \text{ kg}$$
$$R_{enz} = \frac{1}{2}(5 \text{ nm}) = 2.5 \times 10^{-9} \text{ m}$$
$$I = \frac{2}{5}MR^2 = 5.1892 \times 10^{-49} \text{ kg m}^3$$

The resulting entropy of rotation for the enzyme is:

$$S_r^{(enz)} = N_{enz}k_B \ln\left(\alpha e^{3/2}T^{3/2}\right) \tag{133}$$

At a temperature of $T = 309.65$ K, the resulting entropy of rotation contribution by the enzyme is given by (134):

$$S_r^{(enz)} = 0.592884N_{enz}k_B = 0.592884\eta k_B N_{sus} \tag{134}$$

2.5.2.5 Entropy of equilibrium

Summing of all the contributions to the nondimensionalized entropy, (123), (124), (126), (128), (132), (134), the resulting expression is given in (135):

$$\frac{S_{eq}}{k_B N_{sus}} = 80.3875 + \eta 1.82029 + 0.0984549(1 + \eta) + 12.0203 + 0.0127706\eta + 20.8999 + 0.592884\eta \tag{135}$$

2.5.3 Entropy of fluctuations

The entropy of fluctuation is made noticeable in the system once the interaction between enzyme and substrate begins. This moment in time will be labelled as $t = 0$.

According to the Michaelis-Menten model, it is enough to follow the substrate and the enzyme-substrate complex to have a proper understanding of the system. Under such consideration, we will see that there is a decrease in entropy.

The computer simulation was carried out with the reaction rates shown in Table 5 [64] below. As shown in previous sections, the simulation displays three stages of the chemical reaction. Figure 14 shows the functions fitted to the means of N_2/Ω and N_3/Ω, where, as before, $N_2 = S$, $N_3 = ES$ and $\Omega = N_{10} + N_{20}$.

k_1'	41×10^6	1/mol
k_2	2320	1/s
k_3	3610	1/s

Table 5. Transitions rates used in the simulation of the penicillin hydrolysis catalyzed by beta-lactamase.

The method used to calculate the means was the following:

1. The simulations were carried out p number of times, with $p = 1000$.
2. Of the p realizations, the one with the longest duration was selected. Its time was divided into I intervals of equal width, with $I = 100, 1000, 10000$.
3. The datapoints of the p realizations that fell in each interval were averaged.

The curves fitted serve as confirmation of an initial stage when the substrate decreases rapidly as the enzyme-substrate complex increases drastically towards the second stage. During the second stage, almost all enzymes are in the enzyme-complex state, in other words, the concentration of free enzymes fluctuates near zero; this stage is what is called the stationary state in biochemistry. The third stage is reached when substrate is depleted, therefore the concentration of enzyme-substrate complex decreases exponentially. The time duration of each stage and the functions fitted for the substrate and enzyme-substrate complex during each of these can be seen in Table 6, the curves are shown in Figure 14.

	Duration (s)	S fit	ES fit
1st stage	$0 < t < t_1 = 3.38985 \times 10^{-4}$	$\psi_1(1) = 0.980388 - 111.03901t$	$\phi_1(t) = 57.5649t$
2nd stage	$t_1 < t < t_2 = 0.013559$	$\psi_2(t) = 0.966669 - 70.56632t$	$\phi_2(t) = 0.01951$
3rd stage	$t_2 < t < t_3 = 0.0169$	$\psi_3(t) = 0.00983$	$\phi_3(t) = e^{38-3090t}$

Table 6. Time functions that parametrize the substrate and enzyme-substrate complex concentrations in 1st, 2nd and 3rd stage.
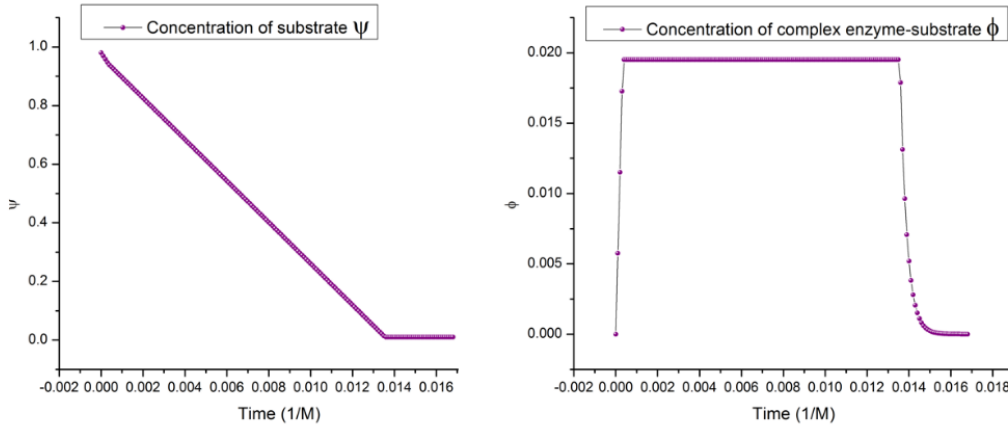
Figure 14. Time evolution of the substrate (left) and enzyme-substrate concentration (right).

Equations (32) were solved numerically, then $S(t)/Nk_B$ was found using expression (36). The computer simulation allows us to find the entropy of fluctuations $\Xi_{jj}(0)$ but, even though we consider the precision to not be enough to quantitively determine $\Xi_{jj}(t)$, we can provide an approximation using the following initial conditions:

$$\Xi_{11}(0) = 0.377676 \qquad \Xi_{22}(0) = 0.377676 \qquad \Xi_{12}(0) = 0$$

Adding the approximation of the entropy of fluctuations to the previously obtained entropy of equilibrium, S_{eq}/Nk_B, the result can be seen in Figure 15. Some relevant values of the time evolution of S_{eq}/Nk_B are shown in Table 7.
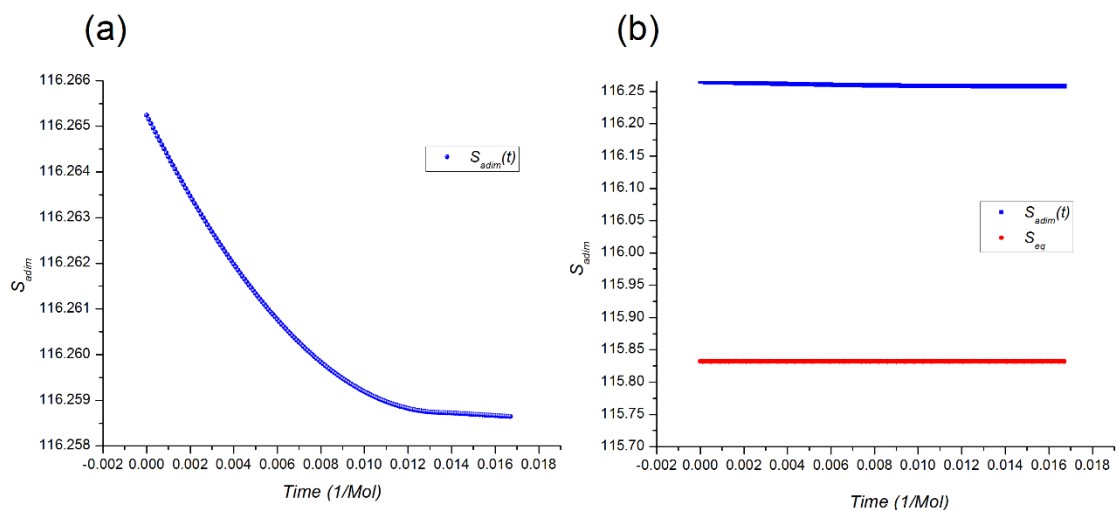
Figure 15. Left: Time evolution of the entropy of fluctuation. Right: Comparison between total entropy at $t > 0$ (start of the reaction), and entropy of equilibrium at $t \leq 0$.

S_{eq}/Nk_B	115.83
$\Delta S_+/Nk_B$	0.433
$S_T(t > 0)/Nk_B$	116.265
$S_T(t_3)/Nk_B$	116.259
$\Delta S/Nk_B$	-6.602×10^{-3}

Table 7. Numerical values of the entropy. S_{eq}: entropy of equilibrium. ΔS_+: entropy of fluctuation during $0 < t < t_3$. $S_T(t > 0)$: Total entropy at the start of the reaction, $t > 0$. $S_T(t_3)$: Total entropy at t_3 (the end of the catalytic reaction). ΔS: Decrease in entropy of fluctuation ($S_f(t_3) - S_f(t > 0)$).

The intriguing result seen in Figure 15 and Table 7 can be stated in two aspects:

1) It is clear that the net entropy of the reaction is greater than it was before the start of the reaction, therefore it is a spontaneous process.
2) The curve displayed in Figure 15a shows a decrease in entropy, something that is only possible if there is an external energy source.

Before the reaction, the value of the total entropy is S_{eq}/Nk_B. Once the reaction starts (at $t > 0$), the total entropy suffers a change, increasing a quantity of $\Delta S_+/Nk_B$, so the total entropy at that point is $S_T(t > 0)/Nk_B$. As the reaction takes place, the entropy decreases until the system reaches a state of equilibrium once the catalysis has finished (at $t = t_3$); the resulting decrease in entropy is ΔS, so the total entropy at that point is $S_T(t_3)/Nk_B$. It is important to note that the magnitude of the decrement in entropy, ΔS, is lower than the increase in entropy due to the reaction taking place, ΔS_+; in other words, $\Delta S_+ > \Delta S$. According to the second law of thermodynamics, this decrement is evidence of the existence of work during the process of catalysis.

The value of ΔS is approximately 1.52% of the initial entropy of fluctuations and it is 6.71% of the mixed entropy, this could be (as stated before) because the system is receiving energy in the form of work from an external source. A revision of the existing literature leads us to suggest that it comes from the vibrational degrees of freedom of the enzyme, which will be discussed below. For processes at constant volume, the fundamental equation of thermodynamics establishes:

$$\Delta U = T\Delta S + \mu_2 \Delta N_2 + \mu_3 \Delta N_3$$

The condition of $\Delta S < 0$ leads to the following inequality: $\Delta U < \mu_2 \Delta N_2 + \mu_3 \Delta N_3$. Considering the quasi-stationary state as representative of the majority of the process of catalysis, then $\Delta N_3 = 0$, therefore the inequality takes the form of:

$$\Delta U < \mu_2 \Delta N_2$$

If $\Delta S < 0$ one must have $C_p = T\left(\frac{\Delta S}{\Delta T}\right)_T < 0$, so that this decrease in the entropy is consistent with results previously published: in enzyme catalysis happens that $C_p < 0$ [65], [66]. Also, the negative value in this heat capacity is a condition to show that in enzyme catalysis there is an optimal temperature $T = T_{op}$, where the most efficient catalysis occurs.

The results from our computer simulation of a Michaelis-Menten system allows us to make a prediction that points towards the correct direction, since it reproduces the inequality of $\Delta S < 0$ for the entropy of fluctuations.

However, our model has a limitation in its quantitative aspect. According to Hobbs *et al.* [65] and Arcus *et al.* [66], the values of the heat capacity at constant pressure are within the range $-12\frac{kJ}{mol\,K} < C_p < -1\frac{kJ}{mol\,K}$. If one is to take the right-hand value of the range, at $T = 298.5$ K, with $\Delta T = 1$ K, converting to eV per particle, the resulting value of the change in entropy would be:

$$\Delta S = C_p \frac{\Delta T}{T} = -3.4764 \times 10^{-5} \text{eV K}^{-1}$$

Furthermore, according to our results, the entropy of fluctuations per particle is:

$$\frac{\Delta S}{N} = -5.6875 \times 10^{-7} \text{eV K}^{-1}$$

This leads us to conclude that there is some aspect missing in this model.

2.6   Discussion

The Michaelis-Menten model partially captures the essence of the catalysis phenomenon in absence of cooperativity. It allows the prediction of the existence of a descent in the entropy of fluctuation, which corresponds with the experimental observation of the descent in the heat capacity at constant pressure, C_p, during catalytic processes. Nonetheless, the difficulty of producing quantitatively precise results constitutes a limitation of the model. Although it has demonstrated its usefulness in processes that do not present cooperativity, its simplicity hinders it from capturing a wider range of phenomena specific to each reaction. For example, a revision of the mechanism of hydrolysis of penicillin by the beta-lactamase enzyme produced by bacillus cereus [67], pseudomonas aeruginosa, amongst others, show that the rupture and formation of chemical bonds in the process is more complicated than a catalysis reaction where only one enzyme-substrate complex participates as intermediary. This is a bigger problem than it may seem, as we argue below.

A. Holmberg [68] studied the practical difficulties that appear when estimating parameters in biological processes. He paid special attention to systems described by the Michaelis-Menten equation and proposed a sensibility function to deal with the lack of uniqueness in the results. The problem stems from different parameters reproducing the same experimental results. This indicates that there can be various physical processes that remain hidden within the parameters, which consequently gives way to a set of results being able to model the same substance. This leads one to think that, in the model, a compound as the enzyme-substrate complex can, in the real phenomenon, be two molecules even though in the Michaelis-Menten formulation appears only one.

J. Kim and J. Lee [69] pick up the topic of the difficulty faced when elaborating mathematical models to describe specific phenomena. They explore the case where differential equations with adjustable parameters, obtained from experimental data, are used with these purposes. Their suggestion is a set of mathematical tools to estimate the quality of the adjusted parameters. It is this complexity in the analysis that clearly displays the issues confronted when modelling from experimental data.

A similar problem appears in systems modelled with the Langevin equation and the Fokker-Planck equation. In one dimension both formulations are equivalent, but in two or more dimensions, two Langevin equations corresponding to two different physical systems lead to the same Fokker-Planck equation.

In conclusion, while it is praiseworthy that the Michaelis-Menten model sheds light on the qualitative understanding of the role of the entropy in the catalytical process, its quantitative prediction is a much more complicated field of study.

2.7   Possible repercussions in pharmaceutical technology

In recent years, there have been developments in the use of nanostructures as drug carriers [70]. In the design of these processes, it is often suggested that drug carriers could accumulate in specific

sites where they would then release their load, thus increasing the efficiency of the medicine [71], as well as reducing its toxic effects in the patient undergoing treatment. If one supposes that these nanocages have a specific size, for example a diameter of 50 nm, it is possible to estimate the capacity of each drug carrier: If $R = 25$ nm, and the carrier is spherical, its effective volume would be $V_{ef} = 8.1812 \times 10^{-24}$ m^3; now, if the volume occupied by a molecule of a drug like amoxicillin is that of a square prism of sizes $0.725 \times 0.423 \times 0.930$ nm [72], giving the amoxicillin molecule an effective volume of $V_{amox} = 2.8521 \times 10^{-28}$. If the volume within the nanocage is occupied by this drug, the maximum quantity of molecules it could carry would be $N_{amox} = \dfrac{V_{ef}}{V_{amox}} = 28685$. However, if the nanocage carries an aqueous solution of amoxicillin and clavulanic acid, in proportions similar to those found in injectable solutions $(0.0472, 0.009, 0.94)$ [73], the antibiotic occupies approximately only 5% of the space, meaning that there are of the order of 1434 molecules of antibiotic in the load. This means that purely deterministic models would only offer a partial understanding of the system.

With regard to stochastic mathematical models used to describe the transport and release of drugs in living tissue, these tend to focus on the concentration of the drug over time [74] and are based on basic equations, like the Fick law of diffusion in different geometries. These can also incorporate other relevant details, such as local tissue inflammation and degradation of the polymer drug carrier.

With this in mind, we believe that the inclusion of other thermodynamic magnitudes, beside particle concentration, in the description of the process would prove useful. One such magnitude could be the elastic properties of the beta-lactamase molecule during the hydrolyzation of the antibiotic.

The usual approach for studying molecular vibrations consist in supposing that the force constants between atoms are independent of the temperature of the medium. This idea is introduced in statistical physics through the occupation of energy levels, without considering the possibility that the vibration frequency of the particles that give form to the molecule depend on the temperature. In contrast with this methodology, Kolesov [75] considers the changes in temperature as a means to fine tune atomic bond length and atomic interaction. He suggests that $\omega(0)$ is the vibration frequency at a temperature of $T = 0$ K, and for increasing values of T, the relation $\omega(T) = \omega(0) + f(T)$ is followed.

If the approach by Kolesov is true, it could open the way to new processes and techniques that would allow the local manipulation of temperature to interfere with the normal vibration modes of the molecule, aiding in the transfer of energy towards the process of catalysis.

2.8   Conclusions

The treatment by Bartholomay was reformulated by van Kampen through his omega expansion. The (N, M) state space, for substrate and enzyme-substrate complex molecules, respectively, was split in two spaces:

- A state space for the macroscopic concentrations. This reproduces the dynamics of the Michaelis-Menten that are found in textbooks.
- A state space for the fluctuations, known as the fluctuation space. It is studied through time dependent Ornstein-Uhlenbeck processes, adding to the understanding of the enzymatic reaction kinetics that can be described by the Michaelis-Menten model.

A simulation based in the Gillespie algorithm allows a clear configuration of the quasi-stationary state under study. The theory and the simulation help us demonstrate that the probability density in the fluctuation space is a gaussian function that rotates clockwise. The auto-correlation functions tend to a constant at the end of this stage.

The formalism of stochastic velocities proves useful when studying the fluctuations described by gaussian probability densities. The curl of the total stochastic velocity is negative, explaining the tendency of the probability density to rotate. It is this tendency to rotate that explains the lack of detailed balance during the quasi-stationary state

The estimation of the entropy displays a sudden increase in its value once the reaction starts, and a subsequent minor descent as it progresses. Here, two important aspects of the process combine:

1. The increase in entropy indicates a spontaneous chemical reaction.
2. Its descent supports the existence of a rearrangement process during catalysis, as well as the presence of work being performed on the system.

We propose that the source of this energy are the normal vibration modes of the enzyme inside a medium at a given temperature. This also backs up the negative sign in the change of heat capacity at constant pressure, C_p, that has been found by other researchers, who consider it a fundamental part for the existence of an optimal temperature in the efficiency of the catalytic ability of enzymes. The Michaelis-Menten model has been notably successful in this aspect, but it shows an important limitation when quantitatively predicting the magnitude of the descent of C_p.

3 Chapter II: A finite Hopfield neural network model for the oxygenation of hemoglobin

3.1 Objective

In the present chapter we develop a model based in a finite Hopfield neural network to analyze the oxygenation process of Hb, to explore the extent of the similarities between experimental ODCs (Oxygen Dissociation Curves) and the simulated saturation curves, based in a small set of hypotheses. It seeks to simulate the phenomenon within the lung alveoli as a probabilistic process governed by the probability that each of the four binding sites of an Hb molecule is occupied or vacant. The oxygen partial pressure, PO_2, is introduced as an external field. The influence between the binding sites in an Hb molecule is added by a cooperativity parameter J, which represents an interaction between the binding sites. The term used is analogous to a ferromagnetic system that can be described by the Ising model of spins, where the spin of a particle can affect the spin of its neighbors. The neural network simulation lets us obtain ODCs, which are then analyzed in order to explore their possible compatibilities with the ODCs used in scientific literature and medical practice. The finite nature of the network grants the possibility of adjusting the model to nanometric oxygenation devices.

This work is organized as follows: Section 2 shows the complexity of the system by means of a brief review of the physical and chemical aspects involved in the natural process of oxygenation of Hb. The usual reasoning behind obtaining the ODC from the mass action law is revised, as well as the properties of the resulting Hill equation from an analysis of the system in equilibrium. Section 3 presents our probabilistic approach based in neural networks. It is pointed out that this model depends on two parameters: the cooperativity parameter, J; and the network temperature parameter, T. We briefly discuss the usual form of the transition rates, $w_\pm$ [42]; and show the results of a simulation to explain how these change with the partial pressure of oxygen, PO_2. In the fourth section we present the simulation results to clarify how the oxygen saturation in Hb evolves with time, given a value of PO_2, therefore identifying the tendency towards equilibrium. An estimation is made to explore the relation between the algorithmic time of the network and the real oxygenation time of Hb in the alveoli. We obtain simulated ODCs for different values of J and inspect their relation to the ODCs found in experiments. In the fifth section we revise qualitative aspects of the simulated ODCs and their relation to the P_{50} parameter. In the sixth section we obtain values of the Hill coefficient, n_H; partial pressure at half saturation, P_{50}; and k_D (which we define as the inverse of the constant equilibrium k), as well as the values of maximum saturation for various pairs of J and T. In the seventh section the numerical values of the parameters obtained from the resulting simulation data is shown. In the eight section the find the relation between parameters n_H and P_{50} to cooperativity parameter J. In the ninth section we establish the relation between the network temperature T, and the temperature in Celsius of the medium of the Hb, T_h. In the tenth section the connection between J and experimental pH is revealed. In the eleventh section we study the Gibbs free energy, and in the twelfth section the value of the enthalpy for the values of J considered relevant. The behavior of the noise in terms of the model parameters is analyzed in its

own section. A brief discussion follows in the further section and conclusions are presented in their own section. The appendix provides various tables of simulation data.

3.2   Complexity of the physical system

3.2.1   Some physical and chemical aspects of the Hb structure

The proteins are considered dynamic systems due to their complex structures and because their functions depend on their interactions with other particles. These interactions can have subtle effects or made very evident in the folding or de-folding of the protein structure, that is to say, their conformational changes. Their functions often involve the reversible binding of other particles, these are called ligands or substrates, and they may be any kind of particle, from a simple ion to another protein. The reversible nature of said interactions are considered critical to life as we know it, as they allow organisms to perform a myriad of processes, digestion and DNA replication being examples of them.

A ligand binds to a specific part of the surface of the protein called the binding site or active site, which is complementary to the shape, size and charge density of the ligand. This causes the protein to display a distinctive property, that of specificity, which is the ability of the protein to discriminate among the various particles in the medium and selectively bind to one or a small set of ligands. The binding process involves a conformational change of both the ligand and the protein, resulting in a tighter binding between the two. In the case of a multi-subunit protein, like the hemoglobin, this induced fitting of one subunit often affects the shape of the other subunits; like increasing or diminishing the affinity of the protein to the ligand.

The binding of ligands may be regulated by the binding of effector molecules to sites different than the binding or active sites, called allosteric sites; these may cause conformational changes in the protein that can either activate or deactivate the protein's binding abilities, thus boosting or diminishing the catalytic or transport activity the protein population realizes.

To have an efficient distribution of oxygen, large multicellular animals depend on proteins responsible of oxygen transportation to the various tissues of a living organism. To carry out this duty, a heme prosthetic group, which is a protoporphyrin ring with an iron atom in its ferrous (Fe^{2+}) state as its core, is often part of a protein structure; this is so the iron atom in the prosthetic group binds to the oxygen molecule, and the protein fulfills the role of transporting the oxygen molecule through the body to the tissues that require it.

One kind of oxygen-carrying protein is myoglobin, which is a relatively simple oxygen-binding protein primarily found in muscle tissue. Myoglobin is part of the globin family of proteins and is constituted a single polypeptide unit of 153 amino acid residues with one heme molecule.

Hemoglobin, found in erythrocytes, is another oxygen-carrying protein and serves as transport for most of the oxygen in the blood in animals. It is a tetrameric protein containing four heme groups associated with each subunit, it has a roughly spherical shape with a diameter of approximately 5.5

nm. Adult hemoglobin contains two alfa chains, each with 141 amino-acids each, and two beta chains, with 146 each.

Its purpose as a transport protein means that it must bind oxygen efficiently in the lungs and release it in the tissues that require it. An important aspect of hemoglobin that allows it to fulfill this purpose is its variable affinity, which changes depending on the concentration of dissolved oxygen in the medium, of 2,3 biphosphoglycerate (2, 3 BPG), temperature and pH level caused by cellular respiration of the tissues; these can affect the affinity of hemoglobin and facilitate the binding or release of O2. This aspect makes it a better transport protein than myoglobin, which is relatively insensitive to these changes.

This variability in affinity is given the name of cooperativity, and it is understood as the alteration in the ease of binding of subsequent ligands after the binding of an initial ligand. This property can be observed in a plot of initial rates as a function of initial substrate concentrations, where the behavior displayed is a nonhyperbolic curve. For hemoglobin, this means that upon the binding of an oxygen molecule to one of its four binding sites, the next O_2 will have an easier time binding to one of the remaining three, then the third molecule will experience the same phenomenon, as does the fourth. This kind of cooperativity is called positive cooperativity, and it involves a series of complex conformational changes of the protein.

It is thought there are two major states: the R (relaxed) state and the T (tense) state; although it is possible for oxygen to bind to both states, it has a significantly higher affinity to the R state of hemoglobin. When an O_2 binds weakly to one of the subunits in the T state, it triggers a change to the R state, this in turn changes the affinity of the other subunits, facilitating the binding of other oxygen molecules. The last O_2 molecule to bind is thought to do so to a subunit already in the R state, which has a higher affinity than the first subunit.

There are two models that suggest mechanisms explaining the cooperative binding of ligands to multi-subunit proteins:

- Concerted model: It assumes that all subunits undergo the transition from T to R state simultaneously. The ligand can bind to any conformation but binds more readily to the R state. The successive binding of a ligand makes a transition from the low-affinity state to the high-affinity state more likely.
- Sequential model: The binding of a ligand can induce a conformational change in an individual subunit, subsequently this subunit can trigger one such change in an adjacent subunit as well as increasing the likelihood of the binding a second ligand.

It is worth mentioning that these are not mutually exclusive.

Hb is a complex macromolecule, thus small changes in its structure can cause blood disorders; as is the case of sickle-cell anemia, a genetic disease caused by a substitution of a Glu6 to Val6 in each beta subunit. This change produces a hydrophobic patch on the macromolecule's surface, causing it to aggregate into fibers. Another is the oxidation state of the iron core of at least one of the heme

groups in Hb, if it's in the ferric state (Fe^{3+}) instead of the ferrous state (Fe^{2+}) the oxygen affinity of the remaining hem sites is increased, leading to a reduced ability of the Hb to release the O_2 to the surrounding medium, causing tissue hypoxia.

3.2.2 Obtaining the oxygen-hemoglobin dissociation curve (ODC) through the law of mass action

The Hill equation is a simple expression often used to fit experimental data to an ODC. With the purpose of clarifying the theoretical foundation of this method, we proceed with an examination of the usual manner with which it is obtained in the literature.

The oxygenation process of a Hb is realized in four stages, one for each of the four Fe atoms seated at the center of a porphyrin ring. Schematically it is represented as follows:

$$
\begin{aligned}
Hb + O_2 &\underset{k_r}{\overset{k_f}{\rightleftharpoons}} HbO_2 \\
HbO_2 + O_2 &\underset{k_r}{\overset{k_f}{\rightleftharpoons}} HbO_4 \\
HbO_4 + O_2 &\underset{k_r}{\overset{k_f}{\rightleftharpoons}} HbO_6 \\
HbO_6 + O_2 &\underset{k_r}{\overset{k_f}{\rightleftharpoons}} HbO_8
\end{aligned}
\tag{136}
$$

Where $k_i, i = 1, \dots, 4$, are the equilibrium constants. From now on, $[X]$ denotes the concentration of a chemical substance X. Using the law of mass action, the next expressions will follow:

$$
\begin{aligned}
\frac{[HbO_2]}{[Hb][O_2]} &= k_1 \\[1em]
\frac{[HbO_4]}{[HbO_2][O_2]} &= k_2 \\[1em]
\frac{[HbO_6]}{[HbO_4][O_2]} &= k_3 \\[1em]
\frac{[HbO_8]}{[HbO_6][O_2]} &= k_4
\end{aligned}
\tag{137}
$$

Operating on them and defining $k = k_1 k_2 k_3 k_4$, results:

$$
k = \frac{[HbO_8]}{[Hb]([O_2])^4}
\tag{138}
$$

From this expression, (139) can be obtained

$$
[HbO_8] = k[Hb]([O_2])^4
\tag{139}
$$

If one is to suppose that the four reactions occur so rapidly that all Hb molecules are found in their oxygenated state HbO_8, so that all other intermediate states are irrelevant for the analysis, it can be established that

$$
[Hb]_{tot} = [Hb] + [HbO_8]
\tag{140}
$$

Now defining the oxygen saturation in hemoglobin, Sa_{O_2}, as

$$Sa_{O_2} = \frac{[HbO_8]}{[Hb]_{tot}} \tag{141}$$

From (139) and (140), (141) becomes

$$Sa_{O_2} = \frac{k[Hb]([O_2])^4}{[Hb] + [HbO_8]} = \frac{k[Hb]([O_2])^4}{[Hb] + k[Hb]([O_2])^4} \tag{142}$$

$$Sa_{O_2} = \frac{k([O_2])^4}{1 + k([O_2])^4} \tag{143}$$

Expression (143) bears a close resemblance to the Hill equation found in literature. The Hill equation for the hemoglobin is shown below

$$S_{HbO_2} = \frac{k([O_2])^{n_H}}{1 + k([O_2])^{n_H}} \tag{144}$$

Where n_H is given the name of Hill coefficient. The form with which it will be utilized in this work is

$$S_{HbO_2} = \frac{([O_2])^{n_H}}{k_D + ([O_2])^{n_H}} \tag{145}$$

With $k_D = \frac{1}{k}$.

Therefore, it is clear that there are two hypotheses sustaining (145):

- The law of mass action is applicable.
- The intermediate oxygenation states are irrelevant.

3.2.3 Analysis of the sigmoid function

Next is shown the expression for the ODC, and the importance of parameters k_D and n_H will be made evident further below

$$\theta(x) = \frac{x^{n_H}}{k_D + x^{n_H}} \tag{146}$$

It is easily demonstrable that $\lim_{x \to \infty} \theta(x) = 1$ and $\lim_{x \to 0} \theta(x) = 0$ are satisfied, from these it follows that for $x \geq 0$ it is true that $0 \leq \theta \leq 1$. Also, if we are to define the midpoint of $\theta(x)$ as $\theta_m = \theta(x_m) = \frac{1}{2}$ it is straightforward to demonstrate that

$$x_m = k_D^{\frac{1}{n_H}} \tag{147}$$

Where it is plain to see that the value of x_m is determined by the Hill coefficient n_H and by k_D.

Studying the derivative of $\theta(x)$

$$\theta'(x) = \frac{n_H x^{n_H - 1}}{k_D + x^{n_H}} - \frac{x^{n_H}}{(k_D + x^{n_H})^2} \tag{148}$$

one can see that it has an asymptotic conduct: a) $\lim\limits_{x \to \infty} \theta'(x) = 0$, b) $\lim\limits_{x \to 0} \theta'(x) = 0$. Hence, $\theta'(x)$ must have an extreme point x_2 that can be found by setting to zero de derivative:

$$x_2 = \left[\frac{k_D (n_H - 1)}{n_H + 1} \right]^{\frac{1}{n_H}} \tag{149}$$

This is the point where the sigmoid curve $\theta(x)$ reaches its highest slope. By calculating $\theta'(x_2)$ one can find the highest value that the Hill curve can take.

In this work the independent variable will be x, which is the partial pressure, PO_2, divided by 100: $x = \frac{PO_2}{100}$, with range $0 \le x \le 1$. The saturation Sa_{O_2}, is the dependent variable. It will be denoted as $\theta(x)$ and can be in the range $0 \le \theta \le 1$, or with percentage to connect with the language used in medical practice.

This work calls into question the validity of the hypotheses that arrive to expression (146), due to the following reasons:

- It rests on the law of mass action which, according to statistical physics, is only valid if the process is in dynamic equilibrium. Instead, we set out from the fact that there is a gradient of PO_2 between the interior of the erythrocyte and the surrounding medium that influences the oxygenation process of Hb, and this gradient is such that it transfers O_2 molecules from the exterior into the erythrocyte and eventually towards the Hb bindings sites. Therefore, this is an out of equilibrium process where oxygenation occurs when the system is proceeding towards equilibrium.
- It also supposes that the intermediate states of Hb oxygenation are irrelevant, when it is not necessarily true since the erythrocyte remains in the lung alveoli between 0.2 and 0.75 seconds. It is sound to assume that the forms HbO_{2r}, with $r = 0,1,2,3$ are also present.

3.3   Probabilistic approach and neural network method

The phenomenon of O_2 capture by an iron atom located at the core of a porphyrin ring is of a stochastic nature that depends on many factors. Some of these have already been mentioned above, in the section that addresses the complexity of the system. In essence, this problem is a process of diffusion of an ensemble of O_2 gas molecules that come near an erythrocyte, penetrate it, and then follow a random path among many Hb molecules with which they can collide with. A collision between an O_2 and an Hb can happen at any part of the geometry of the Hb molecule, some of which could occur where there is a Fe atom with which they can bind to, but also against parts where binding cannot happen. Therefore, every O_2 molecule bound to an iron core is the result of a successful collision that does not occur with a probability of 1.

What has been said thus far can be synthesized as the need to formulate a model that contemplates the stochastic nature of O_2 binding to an Hb. The probabilistic focus being developed in this work

seeks to attend this problem. By doing so it tries to simplify all fortuitous aspects that influence this process into a single fact: that the binding either happens or it does not. This approach consists in considering that each binding site has a probability of becoming occupied or vacant. The simplicity of this model arises from the use of only two parameters in the description of the transition rates: The parameter J, related to the cooperativity; and the parameter T, called the temperature of the neural network, which is related to the temperature of the medium of the hemoglobin, T_h.

The optimization method for the transport of oxygen in blood is based on the affinity of the Hb molecule towards O_2, but affinity can change rapidly when erythrocytes pass through blood vessels. This is due to allosteric effects caused by substances acting on the Hb, such as 2,3-Bisphosphoglyceric acid, hydrogen ions and CO_2.

This model supposes that all external agents can be represented by the cooperativity parameter J, regardless of the number of different types of compounds involved. The challenge is determining how much information can be elucidated from these simplifications.

Statistical conclusions are taken in this work by using 500 or 100 realizations. This criterion is based on the central limit theorem. According to this, if one has a population with mean μ, from where a sample of size n and mean $\langle x \rangle$ is taken, the theorem describes how the distribution of the difference in the sample and population means ($\langle x \rangle - \mu$) changes with respect to the sample size. Pfanzagl and Sheynin [76] show that the error decreases as $\pm \sqrt{\frac{\pi-2}{2(n-1)}}$, so that for $n = 30$ one finds that this goes from ± 0.53 if $n = 3$ to ± 0.14 when $n = 30$. The significance of this is that the convergence happens fairly quickly, and for this reason the practice has been to consider that $n \geq 30$ is sufficient. On the other hand, for small samples these results do not hold and the t-distribution is more appropriate.

3.3.1   Transition rate and its behavior during the simulation

We consider a physical system comprised of M macromolecules, each with n binding sites; making up a total of $N = nM$ binding sites, each of which can be modeled by a bivalued variable σ_i, with $i = 1, \dots, N$. When the i-th binding site is vacant $\sigma_i = -1$, and when it captures an O_2 molecule $\sigma_i = +1$. Considering that the Hopfield neural network is based on the Ising spin model, it is possible to make an analogy between a neuron that sends a $+1$ or -1 signal, a binding site that is occupied or vacant, and a spin that is aligned with or against an external magnetic field $\vec{\mathcal{H}}$. The interconnection of the neurons in the network can be understood as the interaction between neighboring spins; this interaction generates a field that adds to the external field that represents PO_2. Such a system can be described as a vector state:

$$\vec{\sigma} = (\sigma_1, \sigma_2, \dots, \sigma_N)$$

In statistical physics, a system at a temperature T with N distinct states, each with energy E_i is said to follow that the probability for a state to be occupied can be described by

$$P(E_i) = \frac{e^{-\beta E_i}}{Q}$$

where $Q = \sum_j e^{-\beta E_j}$ is the partition function. For a system with two states such that its energies are $E = \pm\mu H$, $P(E_i)$ takes the form of

$$P_\pm = \frac{e^{\pm\beta\mu H}}{e^{\beta\mu H} + e^{-\beta\mu H}}$$

Two transition rates can be proposed, each taking the form

$$w_\pm = \frac{1}{2}[1 \pm \tanh\beta\mu H]$$

such that each state σ_i has a probability rate w_+ of its spin to point upwards, aligned parallel to an external field H, or w_- to point downwards, aligned antiparallel to H. For a neural network operating at a temperature T, the external field H is given by the next expression:

$$H = h + h_r$$

where h is the field resulting from a parameter that controls the experiment, which in this work is the oxygen partial pressure divided over 100, and $h_r = \sum_{j=0}^{r} J_{ij}\sigma_j$, that corresponds to the mutual influence between the r neighboring states that give rise to cooperativity. The factor J_{ij} is a measure of this mutual influence between states i and j.
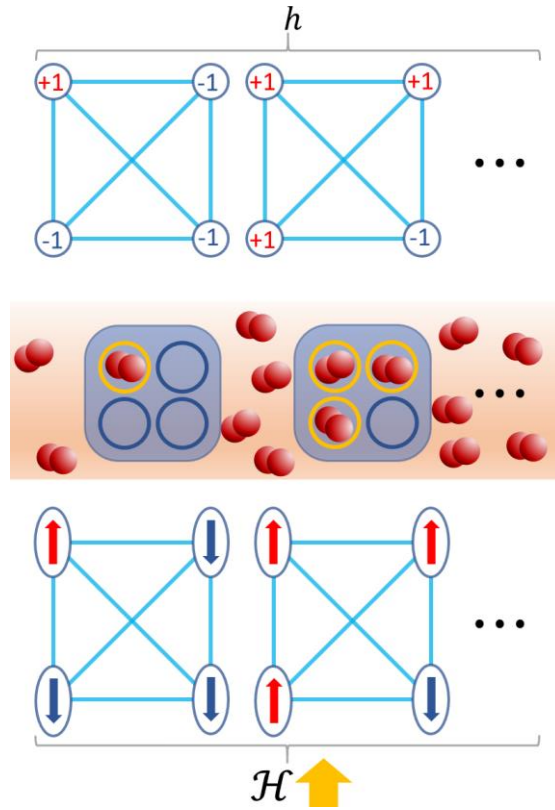
Figure 16. Three model analogies. An occupied site is assigned the value of $+1$ and -1 if it is vacant.
Each $+1$ is a spin aligned with external field $\vec{H}$ and -1 aligned against it.

This model was adapted to the case of one hemoglobin, with 4 binding sites each capable of binding to an O_2 molecule. The simplest model consists in supposing that all interactions between these four sites is equal. We propose:

$$h_1 = 0, h_r = J \sum_{j=0}^{r} \sigma_j , r = 2,3,4$$

So that the argument of the hyperbolic tangent is modified during the process of capturing O_2 of the hemoglobin.

In order to understand the change in the transition rates during the simulation, we studied the $w_\pm$ in the neural network when $J = 0.35$ and $T = 0.75$. Five hundred realizations were carried out and the mean and standard deviations were calculated for each value of $x = \frac{PO_2}{100}$. The resulting plots are shown in Figure 17:
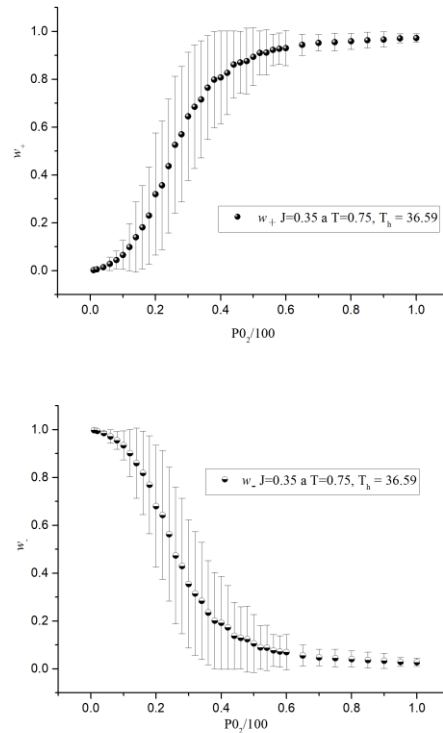
Figure 17. Values of $w_{\pm}$ as function of PO_2 for sufficiently long times. w_+ tends to 1, while w_- tends to zero. Black dots represent mean values, vertical bars are standard deviations. The latter tends to zero at the extremes and take higher values in the transition between vacant to occupied states. Statistical calculations were performed over 500 realizations. $J = 0.35, T = 0.75$.

One can observe that w_+ asymptotically grows towards 1, while w_- decreases towards 0. The vertical bars indicate the magnitude of the standard deviation of the probabilities; these make evident the relevancy of the random nature of the process. From this it results that the probabilities of occupation, w_+, tend towards 1, while that of vacancy, w_-, tend towards 0.

3.4   Computer simulation and its methodological significance

In this section we present the results from the simulations and explain their meaning. The scenario that is being sought to simulate is that of an ensemble of deoxygenated Hb molecules that enter a lung alveolus. Once there they find themselves within a medium with a high concentration of O_2. The O_2 molecules travel between many Hb molecules and are subject to collisions, some of these will be against iron atoms from an Hb, and some of these will have enough energy for the O_2 to bind to an iron atom. From the perspective of one of the Hb molecules, an iron atom from one of its four porphyrin rings will suddenly bind to an O_2. This is a stochastic phenomenon that can occur with probability w_+. Similarly, the process of a loss of an O_2 can occur with probability w_-. It is notable that both w_+ and w_- are equal only in two cases: when $PO_2 = 0$, and when all binding sites are

vacant. When PO_2 increases, so does w_+ but w_- decreases; when that happens, O_2 molecules begin to bind to Hb binding sites, triggering the phenomenon of cooperativity, which also affects the increase in w_+. If PO_2 is kept constant, the saturation reaches a level where the fluctuations of saturation are around a stable value.

This oxygenation phenomenon develops in real time while the Hb is inside the lung alveoli. This real time is related to an algorithmic time of the neural network. This algorithmic time is the time that transpires during the iteration of the network, such that, given a PO_2 value, the oxygen saturation increases until reaching a stable value.

Due to the fact that each erythrocyte carries approximately 2.7×10^8 Hb molecules [77], it is possible to apply the limit when the number of neurons tend to infinity, nonetheless, beside the increase in computational demands, they leave out the effects that may appear if there is intention of designing nanometric artificial oxygenator devices. These could consist of cylindrical gas exchangers, or other artificial nanostructures, of which Hb molecules are made to flow through. In the case of small devices, these could be placed inside intravenous catheters used in the treatment of patients with acute or chronic lung deficiencies [78]. A mathematical model that studies this phenomenon can be consulted in [79]. In extremely small devices what will happen is that the reduction in participating molecules will increase the presence of the random nature of the phenomenon, giving way to the presence of noise that must be accounted when designing such devices.

The presence of noise due the reduction in size can be replicated by a neural network model if it is finite in size, with the advantage of preserving the macroscopic properties by means of calculating the averages of the participating quantities.

3.5 Results and interpretation

3.5.1 Algorithmic time and real time

When a neural network is updated through a sequential dynamic process, it is considered that one unit of time corresponds to N update cycles; thus, a single cycle is associated to a time step of $\Delta t_a = \frac{1}{N}$. Here we call this the algorithmic time t_a. In a process of 2×10^4 iterations, the final algorithmic time is $t_a = 10$. The units of t_a don't have a direct physical meaning, but it is possible to draw a relation between them and the real oxygenation process. For this purpose, it is considered that each red blood cell remains within the lung alveoli $0.2\ s < t_a < 0.75\ s$. Therefore, $1\ t_a = 7.5 \times 10^{-2}\ s$ for the case of the largest value in the range of t_a.

In Figure 18 the reader can see the evolution process of a neural network with the cooperativity parameter $J = 0.35$ and network temperature $T = 0.75$, which, as will be demonstrated later in this chapter, corresponds to a hemoglobin temperature $T_h = 36.59\ °C$. The update process of the neural network simulates the binding of O_2 to a portion $M = 500$ hemoglobin molecules (making a total of $N = 2000$ binding sites. This system, as previously mentioned, is about the transit of Hb molecules through the lung alveoli that causes them to undergo a non-equilibrium process
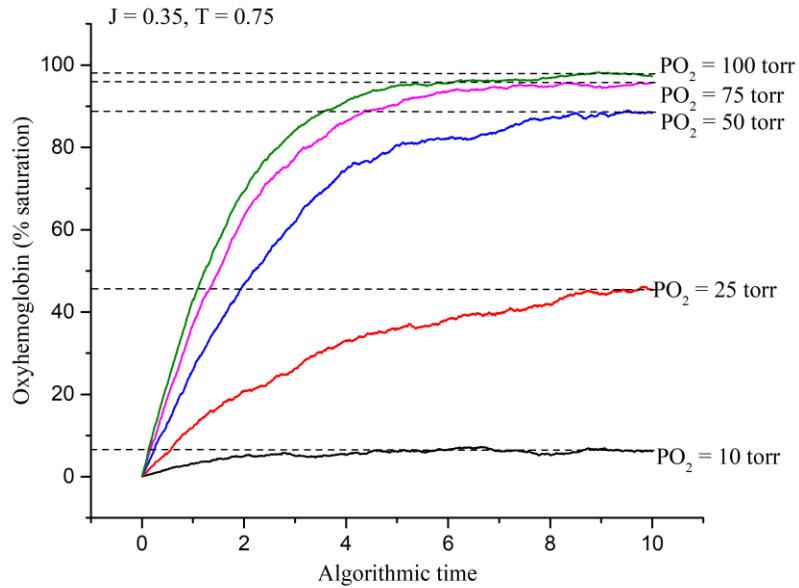
Figure 18. Hemoglobin saturation percentage as a function of algorithmic time. PO_2 is a fixed parameter for each curve. The saturation increases asymptotically until an equilibrium value is reached. $J = 0.35$, $T = 0.75$.

This system, as previously mentioned, is about Hb molecules undergoing a non-thermodynamic equilibrium process as a consequence of being carried through the lung alveoli, where there exists a transference of O_2 molecules from the surrounding medium towards the Hb binding sites. Figure 18 shows the time evolution of one realization of five cases with different PO_2. Dynamic equilibrium is reached once the evolution curves asymptotically approach a horizontal line. The final values of partial pressure of oxygen and saturation are shown in Table 8, where it can be appreciated that higher PO_2 correspond to higher saturation values. Going forward, the focus of this study will be the end state of the system, in other words, the equilibrium state.

PO_2 (torr)	θ_{end} (%)
10	6.1
25	45.4
50	88.4
75	95.7
100	97.25

Table 8. Asymptotic values (long times) of oxygen saturation for the given partial pressures. The left-hand column is the partial pressure of oxygen. The right-hand column is the saturation value at the given partial pressure.

3.5.2 Equilibrium state

The next step in the simulation process was the study of the equilibrium states. For this purpose, a list of the PO_2 values used by Severinghaus [80] was created, then picked the first PO_2 value from the list, set the network temperature T and the cooperativity parameter J. One hundred realizations were carried out, each with 2×10^4 iterations. In each realization the final value of the normalized occupation number was recorded, and from the 100 realizations simple statistical calculations were performed, producing a set of three data values: the mean occupation number $\langle s \rangle$, where $-1 \leq \langle s \rangle \leq 1$; the standard deviation, σ_s; and the PO_2 value. Each value of $\langle s \rangle$ is transformed using $\theta = \frac{\langle s \rangle + 1}{2}$, where $0 \leq \theta \leq 1$. This way 39 (x, θ) data pairs can be generated for any given pair of (J, T). The values of J considered were $J = 0.35 + 0.5j$, with $j = 0, \dots, 10$; and the range of T that were used for the majority of simulations was $0.55 \leq T \leq 0.80$, with a $\Delta T = 0.5$ between each value of T.

The end products were sigmoidal curves of which properties are studied in further sections. These are compared with the properties displayed by the ODCs utilized in medical practice and scientific research. We then show that these are compatible with the results of the simulations in this work.

3.5.3 Affinity

In this section we review the relation between the parameter J introduced in this model with the concept of affinity used in physical chemistry studies of hemoglobin. Figure 19 shows that as J increases the ODC shifts to the left and vice versa. This phenomenon related to the pH in the medium surrounding the Hb, as well as the aspects of the values of P_{50} of the simulation, will be discussed in sections below.
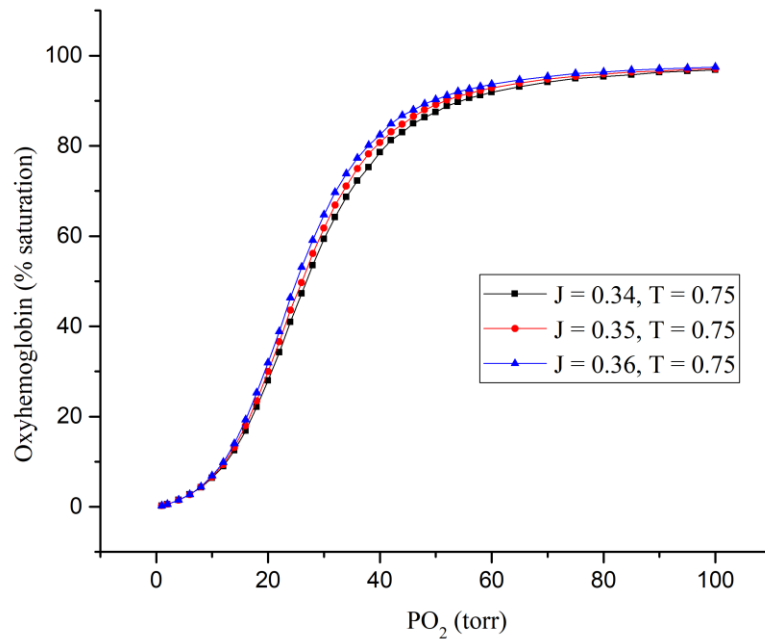
Figure 19. Hemoglobin oxygenation percentage as a function of PO_2. Statistical calculations were performed over 100 realizations. The curves take a sigmoidal shape. When affinity grows the curve shifts to the left. $T = 0.75$, $J = 0.34, 0.5, 0.36$.

It is possible to compare the results from the simulation with parameters $J = 0.35$ and $T = 0.75$ with that of adult hemoglobin. Figure 20 displays data measured by Severinghaus [80], along with the simulation with $N = 2000$ neurons organized in $M = 500$ Hb molecules using the parameters of J and T mentioned earlier, and with a curve fitted using the Hill equation with parameters n_H and k_D. The simulated curve is the result of averaging 100 realizations, the red and blue dashed curves indicate the region of random fluctuations of θ; the curve of Severinghaus falls within this region.
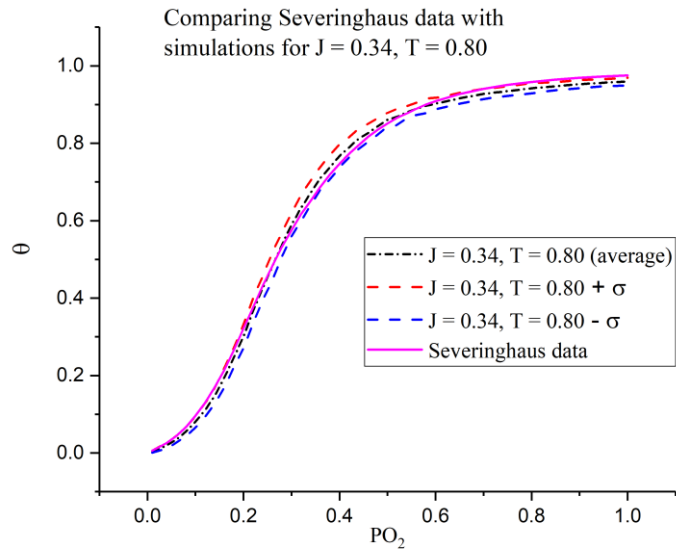
Figure 20. Hemoglobin oxygenation percentage θ as a function of normalized PO_2. Mean curve contained within the region demarcated by the standard deviation. Fluctuations are greater in the transition between vacant binding sites to occupied binding sites.

The difference between these three curves is small enough to have grounds for believing that a neural network may be of use to simulate an ODC.

3.6   Qualitative aspects based on the P_{50} value

In this section we explore the relation between the P_{50} obtained through the simulation with a variety of P_{50} values found in the medical practice. Figure 21 presents which values of the pair (J, T) give simulated OCDs with P_{50} values that lie within regions known in the literature to be associated with fetal Hb (19.8 $torr$), Hb from infants younger than 10 months of age (30 $torr$), and adult Hb (26.8 $torr$).
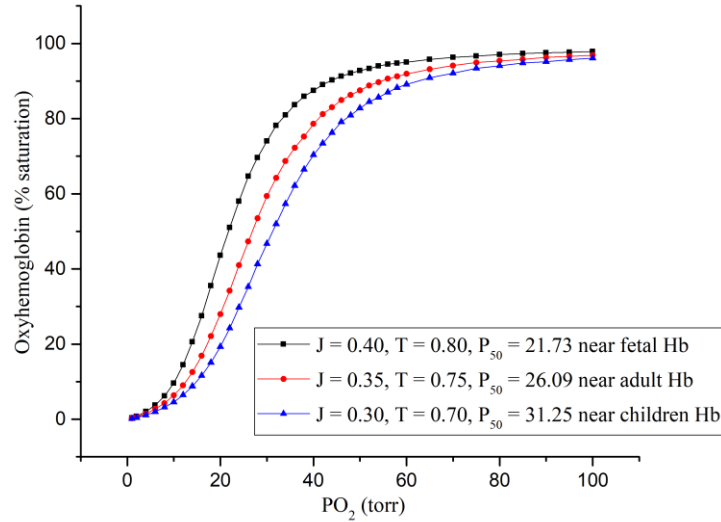
Figure 21. Hemoglobin oxygenation percentage as a function of PO_2. Statistical calculations were performed over 100 realizations. Modifications in the values of J and T qualitatively replicate cases of hemoglobin found in fetal, adult and infant younger than 10 months subjects.

Figure 21 illustrates the manner with which this model operates. Fetal hemoglobin differs from adult hemoglobin in two β subunits being substituted by two γ subunits, in other words, adult hemoglobin is formed by $\alpha_2\beta_2$ chains and fetal hemoglobin by $\alpha_2\gamma_2$ chains. The space where 2,3-Bisphosphoglyceric acid (2,3-BPG) would fit in adult hemoglobin also differs in fetal hemoglobin; while in the adult form the residues in this space are positively charged, in the fetal form these are neutral. Due to the negative charge of 2,3-BPG, it can easily bind to adult Hb, causing allosteric changes in the molecule that result in a decrease in affinity to O_2; in fetal Hb these changes do not take place, hence affinity remains unchanged, this way the hemoglobin of the fetus can compete with that of the mother in the capturing of oxygen. The model presented here condenses these aspects of the physical system into parameters J and T.

3.7 Obtaining parameters n_H, P_{50}, k_D and θ_{max}

Denoting saturation as θ and $x = P_{50}$, the Hill equation can be written as

$$\theta(x) = \frac{x^{n_H}}{k_D + x^{n_H}} \tag{150}$$

with $k_D = \frac{1}{k}$. This saturation parameter θ provides the saturation percentage when multiplied by 100.

The method of obtaining n_H is delineated next:

1. The 39 ordered pairs (x, θ) were used to compile a list of 39 data pairs of the form $\left(\ln x, \ln\frac{\theta}{1-\theta}\right)$.

66

2. Of the pair compiled in point 1, the numerical derivative was calculated using a finite difference method.
3. Finally, the mean of the local derivatives was found.

In Figures 22 and 23 are shown the curves obtained when $J = 0.35$ and $T = 0.75$ in points 1 and 2 respectively, where the obtained value was $n_H = 2.82864$
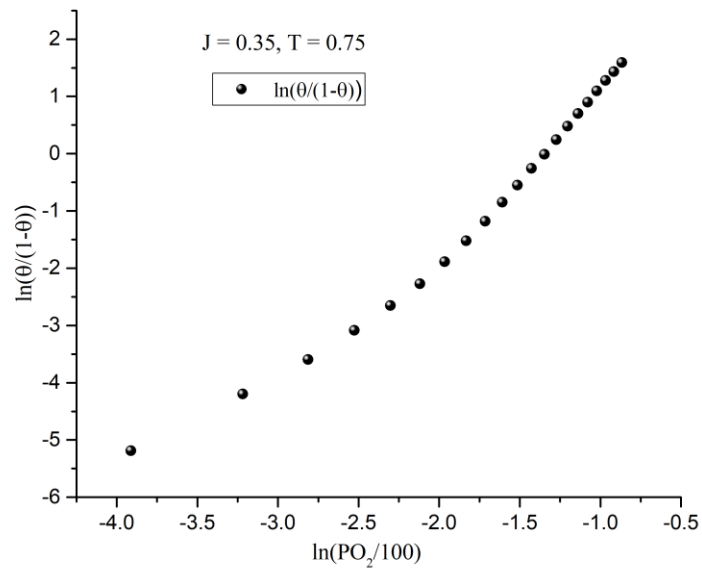
Figure 22. Values of $\ln \frac{\theta}{1-\theta}$ as function of normalized PO_2. Statistical calculation were performed over 100 realizations. Process for obtaining the parameters for a Hill curve. Shown here is for $J = 0.35, T = 0.75$.
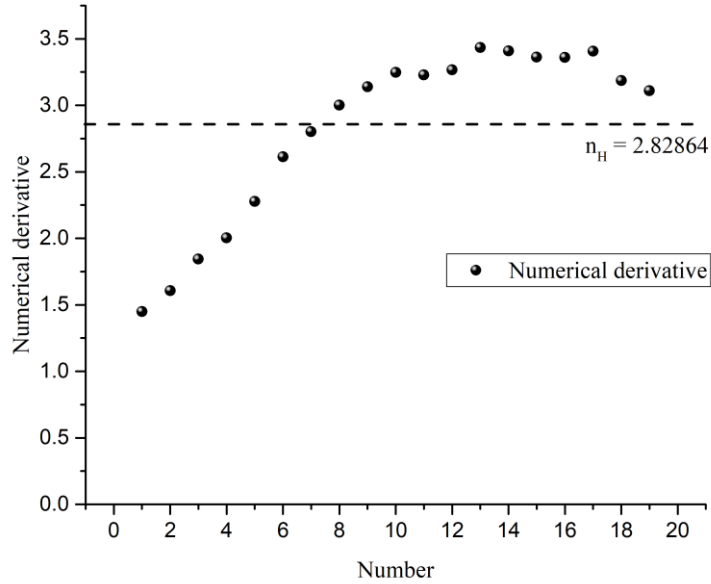
Figure 23. Numerical derivative of the curve shown in Figure 22. Statistical calculations performed over 100 realizations. Its mean is interpreted as the Hill coefficient n_H.

To calculate the P_{50}, the method used is delineated next:

1. A pair (x_1, θ_1) is taken such that θ_1 is the value immediately before $\theta = 0.5$, and a pair (x_2, θ_2) is taken such that θ_2 is the value immediately after $\theta = 0.5$.
2. The slope of the line joining (x_1, θ_1) and (x_2, θ_2) was calculated.

The value of k_D was calculated by the expression $k_D = P_{50}^{n_H}$. These values were plugged into the Hill equation and plotted along with a simulated ODC, as shown in Figure 24.
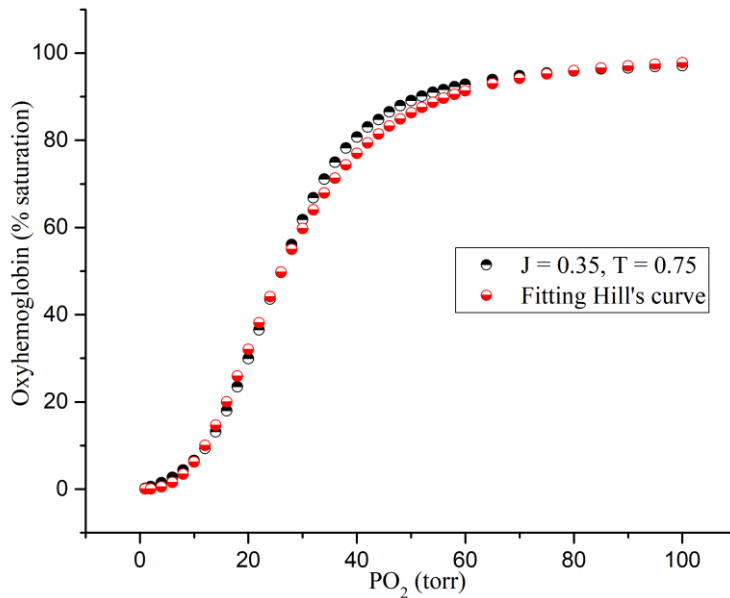
Figure 24. Comparison between the Hill curve produced by k_D and n_H and the mean curve given by the neural network simulation. Statistical calculations were performed over 100 realizations. $J = 0.35$, $T = 0.75$.

The curves match closely in the region with 50% saturation and in the asymptotic growth towards θ_{max}, which occurs when $x = 1$, or $PO_2 = 100\ torr$.

3.8 Analysis of simulations

The results offered by this Hopfield neural network model for the ODC are discussed in this section. Simulations were carried out for the ordered pair (J, T) with the values $J = \{0.30, 0.32, 0.34, 0.35, 0.36, 0.38, 0.40\}$ and from $T = 0.50$ to $T = 0.80$, or from $T = 0.60$ to $T = 0.90$ as the case may require. For each (J, T) 100 realizations were carried out to obtain pairs of (x, θ), where x is the normalized PO_2. The saturation variable was also normalized to maintain it within the interval $0 \leq \theta \leq 1$. The resulting data was then scaled to recover the ranges used to measure $PO_2\ (torr)$ and saturation in percentage. As previously explained, once obtaining the data set of each realization, the mean and standard deviation were calculated, forming a three-element data set $\{x, \theta, \sigma_\theta\}$.

With this analysis we composed seven tables, of which one of them is shown below, the remaining six are in the appendix:

T	n_H	P_{50}	k_D	θ_{max}	J
0.55	4.07487	28.087	0.00565865	99.33	0.35

0.60	3.73575	27.292	0.00781959	98.95	0.35
0.65	3.40201	26.712	0.0112116	98.52	0.35
0.70	3.07437	26.266	0.0164068	97.89	0.35
0.75	2.82864	26.095	0.0223698	97.1	0.35
0.80	2.59123	25.783	0.0298295	96.34	0.35

Table 9. Cooperativity parameter, $J = 0.35$, network temperature, T, is on the leftmost column. The calculated values are for: Hill coefficient (n_H), partial pressure at half saturation (P_{50}), dissociation constant (k_D), and maximum saturation achieved (θ_{max}).

In a later section will be demonstrated that the network temperatures $T = \{0.65, 0.70, 0.75\}$ correspond to temperatures $T_h = \{37.23\,°\text{C}, 36.90\,°\text{C}, 36.59\,°\text{C}\}$, which are the temperatures were the hemoglobin is found within a living human. Table 9 lets us reach the next conclusions:

- The method used to calculate the Hill coefficient, n_H, allows the interpretation of it being the average of occupied states over all the points in the ODC. Therefore, the result obtained at $T = 0.55$ lacks any physical meaning. Also, the Hill coefficient is a dimensionless parameter that has been used as a measure of cooperativity, originally obtained by A. V. Hill in 1910 and brought back by J. Wyman in 1964 [81]. This aspect will be further discussed at another section.
- The network temperature range $T = 0.60 + 0.5j$, where $j = 0,1,2,3,4$, offers the P_{50} values considered as normal for human adult hemoglobin. It will later be demonstrated that these correspond to hemoglobin temperatures within the range $36.59 \leq T_h \leq 37.23$, which are the temperatures measured in healthy human adults.
- From temperatures T and T_h presented here it is clear that when T increases T_h decreases. This lets us affirm that if T_h is to decrease, n_H will decrease as well.

3.9   Dependence of n_H and P_{50} of cooperativity J

The relation between the parameters n_H and P_{50} as functions of parameter J is presented in this section. For this it was taken the temperature $T = 0.75$ as a case study and the data found in Tables 9, 16, 17, 18, 19, 20 and 21 were used with the values for the cooperativity parameter J found there. The values for n_H, P_{50} and θ_{max} found were compiled in the next table:

J	n_H	P_{50}	θ_{max}
0.30	2.52804	30.977	94.946
0.32	2.66238	28.829	95.968
0.34	2.77168	26.873	96.876

0.35	2.82864	26.095	97.100
0.36	2.87214	25.092	97.480
0.38	2.98723	23.559	98.048
0.40	3.08659	22.083	98.465

Table 10. Cooperativity parameter (J) is on the leftmost column. The calculated values are the Hill coefficient (n_H), partial pressure at half saturation (P_{50}), and maximum saturation achieved (θ_{max}).

It was found that the values nearest to the healthy adult human vitals are within $0.34 \leq J \leq 0.36$ with $T = 0.75$. Further below ΔpH and other parameters are calculated $J = 0.35$ and $T = 0.75$ using as reference.

Comparing the first and second columns in Table 10, it is evident that n_H linearly increases with J. The equation of the line fitted to this data is shown next:

$$n_H(J) = 0.886388 + 5.52344J$$

From this it results that the derivative $dn_H = C(T)dJ$, where $C(T)$ is a function only of the network temperature T, demonstrating that n_H depends on the cooperativity parameter J. For this case $C(T) = 5.52344$.

Comparing the first and third columns, it can be seen the value of P_{50} diminishes linearly with J. This relation supports the affirmation presented in a previous section that P_{50} is a function of J. The equation of the line fitted is:

$$P_{50}(J) = 57.2436 - 88.6521J$$

This means that an increase in the cooperativity parameter triggers a faster oxygenation process, which can also be seen in the differential equation $dP_{50} = D(T)dJ$. In other words, they are directly proportional. For this case $D(T) = -88.6521$.

Comparing the first and fourth columns shows that the maximum saturation, θ_{max}, increases with J. This relation can be described by a quadratic expression of the form:

$$\theta_{max}(J) = 62.5505 + 162.888J - 182.815J^2$$

From Table 9 one can arguably conclude that the ODC obtained with parameters ($J = 0.75, T = 0.35$) is closest to what the measures of a healthy adult would be like. In the next section will be shown that the Hb temperature for this case is $T_h = 36.59\ °C$, which is close to body temperature of a healthy person. Below we present a comparison between the simulated ODC, the resulting curve from fitting (150) and the data from Severinghaus.
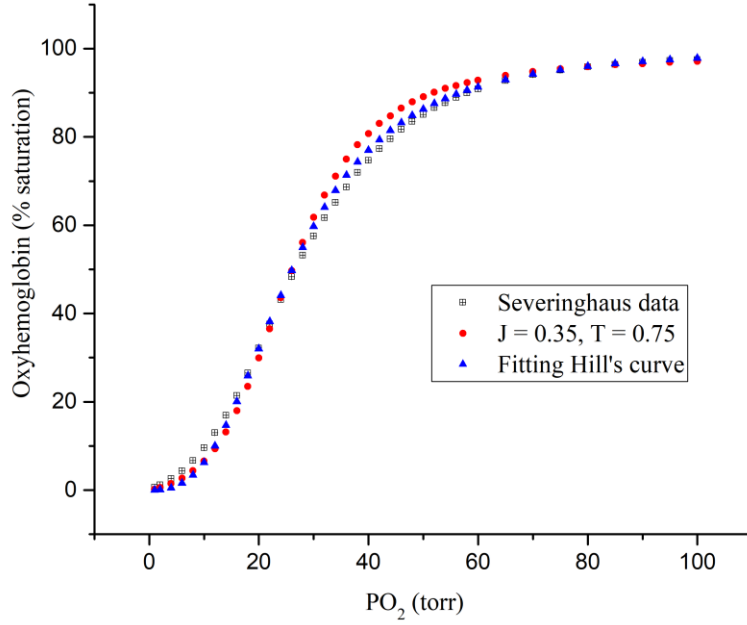
Figure 25. Comparison between the mean curve obtained from the neural network simulation, the Hill curve and the data from Severinghaus [80]. $J = 0.35$, $T = 0.75$. The curves shown share strong similarities.

3.10 Relation between network temperature and hemoglobin temperature

In this section we establish the relation between the neural network temperature T and the hemoglobin temperature T_h. The process consists in:

1. Obtaining a functional relation between P_{50} and T_h through experimental studies found in the scientific literature.
2. Use the simulation data from this work to find another functional relation between P_{50} and T.
3. Match both expressions and establish the relation between T and T_h.

To relate P_{50} and T_h we assume that the expression studied by Samaja *et al.* [82] is true: $\frac{d(\log_{10} x)}{dT_h} = c$, with $x = P_{50}$, and for the conditions considered in the reference $c = 0.0229$. Taking the limit, we obtain the differential equation:

$$\frac{d(\log_{10} x)}{dT_h} = c \tag{151}$$

with T_h measured in Celsius. Considering that $\log_b x = \frac{\ln x}{\ln b}$, it is possible to write (151) as:

$$\frac{d\left(\frac{\ln x}{\ln 10}\right)}{dT_h} = c \tag{152}$$

72

Rearranging and integrating (152), it is possible to rewrite it as

$$ln\, x = (c\, ln\, 10)T_h + c_1 \tag{153}$$

where c_1 is an integration constant. Elevating an exponential in both sides and imposing the conditions: $P_{50} = 10.3\, torr$ if $T_h = 19\,°C$, it results:

$$x(T_h) = P_{50}(T_h) = 3.7821 e^{(c\, ln\, 10)T_h} \tag{154}$$

A numerical approximation for the exponent is $c\, ln\, 10 = 0.0527292$.

From the results reported in Table 9 above and Tables 18 and 19 in the appendix, it is possible to do a line fitting for P_{50} and T:

$$P_{50} = a(J) - b(J)T$$

where $a(J)$ and $b(J)$ take the values shown in the table below:

J	$a(J)$	$b(J)$
0.34	41.996	6.52
0.35	41.3315	6.32571
0.36	42.9142	9.64571

Table 11. Cooperativity parameter (J) is on the leftmost column. Values of the coefficients of the line equation fitted to obtain the dependence of the partial pressure at half saturation (P_{50}) as a function of J.

The line equations were matched with the right-hand side of equation (154), obtaining:

$$a(J) - b(J)T = Ae^{BT_h}$$

with $A = 3.7821$ and $B = c\, ln\, 10 = 0.0527292$. Rearranging results the relation between T and T_h:

$$T_h = \frac{1}{0.0527292} ln\left(\frac{a(J) - b(J)T}{3.7821}\right)$$

This equation produces the next relations between T and T_h:

	$J = 0.34$	$J = 0.35$	$J = 0.36$
T	T_h	T_h	T_h
0.55	38.40	37.84	37.59
0.60	38.09	37.54	37.13

0.65	37.76	37.23	36.66
0.70	37.44	36.91	36.18
0.75	37.11	36.59	35.68
0.80	36.77	36.26	35.18

Table 12. Network temperature (T) is on the leftmost column. Values of the temperature of the medium of the hemoglobin (T_h) when the cooperativity parameter is $J = 0.34, 0.35, 0.36$, respectively.

We have found that there is an inverse proportionality between T and T_h; in other words, as the network temperature T increases, the temperature of the medium of the hemoglobin T_h decreases.

Compiling a table of P_{50} as a function of T_h is straightforward, as is fitting a curve. This was done for $J = 0.5$, and the quadratic equation is:

$$P_{50}(T_h) = 1028.1 - 55.4675T + 0.767422T^2$$

This result matches qualitatively with Figure 5 of Samaja *et al.* [82], as it shows the increase of P_{50} with temperature from 10 °C to 40 °C.

3.11 Relation of pH to the cooperativity parameter J

In this section we show the relation between the cooperativity parameter J with the experimental hydrogen potential pH.

In humans, the normal blood pH levels are found within 7.35 and 7.45. If $pH < 7.0$ it is considered severe acidosis, and if $pH > 8.0$ it is considered severe alkalosis; either of these could be fatal. This indicates that if one is to find a normal value of pH and there is a $\Delta pH = 0.55$ or $\Delta pH = -0.35$, it is classified as abnormal. With this in mind, in this section we establish a relation between parameter J and ΔpH, predicted by the neural network simulation. For this purpose, we set off from the expression found by Reeves [83]:

$$\frac{\Delta(\log_{10} P_{50})}{\Delta(pH)} = B$$

where B is a numerical value within the range $-0.53 \leq B \leq -0.41$. Taking the limit, it gives us the following differential equation:

$$\frac{d(\log_{10} P_{50})}{d(pH)} = B$$

Integrating and solving for pH results:

$$pH(J) = \frac{1}{2.3B} \ln\left(\frac{P_{50}(J)}{P_{50}(J_0)}\right)$$

Considering the network temperature T as constant, then taking the average value of $B = -0.47$ and $J_0 = 0.35$ as reference, Tables 9, 16, 17, 18, 19 and 20 were used to compile Table 13. This should not be mistaken with this meaning that the temperature of the medium of Hb, T_h, is constant.

J	ΔpH
0.30	-0.370
0.32	-0.215
0.34	-0.071
0.35	0
0.36	0.062
0.38	0.204
0.40	0.328

Table 13. Change in hydrogen potential (ΔpH) as a function of the cooperativity parameter (J). The value of J = 0.35 is taken as a point of reference.

In all cases studied, the result is that the selected range of variation of parameter J, $0.30 \leq J \leq 0.40$, one obtains $|\Delta pH| \leq 0.4$; this ensures that the variations of pH catalogued as normal appear as consequence of the neural network simulation with a fixed T.

3.12 Gibbs free energy

In this section we present the calculations for the change in the Gibbs free energy, ΔG. This result lets us locate a limitation of this model. ΔG is obtained from n_H and k_D, where $k_D = \frac{1}{k}$, with k denoting the equilibrium constant for the change of deoxyhemoglobin, Hb, into oxyhemoglobin, HbO_8. We borrow the expression for the change in the free Gibbs energy from Bordbar *et al.* [84]:

$$\Delta G = -RT\Delta n_H \ln(k) + RT(1 - n_H) \ln(x) \tag{155}$$

with $x = P_{50}$. The result of this was plotted and is shown in Figure 26:
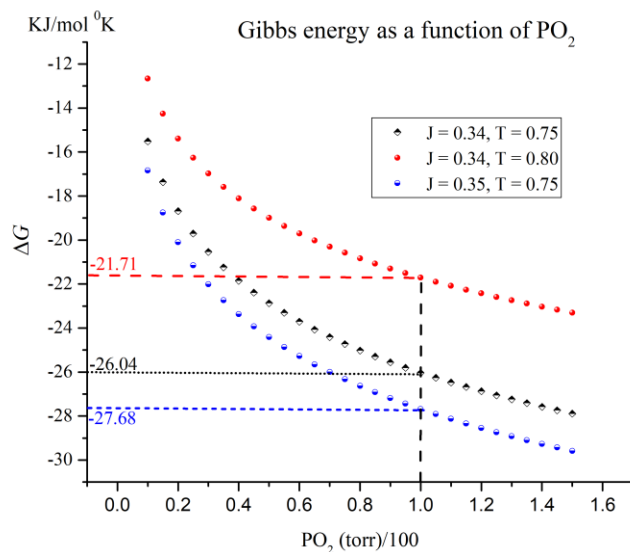
Figure 26. Change in the Gibbs energy as a function of normalized PO_2. Negative values indicate a spontaneous process. When PO_2 increases, ΔG takes more negative values, indicating a more spontaneous process of O_2 binding in the alveoli.

The curves show that ΔG is negative, which means that the process of oxygenation of Hb is a spontaneous reaction. Also, ΔG decreases as PO_2 increases. Although the calculations of the parameter $x = \frac{PO_2}{100}$ increase up to 1.5, it has physical significance until $x = 1\ torr$, which is the pressure that can be reached by the lung alveoli. In other words, when PO_2 increases, ΔG tends to a minimum.

From Figure 26, it is clear that ΔG is more negative when the cooperativity parameter J increases. Also, ΔG is less negative when the network temperature T increases.

Expression (155) was used to calculate ΔG for $x = 1$, which is the maximum pressure in the lung alveoli. The network temperatures T were converted to T_h measured in Celsius as established in Table 12, then converted to Kelvin to plug them in (155). The studied values of ΔG were for $J = 0.34, 0.35, 0.36, 0.38$. The results are shown in Figure 27 below.

76
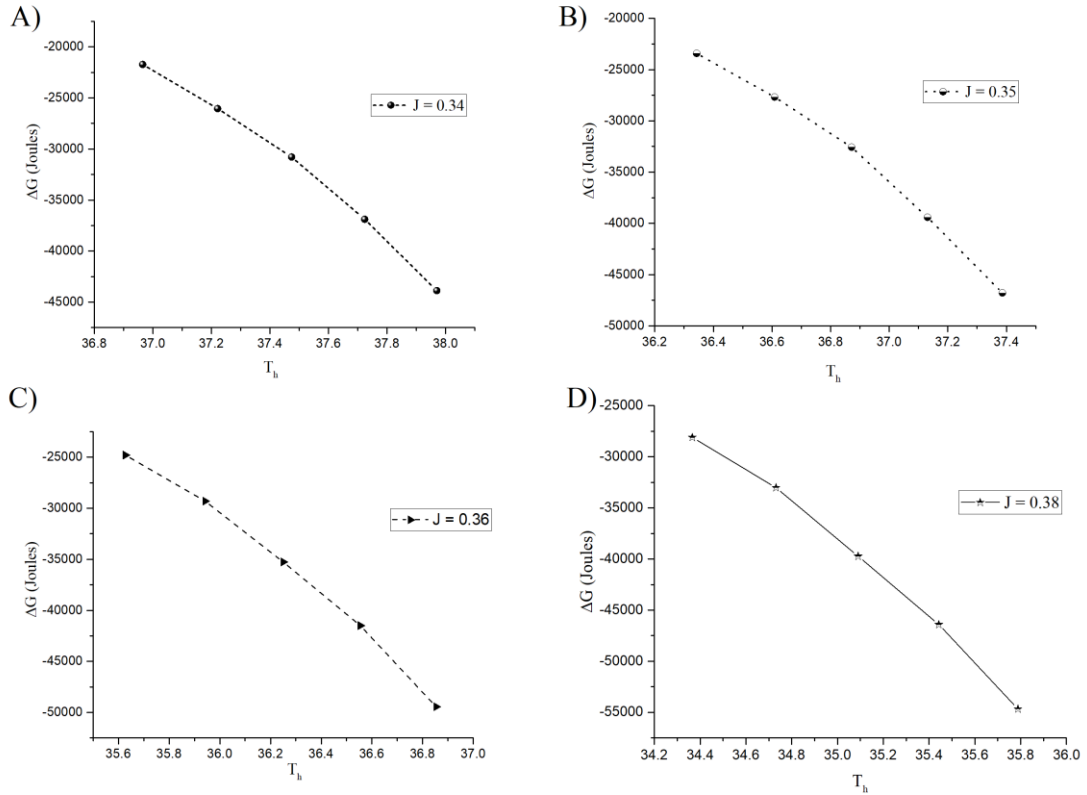
Figure 27. ΔG as a function of T_h. When the cooperativity parameter J increases, the curves shift toward more negative values.

The obtained values are found within the range found by Bordbar *et al.* [84] in their Figure 3, but they are between 39.5% and 48.5% off the value discussed by Holt and Ackers [85]. In the current state of development of this model, it does not have enough elements to obtain the equilibrium constants k_1, k_2, k_3, k_4 and distinguish the free energies that accumulate during the oxygenation process.

3.13 Enthalpy of the model

In a past section, we presented curves in the state space for the Hb saturation as function of PO_2 (θ vs x). These curves display characteristics that make them compatible with the ODCs utilized in medical practice. Each of these curves can be understood as an isotherm in the space $\theta - x$ and associate to it a network temperature T, which has a direct relation to the temperature of the medium of the hemoglobin, T_h. The maximum reachable pressure within the lung alveoli is $x = 1$, therefore, we associate to this parameter the state of thermodynamic equilibrium where the flow of O_2 towards Hb molecules is contained within an erythrocyte. We will show that it is possible to associate a value of enthalpy to a value of J in this model.

In the topic under study, it is not possible to interpret the enthalpy as an exchange of heat in the formation of HbO_8 from Hb. Considering the expression $\Delta H = T\Delta S + V\Delta P$, valid when the number of moles of matter in the system is constant, one can reach the conclusion that ΔH is the heat exchange only if the pressure is held constant. As has been presented above, this is not the case in the Hb oxygenation, as the ODC is obtained by picking values of saturation θ as a function of partial oxygen pressure x.

The calculations are done following the usual procedure found in the literature. First the cooperativity parameter J is set, next one obtains its ΔH value by using the van 't Hoff equation:

$$\frac{d\ln k_{eq}}{dT} = \frac{\Delta H}{RT^2}$$

Denoting $\gamma = \frac{1}{T}$, differentiating and solving for ΔH:

$$\Delta H = -R\frac{d\ln k_{eq}}{d\gamma}$$

Our study focuses on the values of $J = 0.34, 0.35, 0.36$. Using the data from Table 14 below, line equations can be fitted via a standard method.

$J = 0.34$					
T_h	38.09	37.76	37.44	37.11	36.77
$\ln k_{eq}$	4.64135	4.28352	3.94605	3.64216	3.33725
$J = 0.35$					
T_h	37.54	37.23	36.91	36.59	36.26
$\ln k_{eq}$	4.85112	4.49081	4.11006	3.80004	3.51226
$J = 0.36$					
T_h	37.13	36.66	36.18	35.68	35.18
$\ln k_{eq}$	5.04329	4.66891	4.32786	3.97106	3.66578

Table 14. Cooperativity parameters $J = 0.34, 0.35, 0.36$. For each value of J, the first row is the temperatura of the medium of the hemoglobin (T_h) and the second is the natural logarithm of the equilibrium constant (k_{eq}).

The fitted lines for $\ln k_{eq}$ vs γ have the form $\ln k_{eq} = A(J) - B(J)\gamma$. The value of the enthalpy for each line in the space $\theta - x$, shown in Figure 28, can be obtained by calculating their slope. The result is shown in the table 15:

J	ΔH (kcal)
0.34	-22.7616
0.35	-24.1678
0.36	-16.1677

Table 15. Cooperativity parameter (J) is on the left column. The calculated change in enthalpy (ΔH) is on the right column.
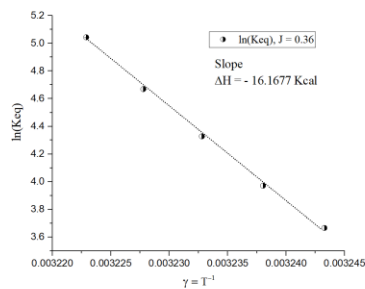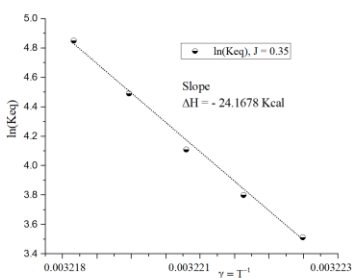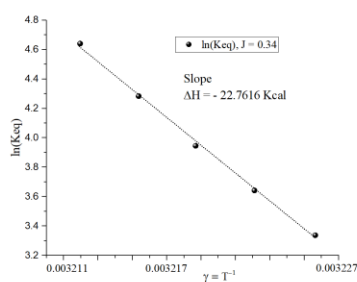
Figure 28. $\ln k_{eq}$ as a function of $\gamma = \frac{1}{T_h}$. The slope is the value of ΔH. Each point has a simulated ODC associated to it.

The results obtained for ΔH are of the order reported in the literature, but they do not match quantitively.

3.14 About the noise

The simulation process presented in this work allows us to obtain the noise that exists as consequence of the finite nature of the number of binding sites in the Hb molecules. The model reflects this trait in the finite nature of the neural network. This phenomenon could be present in small, nano-scaled artificial oxygenators. The uncertainty can be estimated by using the standard deviation, it is possible to draw results shown in Figure 29:
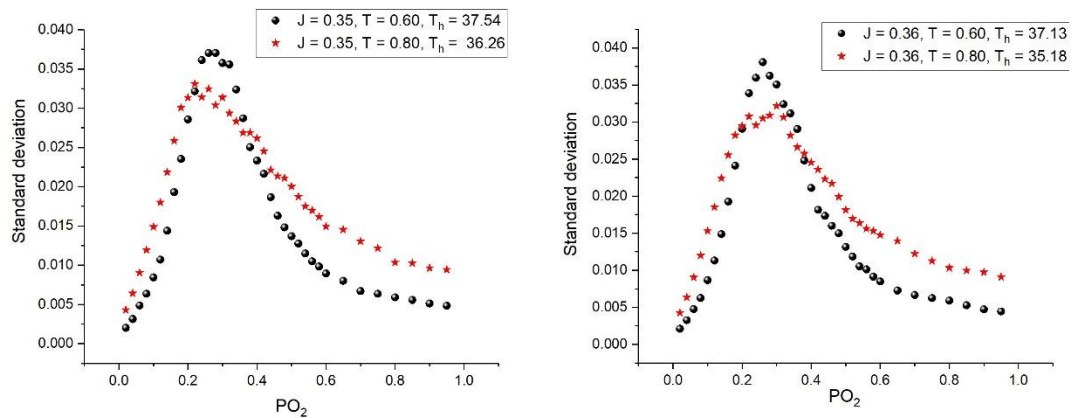
Figure 29. Dependence of the standard deviation respect to $\frac{PO_2}{100}$. To the left hand-side, $J = 0.35$; to the right hand-side, $J = 0.3$. The maximum noise values are in the vicinity of P_{50}. When T_h increases, the curve's height increases and becomes narrower.

For $J = 0.35$ and $J = 0.36$ we present two network temperatures, such that their P_{50} values are near what is considered as normal for healthy human Hb. Both cases display a rapid increase, reaching a maximum in the region associated with a greater value of the slope in the ODC curve. The noise tends to decrease as the system reaches equilibrium for the highest PO_2 values. It can also be appreciated that the curve of the standard deviation turns narrower and higher as T_h increases. On the other hand, this behavior contrasts with the lower noise levels that are reached at maximum saturation. This is more evident when plotting the standard deviation vs. mean Hb saturation:
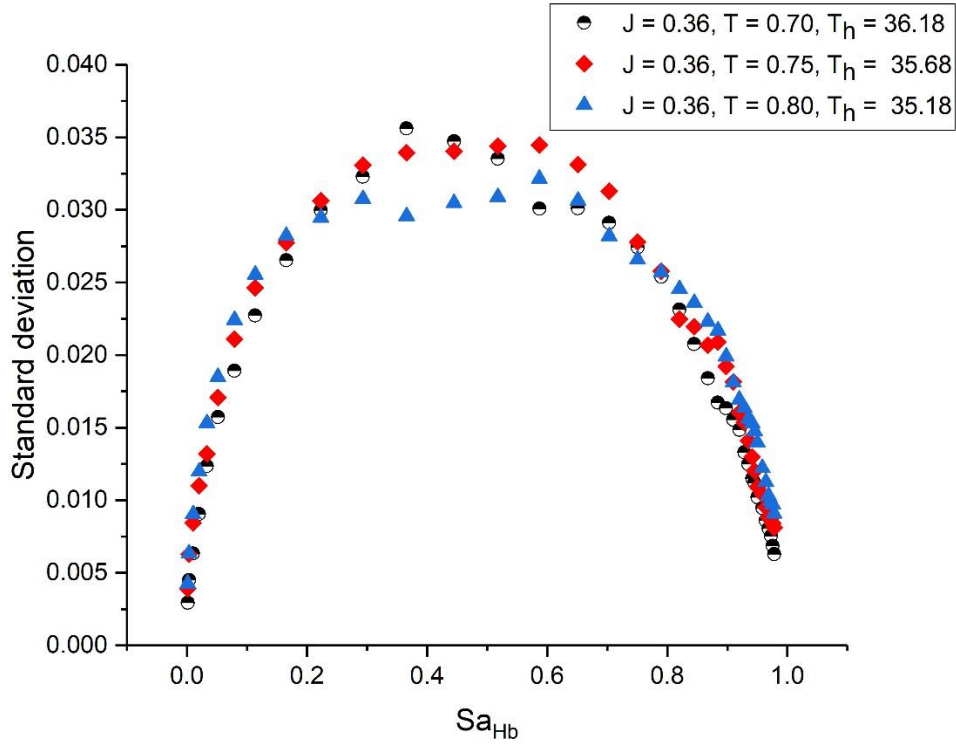
Figure 30. Dependence of the standard debiation respect to the mean Hb saturation. $J = 0.36$ with $T = 0.70, 0.75, 0.80$. The noise reaches its maximum value in the vicinity of P_{50}. The noise decreases to very small values when maximum saturation is reached.

All curves with $J = 0.36$ and $T = 0.70, 0.75, 0.80$ tend to zero as the saturation reaches its maximum. The highest value of the standard deviation occurs when Sa_{Hb} take values between 0.4 and 0.6; that is to say, near P_{50}. As before, the highest noise levels are reached with the highest values of T_h.

Finally, we analyzed the dependence of the standard deviation with respect to cooperativity, which is introduced by the parameter J. The results indicate that the standard deviation shows very little sensibility to changes in parameter J. Table 22 is added to the appendix to show that the changes are, at most, of the order of 10^{-3}, which is not representative of current measurements of oxygen saturation.

3.15 Discussion

The oxygenation of Hb is a process that begins from its T-state and evolves towards its saturated state, called R-state, through an out of equilibrium process. To our knowledge, this topic has been studied since at least 1968 [29]. However, due to their short duration, measurements to monitor the relaxation time of these processes is complicated. To describe these, it is common to see modified diffusion equations, where their exact solutions are difficult to find and instead researchers often opt for numerical methods. Experimental approaches have advanced in the last decades, with the development of techniques that allow the measurement of concentration of O_2

and other substances beside Hb molecules, even if the times involved are very short. There has also been progress in the numerical methods used to solve differential equations. The problem now resides in the fact that the proposed partial differential equations follow the assumption that the quantities involved are continuous. This leaves out stochastic processes that are present and assume greater importance in cases when it is necessary to consider the number of participating molecules, such as miniaturized oxygenators and other devices. In such situations, discrete processes made evident by the finite size of the system may present themselves.

As was mentioned in the introduction of this work, up to now the method of approach to the understanding and control of O_2 transport by biological or artificial means with different geometrical settings, has been in a lot of cases the use of a modified version of expression (145) in this work, or by models like that of Adair. As expressed above, the equilibrium state predicted by some of these approaches coincides with the results obtained here. Comparatively, our model presents an apparent weakness against much of the referenced literature because many of these scientific publications offer a complex and detailed understanding of the physical and chemical phenomena involved. However, one of the relevant aspects in this work is that all of those complex details are reduced to a simple probabilistic problem: the capture or loss of O_2 in each of the four binding sites of an Hb. It is significant that this simplification allows us to reproduce a curve with similar properties to an ODC. On the other hand, although we reference lung alveoli, this model is applicable to any other device where Hb is present in a system where PO_2 increases. In addition, since no special geometry or particular material is required for this model, it is applicable in various situations: from living organisms to mechanical systems designed for the oxygenation of Hb-like molecules.

3.16 Conclusions

Using a finite Hopfield neural network, we developed a stochastic model that simulates the oxygenation process of the hemoglobin. The curves obtained through the simulation of the saturation of the Hb have similar properties to the oxygen-hemoglobin dissociation curve, ODC, that are measured in medical practice and used in scientific research. The process initiates out of equilibrium and evolves towards equilibrium with the passing of the algorithmic time of the network. Each Hb binding site corresponds to a neuron in the network. A number M of Hb molecules give rise to $N = 4M$ binding sites, which correspond to a network of N neurons. The model depends only on two parameters and depends only on transition rates between the states $(+1, -1)$ of each neuron. Figure 19 shows that O_2 saturation, as it evolves, it asymptotically tends towards a horizontal straight line. This horizontal line marks the equilibrium state. The asymptotic values of the O_2 saturation, denoted as θ_{end}, depend on PO_2 as shown in Table 8.

The influence of the oxygen partial pressure was introduced through the field h that affects equally every neuron. The phenomenon of cooperativity is considered by field h_r where the interaction between binding sites is included. The magnitude of this interaction grows whenever a binding site is occupied; with this the cooperative behavior, which appears when an O_2 molecule binds to one of the sites of an Hb, is incorporated in the model.

A list of 39 pairs of (θ vs x) for each pair of (J, T) was generated. The ($\theta - x$) plot shows a sigmoidal shape, which is to be expected for ODCs. The pairs (PO_2, θ_{max}) produce a sigmoidal curve very similar to ODCs. This suggests that the neural network can be used to simulate it. The proper variations in parameters J and T let us replicate the P_{50} values of fetal Hb, early infant Hb and adult Hb. The results were compared satisfactorily with the ODC resulting from the data from Severinghaus; given the simulation data, Figure 21 shows that a Hill curve with $J = 0.35$ and $T = 0.75$ produces a sigmoid curve very similar to the curve by Severinghaus. The curves obtained maintain their shape for different values of (J, T), but their extremes differ slightly. The most notable differences appear in the rapid increase of oxygen saturation. A leftward shift of the ODC was observed when the magnitude of cooperativity parameter was increased.

The simulation results were treated as if they were experimental data. For this, from the 39 pairs of ($\theta - x$), the values were calculated for: the Hill coefficient, n_H; the partial pressure at half saturation, P_{50}; and the equilibrium constant $k = k_D^{-1}$. With these parameters a Hill curve was plotted, then compared with the simulation result, finding a satisfactory fitting. The maximum saturation $\theta_{max} = \theta(x = 1)$ was also obtained. For each (J, T) pair, the quartet of values $(n_H, P_{50}, k_D, \theta_{max})$ can be obtained; these are reported in Tables 9, 16, 17, 18, 19, 20, 21. We also established a functional relation between the network temperature, T, and the medium of the Hb, T_h. Two algebraic relations were found: one between n_H, P_{50} and J, and another between θ_{max} and J. The following relations were found: $n_H(J)$ and $P_{50}(J)$, such that, calculating the derivative, it is possible to find the proportionality relations of dJ with $dP_{50}(J)$, and $dn_H(J)$ with dJ. In other words, the cooperativity parameter J determines the variability of $dn_H(J)$ and dP_{50}.

A relation between the network temperature, T, and hemoglobin temperature measured in Celsius, T_h, was established; it occurs that when T increases, T_h decreases. The values obtained for T_h are within the temperature ranges of healthy human beings. A relation between pH and parameter J was also found, where the difference between the maximum pH value and the minimum pH value are similar to the range of variation considered as normal in the medical practice, meaning, above the state of acidosis and below the state of alkalosis. In qualitative terms, the results are as follows:

- n_H, P_{50}, θ_{max} and k increase when T_h increases.
- The change in pH, ΔPh, is a function that increases as J increases, meaning that an alkaline medium benefits cooperativity.

This last result is consistent with the fact that CO_2 increases acidity, which impacts negatively in cooperativity, in other words, the concentration of CO_2 decreases the cooperative behavior of Hb. This is also consistent with the increase of 2,3-BPG, which decreases affinity of Hb to O_2, contributing with the liberation of oxygen from Hb molecules to tissues in need of oxygenation

The change in Gibbs free energy, ΔG, was calculated in terms of the value of x and it can be seen that, as the oxygen partial pressure increases, the value of ΔG becomes more negative. This indicates that there is a tendency towards a minimum when PO_2 increases. The sign of the results of ΔG indicate that the oxygenation of hemoglobin is a spontaneous reaction. The values of ΔG are within the range of those predicted by Bordbar *et al.*, but they do not match quantitatively with the

results discussed by Holt and Ackers. In fact, the model does not provide elements to obtain k_1, k_2, k_3 and k_4 separately.

The value of the change in enthalpy, ΔH, was also obtained for each value of J. It was noted that this cannot be related with the heat exchange, ΔQ, due to each ODC corresponding to a range of pressures, so that the basic condition for identifying ΔH as ΔQ is not met. The values obtained are of the order as those found in experiments, but in the case that was calculated, it does not correspond to the heat of reaction for the reasons put forward in this body of work.

Currently, it is possible to observe the effects of finite size. Some of these experiments are carried out in devices capable of studying properties of single cells by making them flow through structures that can register them individually. Di Caprio *et al.* [86] show in their Figure 3A the ODC and its standard deviation of a single erythrocyte. They indicate that the initial standard deviation is zero, reaches a maximum near P_{50}, and decreases to very small values when PO_2 reaches its highest values.

Their experimental result matches with those obtained in this work. Figure 17 shows how the standard deviation of w_+ and w_- are zero for $PO_2 = 0$, reach a maximum near P_{50}, then decreases when approaching the maximum value of PO_2 achievable in the alveoli. This behavior is due to the finite nature of the neurons in the network, and the finite number of the realizations performed. This noise translates into the simulation data used to plot the simulated ODC curves shown in Figure 20. In both Figure 17 and Figure 20 the standard deviation reaches it minimum when PO_2 is very low and when it is very high, while the maximum value is reached when Hb transitions from its T state to R state.

According to experimental observations, when oxyhemoglobin reaches tissues that metabolize O_2 it reduces its affinity and releases its cargo with more ease. Instead, the behavior in this model is that affinity increases with T_h, which agrees with kinetic theory of gasses. This theory states that the number of collisions between reactants, in this case Hb binding sites and O_2, increases with temperature, in this case T_h; giving way to an increase in the probability of some of these collisions to be in the correct place and with enough energy for the O_2 molecule to bind to the Fe of the porphyrin ring. This conflicts with medical observations and biochemical analysis shows a limitation of our model but could also indicate that T_h has influence over chemical mechanisms that are not being considered in the model due to the simplicity of the hypothesis this model is based upon.

4 Significance in nanoscience and nanotechnology

From the results in this work can be drawn functional understanding that can potentially prove useful for future research and development.

In the realm of nanotechnology, both approaches developed here, for non-cooperative and cooperative enzymatic reactions, allow for the replication of simulated experiments that could be strenuous and costly if performed in a chemistry laboratory. Instead, in the span of minutes or seconds, this effort can be performed hundreds or thousands of times, change the reaction under

study by simply modifying the parameters involved, and repeat the process as many times as needed.

Their rapid data generation and versatility can aid in the design of nano-scaled devices focused in catalyzing reactions occurring within small volumes, where the participating substances are in the order of tens, hundreds or thousands; causing the stochastic component of the phenomenon to become a key factor that cannot be neglected. The theoretical knowledge and understanding of this stochastic component could allow discrimination between the noise inherent of these scales, and noise coming from other sources. This in turn would allow for adequate filtering and averaging of the measurements, granting more refined data to be studied.

In the specific case of the hemoglobin simulation, the reproduction of the ODC (Oxygen Dissociation Curve) could aid in the miniaturization of oxygen concentrators already in the market today; their reduction in size bringing some relief to the burden on patients who must use them in a daily basis.

In the realm of nanoscience, for the non-cooperative reactions, we have the ability to know the conduct of the entropy during the reaction. The reduction of its value over time suggests the existence of an energy source fueling the reactions, which we propose comes from the normal vibration modes of the enzymes. The fact that enzymes are flexible, allowing for the oscillation of their structure, means that their vibrations have specific frequencies. They are these frequencies that, we propose, are related to the specificity observed in enzymes. In other words, substrate molecules must resonate with the active site of the enzyme for the reaction to be catalyzed. This aspect, if correct, deserves further exploration because it would mean that physical chemistry could prove an invaluable asset in the understanding and design of artificial catalysts for specific substrate molecules.

5 References

[1]   P. W. A. J. De Paula, *Atkins' Physical chemistry*, 9ed. W.H. Freeman, W. H. Freeman, 2010.

[2]   S. Schnell, "Validity of the Michaelis-Menten equation - steady-state or reactant stationary assumption: that is the question," *FEBS J.*, vol. 281, no. 2, pp. 464–472, Jan. 2014, doi: 10.1111/febs.12564.

[3]   A. B. Kolomeisky, "Michaelis–Menten relations for complex enzymatic networks," *J. Chem. Phys.*, vol. 134, no. 15, p. 155101, 2011, doi: 10.1063/1.3580564.

[4]   G. Dell'Acqua and A. M. Bersani, "A perturbation solution of Michaelis–Menten kinetics in a 'total' framework," *J. Math. Chem.*, vol. 50, no. 5, pp. 1136–1148, May 2012, doi: 10.1007/s10910-011-9957-6.

[5]   A. M. Bersani, E. Bersani, G. Dell'Acqua, and M. G. Pedersen, "New trends and perspectives in nonlinear intracellular dynamics: one century from Michaelis–Menten paper," *Contin. Mech. Thermodyn.*, vol. 27, no. 4–5, pp. 659–684, Sep. 2015, doi: 10.1007/s00161-014-0367-4.

[6]   B. Li and B. Li, "Quasi-Steady-State Laws in reversible model of enzyme kinetics," *J. Math. Chem.*, vol. 51, no. 10, pp. 2668–2686, Nov. 2013, doi: 10.1007/s10910-013-0229-5.

[7]   A. F. Bartholomay, "A Stochastic Approach to Statistical Kinetics with Application to Enzyme Kinetics *," *Biochemistry*, vol. 1, no. 2, pp. 223–230, Mar. 1962, doi: 10.1021/bi00908a005.

[8]   S. Hasstedt, "Stochastic models for an open biochemical system.," *Biosystems.*, vol. 10, no. 4, pp. 319–28, Dec. 1978, [Online]. Available: http://www.biomednet.com/db/medline/78134145%5Cnhttp://www.biomednet.com/db/medline/79145694.

[9]   P. Arányi and J. Tóth, "A full stochastic description of the Michaelis-Menten reaction for small systems.," *Acta Biochim. Biophys. Acad. Sci. Hung.*, vol. 12, no. 4, pp. 375–88, 1977, [Online]. Available: http://www.biomednet.com/db/medline/78183714.

[10]   X. Xie Sunney and J. K. Trautman, "OPTICAL STUDIES OF SINGLE MOLECULES AT ROOM TEMPERATURE," *Annu. Rev. Phys. Chem.*, vol. 49, no. 1, pp. 441–480, Oct. 1998, doi: 10.1146/annurev.physchem.49.1.441.

[11]   T. Funatsu, Y. Harada, M. Tokunaga, K. Saito, and T. Yanagida, "Imaging of single fluorescent molecules and individual ATP turnovers by single myosin molecules in aqueous solution," *Nature*, vol. 374, no. 6522, pp. 555–559, Apr. 1995, doi: 10.1038/374555a0.

[12]   H. P. Lu, L. Xun, and X. S. Xie, "Single-Molecule Enzymatic Dynamics," *Science (80-.).*, vol. 282, no. 5395, pp. 1877–1882, 1998, doi: 10.1126/science.282.5395.1877.

[13]   H. Qian and E. L. Elson, "Single-molecule enzymology: stochastic Michaelis–Menten kinetics," *Biophys. Chem.*, vol. 101–102, pp. 565–576, Dec. 2002, doi: 10.1016/S0301-4622(02)00145-X.

[14]   M. O. Stéfanini, a J. McKane, and T. J. Newman, "Single enzyme pathways and substrate fluctuations," *Nonlinearity*, vol. 18, no. 4, pp. 1575–1595, Jul. 2005, doi: 10.1088/0951-

7715/18/4/008.

[15]   A. M. Bersani, E. Bersani, and L. Mastroeni, "Deterministic and stochastic models of enzymatic networks—applications to pharmaceutical research," *Comput. Math. with Appl.*, vol. 55, no. 5, pp. 879–888, Mar. 2008, doi: 10.1016/j.camwa.2006.12.092.

[16]   J. Puchałka and A. M. Kierzek, "Bridging the Gap between Stochastic and Deterministic Regimes in the Kinetic Simulations of the Biochemical Reaction Networks," *Biophys. J.*, vol. 86, no. 3, pp. 1357–1372, Mar. 2004, doi: 10.1016/S0006-3495(04)74207-1.

[17]   T. E. Turner, S. Schnell, and K. Burrage, "Stochastic approaches for modelling in vivo reactions," *Comput. Biol. Chem.*, vol. 28, no. 3, pp. 165–178, Jul. 2004, doi: 10.1016/j.compbiolchem.2004.05.001.

[18]   V. Saks, N. Beraud, and T. Wallimann, "Metabolic Compartmentation – A System Level Property of Muscle Cells," *Int. J. Mol. Sci.*, vol. 9, no. 5, pp. 751–767, May 2008, doi: 10.3390/ijms9050751.

[19]   F. Hinzpeter, U. Gerland, and F. Tostevin, "Optimal Compartmentalization Strategies for Metabolic Microcompartments," *Biophys. J.*, vol. 112, no. 4, pp. 767–779, 2017, doi: 10.1016/j.bpj.2016.11.3194.

[20]   A. Kumar, S. Chatterjee, M. Nandi, and A. Dua, "Emergence of dynamic cooperativity in the stochastic kinetics of fluctuating enzymes," *J. Chem. Phys.*, vol. 145, no. 8, 2016, doi: 10.1063/1.4961540.

[21]   S. L. Berg J.M. Tymoczko J.L., *Biochemistry*, 5th ed. 2002.

[22]   C. C. W. Hsia, "Respiratory Function of Hemoglobin," *N. Engl. J. Med.*, vol. 338, no. 4, pp. 239–248, Jan. 1998, doi: 10.1056/NEJM199801223380407.

[23]   G. S. Adair, "THE HEMOGLOBIN SYSTEM VI. THE OXYGEN DISSOCIATION CURVE OF HEMOGLOBIN," *J. Biol. Chem.*, vol. 63, no. 2, pp. 529–545, 1925, [Online]. Available: http://www.jbc.org/content/63/2/529.full.pdf.

[24]   M. I. Stefan, S. J. Edelstein, and N. Le Novère, "Computing phenomenologic Adair-Klotz constants from microscopic MWC parameters," *BMC Syst. Biol.*, vol. 3, pp. 1–7, 2009, doi: 10.1186/1752-0509-3-68.

[25]   Z. Konkoli, "Safe uses of Hill's model: An exact comparison with the Adair-Klotz model," *Theor. Biol. Med. Model.*, vol. 8, no. 1, pp. 1–17, 2011, doi: 10.1186/1742-4682-8-10.

[26]   J. N. Weiss, "The Hill equation revisited: uses and misuses.," *FASEB J.*, vol. 11, no. 11, pp. 835–841, Sep. 1997, doi: 10.1096/fasebj.11.11.9285481.

[27]   A. V. Hill, "The Combinations of Haemoglobin with Oxygen and with Carbon Monoxide. I," *Biochem. J.*, vol. 7, no. 5, pp. 471–480, Oct. 1913, [Online]. Available: https://www.ncbi.nlm.nih.gov/pmc/articles/PMC1276492/.

[28]   D. A. McQuarrie, *Statistical Mechanics*. HARPER & ROW, 1976.

[29]   W. Moll, "The influence of hemoglobin diffusion on oxygen uptake and release by red

cells," *Respir. Physiol.*, vol. 6, no. 1, pp. 1–15, 1968, doi: 10.1016/0034-5687(68)90014-5.

[30]   P. T. Baxley and J. D. Hellums, "A simple model for simulation of oxygen transport in the microcirculation," *Ann. Biomed. Eng.*, vol. 11, no. 5, pp. 401–416, Sep. 1983, doi: 10.1007/BF02584216.

[31]   A. Clark, W. J. Federspiel, P. A. Clark, and G. R. Cokelet, "Oxygen delivery from red cells," *Biophys. J.*, vol. 47, no. 2, pp. 171–181, 1985, doi: 10.1016/S0006-3495(85)83890-X.

[32]   A. S. Popel, "Theory of oxygen transport to tissue ," *Critical Reviews in Biomedical Engineering* , vol. 17, no. 3. pp. 257–321, 1989, [Online]. Available: http://www.scopus.com/inward/record.url?scp=0024368187&partnerID=8YFLogxK.

[33]   M. Fischer, I. Zinovik, and D. Poulikakos, "Diffusion and reaction controlled dissolution of oxygen microbubbles in blood," *Int. J. Heat Mass Transf.*, vol. 52, no. 21–22, pp. 5013–5019, 2009, doi: 10.1016/j.ijheatmasstransfer.2009.05.013.

[34]   T. Hyakutake and T. Kishimoto, "Numerical investigation of oxygen transport by hemoglobin-based carriers through microvessels," *J. Artif. Organs*, vol. 20, no. 4, pp. 341–349, 2017, doi: 10.1007/s10047-017-0974-5.

[35]   X. S. Chen, H. Nishide, and E. Tsuchida, "Analysis of Facilitated Oxygen Transport in a Liquid Membrane of Hemoglobin," Jan. 1996.

[36]   S. T. Bouwer, L. Hoofd, and F. Kreuzer, "Diffusion coefficients of oxygen and hemoglobin measured by facilitated oxygen diffusion through hemoglobin solutions," *Biochim. Biophys. Acta - Protein Struct. Mol. Enzymol.*, vol. 1338, no. 1, pp. 127–136, Mar. 1997, doi: 10.1016/S0167-4838(96)00197-5.

[37]   S. T. Bouwer, L. Hoofd, and F. Kreuzer, "Reaction rates of oxygen with hemoglobin measured by non-equilibrium facilitated oxygen diffusion through hemoglobin solutions," *Biochim. Biophys. Acta - Gen. Subj.*, vol. 1525, no. 1–2, pp. 108–117, 2001, doi: 10.1016/S0304-4165(00)00177-X.

[38]   A. Kaesler, M. Rosen, T. Schmitz-Rode, U. Steinseifer, and J. Arens, "Computational Modeling of Oxygen Transfer in Artificial Lungs," *Artif. Organs*, vol. 42, no. 8, pp. 786–799, 2018, doi: 10.1111/aor.13146.

[39]   R. Scrima, S. Fugetto, N. Capitanio, and D. Gatti, *Hemoglobin Non-equilibrium Oxygen Dissociation Curve*. 2019.

[40]   E. Agliari, A. Barra, R. Burioni, A. Di Biasio, and G. Uguzzoni, "Collective behaviours: from biochemical kinetics to electronic circuits," *Sci. Rep.*, vol. 3, p. 3458, Dec. 2013, [Online]. Available: https://doi.org/10.1038/srep03458.

[41]   E. Agliari, M. Altavilla, A. Barra, L. Dello Schiavo, and E. Katz, "Notes on stochastic (bio)-logic gates: Computing with allosteric cooperativity," *Sci. Rep.*, vol. 5, pp. 1–11, 2015, doi: 10.1038/srep09415.

[42]   A. Coolen, "Statistical Mechanics of Recurrent Neural Networks I. Statics," Jul. 2000, [Online]. Available: https://nms.kcl.ac.uk/ton.coolen/published/2001/CH14.pdf.

[43] J. M. Castellanos-Jaramillo, "Extensión del modelo Michaelis-Menten a dimensiones nanométricas por medio de física estadística fuera de equilibrio," Universidad de Sonora, 2017.

[44] E. Nelson, "Derivation of the Schrödinger Equation from Newtonian Mechanics," *Phys. Rev.*, vol. 150, no. 4, pp. 1079–1085, Oct. 1966, doi: 10.1103/PhysRev.150.1079.

[45] L. de la Peña-Auerbach, "New Formulation of Stochastic Theory and Quantum Mechanics," *J. Math. Phys.*, vol. 10, no. 9, pp. 1620–1630, Sep. 1969, doi: 10.1063/1.1665009.

[46] E. Santos, "Brownian Motion and the Stochastic Theory of Quantum Mechanics," in *Irreversibility in the Many-Body Problem*, 1st ed., J. Biel and J. Rae, Eds. Boston, MA: Springer US, 1972, pp. 457–470.

[47] A. M. C. (auth. . de la Peña, *The Quantum Dice: An Introduction to Stochastic Electrodynamics*, 1st ed. Springer Netherlands, 1996.

[48] A. Castellanos-Moreno, "Random systems described with stochastic velocities," *Phys. A Stat. Mech. its Appl.*, vol. 316, no. 1–4, pp. 189–202, 2002, doi: 10.1016/S0378-4371(02)01207-4.

[49] D. T. Gillespie, "A general method for numerically simulating the stochastic time evolution of coupled chemical reactions," *J. Comput. Phys.*, vol. 22, no. 4, pp. 403–434, Dec. 1976, doi: 10.1016/0021-9991(76)90041-3.

[50] D. R. Weilandt and V. Hatzimanikatis, "Particle-Based Simulation Reveals Macromolecular Crowding Effects on the Michaelis-Menten Mechanism," *Biophys. J.*, vol. 117, no. 2, pp. 355–368, 2019, doi: 10.1016/j.bpj.2019.06.017.

[51] A. Moreno, A. Jaramillo, A. Corella, S. Gutiérrez-López, and R. Rosas-Burgos, "Stochastic model for computer simulation of the number of cancer cells and lymphocytes in homogeneous sections of cancer tumors," Oct. 2014. https://arxiv.org/abs/1410.3768

[52] H. Risken, *The Fokker-Planck equation: methods of solution and applications*, Softcover. Springer, 1984.

[53] K. R. Albe, M. H. Butler, and B. E. Wright, "Cellular concentrations of enzymes and their substrates," *J. Theor. Biol.*, vol. 143, no. 2, pp. 163–195, Mar. 1990, doi: 10.1016/S0022-5193(05)80266-8.

[54] N. G. Van Kampen, *Stochastic Processes in Physics and Chemistry*. 2007.

[55] C. Gardiner, *Handbook of stochastic methods for physics, chemistry, and the natural sciences*, 3rd ed. Springer-Verlag, 2004.

[56] E. Nelson, *Dynamical theories of Brownian motion*, Second edi. Princeton University Press, 1967.

[57] Y. De Decker, "Stochastic thermodynamics based on an Einstein-Boltzmann definition of fluctuating entropy," *Phys. Rev. E*, vol. 99, no. 3, pp. 1–9, 2019, doi: 10.1103/PhysRevE.99.032143.

[58] O. Ivashchenko, T. Tomila, N. Ulyanchich, T. Yarmola, and I. Uvarova, "Fourier-Transform Infrared Spectroscopy of Antibiotic Loaded Ag-Free and Ag-Doped Hydroxyapatites," *Adv. Sci. Eng. Med.*, vol. 6, no. 2, pp. 193–202, 2014, doi: 10.1166/asem.2014.1473.

[59] B. X. Wang, L. P. Zhou, and X. F. Peng, "Surface and size effects on the specific heat capacity of nanoparticles," *Int. J. Thermophys.*, vol. 27, no. 1, pp. 139–151, 2006, doi: 10.1007/s10765-006-0022-9.

[60] E. Gamsjäger and M. Wiessner, "Low temperature heat capacities and thermodynamic functions described by Debye–Einstein integrals," *Monatshefte fur Chemie*, vol. 149, no. 2, pp. 357–368, 2018, doi: 10.1007/s00706-017-2117-3.

[61] C. di Lauro, "Spectra of Spherical Top Molecules," *Rotational Struct. Mol. Infrared Spectra*, no. 3, pp. 225–245, 2013, doi: 10.1016/b978-0-12-407771-3.00010-0.

[62] E. Ley-Koo and R. Méndez Fragoso, "Properties of the spectra of asymmetric molecules: matrix evaluation in bases of spherical harmonics and common generating function," *Rev. Mex. física*, vol. 54, no. 1, pp. 69–77, 2008.

[63] L. P. P. L. D. Landau, *Statistical physics*, 2nd ed., vol. Part 2. Pergamon Press, 1980.

[64] A. Himoe, K. G. Brandt, R. J. DeSa, and G. P. Hess, "Investigations of the chymotrypsin-catalyzed hydrolysis of specific substrates. IV. Pre-steady state kinetic approaches to the investigation of the catalytic hydrolysis of esters.," *J. Biol. Chem.*, vol. 244, no. 13, pp. 3483–3493, 1969.

[65] J. K. Hobbs, W. Jiao, A. D. Easter, E. J. Parker, L. A. Schipper, and V. L. Arcus, "Change in heat capacity for enzyme catalysis determines temperature dependence of enzyme catalyzed rates," *ACS Chem. Biol.*, vol. 8, no. 11, pp. 2388–2393, 2013, doi: 10.1021/cb4005029.

[66] V. L. Arcus *et al.*, "On the Temperature Dependence of Enzyme-Catalyzed Rates," *Biochemistry*, vol. 55, no. 12, pp. 1681–1688, 2016, doi: 10.1021/acs.biochem.5b01094.

[67] M. I. Page and A. Badarau, "The mechanisms of catalysis by metallo β-lactamases," *Bioinorg. Chem. Appl.*, vol. 2008, no. 5, 2008, doi: 10.1155/2008/576297.

[68] A. Holmberg, "On the practical identifiability of microbial growth models incorporating Michaelis-Menten type nonlinearities," *Math. Biosci.*, vol. 62, no. 1, pp. 23–43, 1982, doi: 10.1016/0025-5564(82)90061-X.

[69] J. H. Kim and J. M. Lee, "Successive complementary model-based experimental designs for parameter estimation of fed-batch bioreactors," *Bioprocess Biosyst. Eng.*, vol. 41, no. 12, pp. 1767–1777, 2018, doi: 10.1007/s00449-018-1999-8.

[70] Y. C. Yeh, T. H. Huang, S. C. Yang, C. C. Chen, and J. Y. Fang, "Nano-Based Drug Delivery or Targeting to Eradicate Bacteria for Infection Mitigation: A Review of Recent Advances," *Front. Chem.*, vol. 8, no. April, pp. 1–22, 2020, doi: 10.3389/fchem.2020.00286.

[71] S. Bhaskar and S. Lim, "Engineering protein nanocages as carriers for biomedical applications," *NPG Asia Mater.*, vol. 9, no. 4, pp. e371-18, 2017, doi: 10.1038/am.2016.128.

[72] H. Nabipour, M. Hosaini Sadr, and N. Thomas, "Synthesis, characterisation and sustained

release properties of layered zinc hydroxide intercalated with amoxicillin trihydrate," *J. Exp. Nanosci.*, vol. 10, no. 16, pp. 1269–1284, 2015, doi: 10.1080/17458080.2014.998301.

[73]   F. de M. UNAM, "AMOXICILINA/CLAVULANATO," 2005. http://www.facmed.unam.mx/bmnd/gi_2k8/prods/PRODS/16.HTM.

[74]   D. Y. Arifin, L. Y. Lee, and C. H. Wang, "Mathematical modeling and simulation of drug release from microspheres: Implications to drug delivery systems," *Adv. Drug Deliv. Rev.*, vol. 58, no. 12–13, pp. 1274–1325, 2006, doi: 10.1016/j.addr.2006.09.007.

[75]   B. A. Kolesov, "How the vibrational frequency varies with temperature," *J. Raman Spectrosc.*, vol. 48, no. 2, pp. 323–326, 2017, doi: 10.1002/jrs.5009.

[76]   J. Pfanzagl and O. Sheynin, "Studies in the history of probability and statistics XLIV a forerunner of the t-distribution," *Biometrika*, vol. 83, no. 4, pp. 891–898, 1996, doi: 10.1093/biomet/83.4.891.

[77]   A. D'Alessandro, M. Dzieciatkowska, T. Nemkov, and K. C. Hansen, "Red blood cell proteomics update: Is there more to discover?," *Blood Transfus.*, vol. 15, no. 2, pp. 182–187, 2017, doi: 10.2450/2017.0293-16.

[78]   K. M. Mihelc, B. J. Frankowski, S. C. Lieber, N. D. Moore, B. G. Hattler, and W. J. Federspiel, "Evaluation of a respiratory assist catheter that uses an impeller within a hollow fiber membrane bundle," *ASAIO J.*, vol. 55, no. 6, pp. 569–574, 2009, doi: 10.1097/MAT.0b013e3181bc2655.

[79]   H. H. Manap, A. K. Abdul Wahab, and F. M. Zuki, "Mathematical Modelling of Carbon Dioxide Exchange in Hollow Fiber Membrane Oxygenator," *IOP Conf. Ser. Mater. Sci. Eng.*, vol. 210, no. 1, 2017, doi: 10.1088/1757-899X/210/1/012003.

[80]   J. W. Severinghaus, "Simple, accurate equations for human blood O 2 dissociation computations.," *J. Appl. Physiol.*, vol. 46, no. 3, pp. 1–2, 2007, [Online]. Available: https://www.nickalls.org/dick/papers/anes/JWSrevised2007.pdf.

[81]   J. Wyman, "Linked Functions and Reciprocal Effects in Hemoglobin: A Second Look," *Adv. Protein Chem.*, vol. 19, no. C, pp. 223–286, 1964, doi: 10.1016/S0065-3233(08)60190-4.

[82]   M. Samaja, D. Melotti, E. Rovida, and L. Rossi-Bernardi, "Effect of temperature on the p50value for human blood," *Clin. Chem.*, vol. 29, no. 1, pp. 110–114, 1983.

[83]   R. B. Reeves, "The effect of temperature on the oxygen equilibrium curve of human blood," *Respir. Physiol.*, vol. 42, no. 3, pp. 317–328, Dec. 1980, doi: 10.1016/0034-5687(80)90122-X.

[84]   A. K. Bordbar, A. A. Saboury, M. R. Housaindokht, and A. A. Moosavi-Movahedi, "Statistical effects of the binding of ionic surfactant to protein," *J. Colloid Interface Sci.*, vol. 192, no. 2, pp. 415–419, 1997, doi: 10.1006/jcis.1997.4999.

[85]   J. M. Holt and G. K. Ackers, *Chapter 7 The Hill Coefficient. Inadequate Resolution of Cooperativity in Human Hemoglobin*, 1st ed., vol. 455, no. A. Elsevier Inc., 2009.

[86]   G. Di Caprio, C. Stokes, J. M. Higgins, E. Schonbrun, and D. A. Weitz, "Single-cell

measurement of red blood cell oxygen affinity," *Proc. Natl. Acad. Sci. U. S. A.*, vol. 112, no. 32, pp. 9984–9989, 2015, doi: 10.1073/pnas.1509252112.

6 Appendix

T_h	T	n_H	P_{50}	k_D	$\theta_{max} \times 100$	J
40.0109	0.70	2.75961	31.251	0.0403667	96.946	0.30
39.9253	0.75	2.52804	30.9768	0.0516794	94.946	0.30
39.8392	0.80	2.31153	30.8963	0.0662074	93.7525	0.30
39.7528	0.85	2.13256	30.7449	0.080844	92.532	0.30
39.666	0.90	1.96491	30.6643	0.0980124	91.197	0.30

Table 16. Cooperativity parameter $J = 0.30$. Value of the temperature of the hemoglobin (T_h) is on the first column, the network temperature (T) is on the second column. The calculated values are for: Hill coefficient (n_H), partial pressure at half saturation (P_{50}), dissociation constant (k_D), and maximum saturation achieved (θ_{max}) multiplied by 100.

T_h	T	n_H	P_{50}	k_D	$\theta_{max} \times 100$	J
38.6345	0.70	2.90031	29.063	0.0277664	96.998	0.32
38.5344	0.75	2.66283	28.8286	0.0364422	95.9685	0.32
38.4337	0.80	2.43348	28.6407	0.0477066	96.027	0.32
38.3325	0.85	2.22959	28.4973	0.0608744	93.8795	0.32
38.2308	0.90	2.06889	28.4649	0.0743068	92.7555	0.32

Table 17. Cooperativity parameter $J = 0.32$. Value of the temperature of the hemoglobin (T_h) is on the first column, the network temperature (T) is on the second column. The calculated values are for: Hill coefficient (n_H), partial pressure at half saturation (P_{50}), dissociation constant (k_D), and maximum saturation achieved (θ_{max}) multiplied by 100.

T_h	T	n_H	P_{50}	k_D	$\theta_{max} \times 100$	J
37.9702	0.60	3.65432	0.280804	0.00964469	98.7835	0.34
37.724	0.65	3.33201	0.276494	0.013794	98.234	0.34
37.4744	0.70	3.02678	0.271522	0.0193309	97.607	0.34

T_h	T	n_H	P_{50}	k_D	$\theta_{max} \times 100$	J
37.2216	0.75	2.77168	0.268726	0.0261957	96.876	0.34
36.9654	0.80	2.52454	0.266622	0.0355345	95.91	0.34

Table 18. Cooperativity parameter $J = 0.34$. Value of the temperature of the hemoglobin (T_h) is on the first column, the network temperature (T) is on the second column. The calculated values are for: Hill coefficient (n_H), partial pressure at half saturation (P_{50}), dissociation constant (k_D), and maximum saturation achieved (θ_{max}) multiplied by 100.

T_h	T	n_H	P_{50}	k_D	$\theta_{max} \times 100$	J
36.8534	0.60	3.80378	0.265573	0.00645246	99.121	0.36
36.5543	0.65	3.45201	0.258589	0.00938253	98.6365	0.36
36.2505	0.70	3.16779	0.255073	0.0131958	98.1855	0.36
35.9417	0.75	2.87214	0.250922	0.0188535	97.4805	0.36
35.6277	0.80	2.63478	0.24875	0.0255841	96.773	0.36

Table 19. Cooperativity parameter $J = 0.36$. Value of the temperature of the hemoglobin (T_h) is on the first column, the network temperature (T) is on the second column. The calculated values are for: Hill coefficient (n_H), partial pressure at half saturation (P_{50}), dissociation constant (k_D), and maximum saturation achieved (θ_{max}) multiplied by 100.

T_h	T	n_H	P_{50}	k_D	$\theta_{max} \times 100$	J
35.7881	0.60	3.92597	0.25135	0.00442092	99.311	0.38
35.4424	0.65	3.58229	0.244274	0.00641504	98.942	0.38
35.0902	0.70	3.2894	0.238651	0.00897867	98.4805	0.38
34.7314	0.75	2.98723	0.235589	0.0133195	98.0485	0.38
34.3657	0.80	2.74719	0.233145	0.0183127	97.326	0.38

Table 20. Cooperativity parameter $J = 0.38$. Value of the temperature of the hemoglobin (T_h) is on the first column, the network temperature (T) is on the second column. The calculated values are for: Hill coefficient (n_H), partial pressure at half saturation (P_{50}), dissociation constant (k_D), and maximum saturation achieved (θ_{max}) multiplied by 100.

T_h	T	n_H	P_{50}	k_D	$\theta_{max} \times 100$	J
34.2256	0.65	3.75959	0.230285	0.00424512	99.1775	0.40
33.8661	0.70	3.38239	0.225159	0.00645461	98.8455	0.40
33.4995	0.75	3.08659	0.220834	0.00944935	98.4655	0.40
33.1258	0.80	2.83299	0.217335	0.0132473	97.876	0.40

Table 21. Cooperativity parameter $J = 0.40$. Value of the temperature of the hemoglobin (T_h) is on the first column, the network temperature (T) is on the second column. The calculated values are for: Hill coefficient (n_H), partial pressure at half saturation (P_{50}), dissociation constant (k_D), and maximum saturation achieved (θ_{max}) multiplied by 100.

J	σ at T=0.70	σ at T=0.75	σ at T=0.80
0.30	0.034	0.034	0.031
0.32	0.035	0.034	0.034
0.34	0.036	0.034	0.036
0.35	0.037	0.034	0.035
0.36	0.040	0.035	0.033
0.38	0.037	0.038	0.038
0.40	0.037	--	--

Table 22. Standard deviation for $J = \{0.30, 0.32, 0.34, 0.35, 0.36, 0.38, 0.40\}$. Network temperatures $T = 0.70, 0.75, 0.80$. The noise displays very little sensibility to changes in J.